Thesis for the degree of Doctor of Philosophy

Oblique Sounding and HF Communication Techniques for Very Long Haul Ionospheric Links

Pau Bergadà Caramés

Enginyeria i Arquitectura La Salle
Universitat Ramon Llull

Barcelona 2014

Oblique Sounding and HF Communication Techniques for Very Long Haul Ionospheric Links

Pau Bergadà Caramés
Research Group in Electromagnetism and Communications (GRECO)
Enginyeria i Arquitectura La Salle
Universitat Ramon Llull
Quatre Camins, 2
08022 Barcelona, Spain

Advisor: Dr. Joan Ramon Regué Morreres
Enginyeria i Arquitectura La Salle, Universitat Ramon Llull, Barcelona, Spain.

This thesis has been prepared using LaTeX.

A la Maria, per tota la seva paciència

Abstract

High Frequency (HF) radio is used by governmental and non nongovernmental agencies worldwide whenever an alternative to satellites for sky wave communication is needed: ships at sea, aircraft out of range of line-of-sight radio networks, military operations, disaster areas with communication infrastructure destroyed or distant regions lacking other communications. It offers an alternative to satellites, or a backup, for long-haul communications, thus avoiding the costs, vulnerabilities and sovereignty concerns of satellite communications.

In this thesis the HF link between the Antarctic Spanish Station Juan Carlos I in Livingston Island, South Shetlands and Spain is studied. The aim of this study is to address the impairments that affect HF propagation (i.e., signal-to-noise plus interference ratio, multipath and Doppler shift and spread) and to design the physical layer of a low rate, low power and long-haul HF link. Some proposals regarding this last issue are addressed, i.e., direct sequence spread spectrum (DSSS) and orthogonal frequency division multiplexing (OFDM). The challenge is to define the symbol characteristics that best fit the link to benefit from time and frequency diversity that offers the HF channel.

Since 2003 several transmission campaigns have allowed to study the HF channel but it is not until the 2009/2010 campaign that we have achieved a whole picture of both diurnal and nocturnal ionospheric activity. In the papers presented in this thesis we have extended the previous research to the whole range of HF frequencies and we have shown the differences on performance between day and night. We have used the results from channel characterization to design and compare the performance of DSSS and OFDM symbols. Both techniques have turned out to be possible candidates to implement a low rate HF link between Antarctica and Spain. However, both techniques stand for different approaches of the modem: DSSS achieves good performance at low data rate in low SNR scenarios, whereas OFDM achieves higher data rate in benign channels.

Keywords: High frequency (HF), sky wave propagation, signal-to-noise ratio (SNR), multipath, Doppler spread, direct sequence spread spectrum (DSSS), orthogonal frequency division multiplexing (OFDM).

Acknowledgments

It is time to finish the research work that began some years ago or at least close this chapter and open another one to keep on satisfying the interest that brought me to this moment. My first thought always goes to thank my parents who were convinced to send their children to University and always supported them to persevere in their studies, regardless of what fulfilled them. My second thought goes to thank my wife, Maria, who has a never-ending faith on his husband who sometimes think he has a lot to do to deserve her love and patience.

The third of my thoughts goes to thank my advisor, Joan Ramon Regué, whom I first met when finishing my Bachelor degree. He introduced me to the digital world and allowed me to become a member of the former Department of Communications and Signal Theory (DCTS) of La Salle Engineering School-Ramon Llull University (URL). He has been a good chief to foster the Antarctic Project, he has fully supported the researchers who were involved in and encouraged them to go further on their studies. Due to his initiatives, proposals and improvements about the project, he has allowed me to gather a lot of data related to new experiments which have derived in contributions published in some journals and finally in this thesis.

As you all may guess, such a big project and its respective parts and tasks have not all been undertaken by this candidate. Therefore, I would like to acknowledge the work carried out by Joan Lluís Pijoan, as the main researcher in this project, for starting such a huge project and for having allowed me to become involved in it. I would also like to thank Carles Vilella, who showed me so many secrets about digital signal processing. He also developed all the work from where I began my research, which turned out to be a solid starting point. A special mention goes to my colleagues Ricard Aquilué, Marc Deumal and Ismael Gutiérrez, with whom I shared a lot of discussions about digital techniques for data transmission and from whom I learned a lot about digital signal processing.

David Badia helped me, and all the group, with all the stuff concerning analogue electronics and EMC problems. As the chief of the former DCTS, he resolved any logistic problem that we came across. I would like to thank him for his patience and for being such an honest man. More recently, Rosa Maria Alsina has pushed me to write this thesis and all the required papers to reach the end of this research period. I have spent so much time with her discussing how to begin each new experiment, discussing

the outcomes and organizing the huge task of writing and correcting the papers. In fact, I would like to keep in contact with her and continue supporting the research activities of the group. I would also like to thank Raul Bardají and Joan Mauricio for sharing with me so good times during the development of the Antarctic project. At last, but not least, I would like to thank Ahmed, Albert, Antonio, Joan Claudi, Miquel, Pablo, Pajares, Sevillano, Simó, Xavi Auñón and Xuti. They are all good people who are always ready to help. I am very grateful to all of them and I miss them from the first moment I left the Department.

This project has been developed with the collaboration of the *Observatori de l'Ebre* (OE), which belongs to the URL and it is also related to the *Centro Superior de Investigaciones Científicas* (CSIC). David Altadill and Santi Marsal, both researchers from this institution, have been very good colleagues with whom I have had very nice moments, specially at the Antarctica. The days working at the OE, deploying the receiver system will remain in my memory for many years. This thesis is based on several projects which has been funded by the Ministry of Science and Innovation of several Spanish Governments. The *Unidad de Tecnologia Marítima*, which belongs to the CSIC, has undertaken all the logistics at the Antarctica to make the research described in this thesis possible. My last thanks go to the Spanish Marine crew of Las Palmas (A-52) for safely carrying the researches from South America to Antarctica and vice versa.

Pau Bergadà
Girona, September 2014

About the author

Pau Bergadà got a Bachelor Degree in Communications from La Salle Engineering School-Ramon Llull University in 2002. In 2003 he got a Master Degree in Electronics and in 2009 he got a Master Degree in Communications from the same University.

From 2003 to 2011 he worked as both assistant professor and researcher focused on projects about wireless and wired communications and software defined radio (SDR) at La Salle Engineering School.

Since 2012 he has worked as electronic engineer for an small engineering and manufacture company, which provides products over a wide range of sectors from LED lighting to industrial automation systems and wireless remote control.

Summary of contributions

This thesis is a compendium of the most relevant contributions of the author. The work carried out in the following three contributions summarize the work undertaken throughout his research project:

- Bergadà, P., M. Deumal, C. Vilella, J.R. Regué, D. Altadill and S. Marsal **Remote Sensing and Skywave Digital Communication from Antarctica**, Sensors 2009, 9, pp. 10136-10157; doi:10.3390/s91210136

- Ads, A.G., P. Bergadà, C. Vilella, J.R. Regué, J.L. Pijoan, R. Bardají and J. Mauricio **A comprehensive sounding of the ionospheric HF radio link from Antarctica to Spain**, Radio Science, vol. 48, 1-12, doi:10.1029/2012RS005-074, 2013

- Bergadà, P., R.M. Alsina-Pagés, J.L. Pijoan, M. Salvador, J.R. Regué, D. Badia and S. Graells **Digital transmission techniques for a long haul HF link: DSSS versus OFDM**, Radio Science, 49, doi:10.1002/2013RS005203, 2014

This thesis is related to the project REN2003-08376-C02-01 "Characterization and modeling of the Antarctic ionospheric channel: Advanced HF communications" whose final goal was to implement a radiomodem capable of transmitting data from a geomagnetic sensor in the Spanish Antarctic Base to the Ebro Observatory in Spain.

The work of the author within this project was mainly to participate on the design of the required equipment and on the design of the preliminary system for data transmission. The design and implementation of the equipment was presented in different conferences. The most important contributions in which he was involved are:

- Bergadà, P., C. Vilella, M. Deumal and J.L. Pijoan, **Sodio: A Software Radio platform for advanced HF communications**, COST-289 Workshop on Spectrum and Power Efficient Broadband Communications, Budapest, 2004.

- Bergadà, P., C. Vilella, J.L. Pijoan, M. Ribó, J.R. Regué and R. Aquilué, **Sondeador ionosférico para un enlace entre la Base Antártica Juan Carlos I y el Observatorio del Ebro**, XX Simposium Nacional URSI, Gandia, 2005.

- Vilella, C., P. Bergadà, M. Deumal, J.L. Pijoan and R. Aquilué, **Transceiver Architecture and Digital Down Converter Design for a Long Distance, Low Power HF Ionospheric Link**, 10^{th} IET International Conference on Ionospheric Radio Systems and Techniques, London, 2006.

Regarding the design of the preliminary system for data transmission, two major modulation techniques have been evaluated: direct sequence spread spectrum (DSSS) and orthogonal frequency division multiplexing (OFDM). The most important contributions in which he was involved were developed within the projects CGL2006 "Monitoring of the geomagnetic and ionospheric variability at the Livingston Island. Advanced techniques for its characterization and data transmission in the HF band" and CTM2009-13843-C02-02 "The Geophysical Observatory on Livingston Island: Installation of a permanent seismic station, improving data transmission system by HF and continuing the collection of historical series of data" and are listed below:

- Bergadà, P., R. Aquilué, I. Gutiérrez and J.L. Pijoan **Estimación del canal inosférico entre la Antártida y el Observatorio del Ebro basada en símbolos OFDM**, XXI Simposium Nacional URSI, Oviedo, 2006.

- Aquilué, R., P. Bergadà, I. Gutiérrez and J.L. Pijoan **Channel Estimation for Long Distance HF Communications based on OFDM Pilot Symbols**, 10^{th} IET International Conference on Ionospheric Radio Systems and Techniques, London, 2006

- Aquilué, R., P. Bergadà, M. Deumal and J.L. Pijoan **Multicarrier Symbol Design for HF Transmissions from the Antarctica Based on Real Channel Measurements**, IEEE Military Communications Conference, Washington D.C., 2006.

- Bergadà, P., M. Deumal, C. Vilella, and J.L. Pijoan **Multicarrier Modulation Proposal for Long Distance HF Data Links**, 12^{th} International Ionospheric Effects Symposium, Alexandria-Virginia, 2008.

- Mauricio, J., P. Bergadà, J.M. Torta, J.L. Pijoan, S. Marsal, J.C. Riddick and J.J. Curto **Codificación de fuente y senalización OFDM ad-hoc para enlace HF de larga distancia**, XXIII Simposium Nacional URSI, Madrid, 2008.

- Alsina-Pagés, R.M., P. Bergadà, J.C. Socoró and M. Deumal **Multiresolutive Acquisition Technique for DS-SS Long-Haul HF Data Link**, 11^{th} IET International Conference on Ionospheric Radio Systems and Techniques, Edinburgh, 2009.

- Bergadà, P., M. Deumal, R.M. Alsina-Pagés and J.L. Pijoan **Time Interleaving Study for an OFDM Long-Haul HF Radio Link**, 11^{th} IET International Conference on Ionospheric Radio Systems and Techniques, Edinburgh, 2009.

- Bergadà, P., R.M. Alsina-Pagés, C. Vilella and J.R. Regué (2012). **Low Rate High Frequency Data Transmission from Very Remote Sensors**, book chapter in "Remote Sensing-Advanced Techniques and Platforms", Dr. Boris Escalante (Ed.), ISBN 978-953-51-0652-4, InTech, doi:10.5772/36053.

Contents

Part II: Contributions

Part I

Overview

Chapter 1

Work frame, motivation and goals

In this chapter the author explains the projects he has been involved in, as well as the different tasks he has undertaken throughout this research period. Moreover, a brief state of the art that has motivated his research activities is reviewed. Finally, the goals pursued by this thesis are explained. The goals of the projects in which he has participated and specifically the work developed by the author have shaped the research topics presented in this thesis.

1.1 Work frame

The research work developed by the author began in 2001 as an undergraduate in the former Department of Communications and Signal Theory (DCTS) of La Salle Engineering School-Ramon Llul University. As a member of the Research Group in Electromagnetism and Communications (GRECO), he participated in several research projects related to the digital communications field.

From September 2001 to June 2003 he worked on the design of a software defined radio (SDR) based digital platform, called SODIO. This digital platform consisted of field programmable gate array (FPGA) devices, high-speed high-resolution A/D/A converters, communication specific ASICs and several input-output buses that assured sufficient connectivity with other platforms and devices. This work was done during the Master degree studies and was presented as his Master's thesis. The funding of this project was provided by La Salle under the internal projects PGR-PR2001-01 "Research on Software Radio Techniques" and PGR-PR2003-06 "Advanced Receivers with Software Radio (ARSODIO)".

Between 2003 and September 2004 he participated in the internal project of La Salle PGR-PR-2004-06 "Study of software architectures. Fitting to SODIO platform", in which software interfaces with SODIO devices and input-output buses were implemented.

In September 2004 he joined the so-called *Antarctic project*: REN2003-08376-C02-01 "Characterization and modeling of the Antarctic ionospheric channel: Advanced HF communications" funded by the Ministry of Education and Science from the Spanish Government. The aim of the Antarctic project was to study the characteristics (i.e., availability, SNR, multipath and Doppler power profile) of the HF channel between Antarctica and Spain; as well as the design of a robust unidirectional system for long haul HF communications through the ionosphere. The radio modem had to be capable of transmitting data with high reliability from a geomagnetic sensor located at the Spanish Antarctic Base in Livingston Island to the Ebro Observatory in Spain. Moreover, due to low power supply and environmental restrictions at the Spanish Antarctic Base simple infrastructure and low power transmissions were required. Another goal of this project was to investigate the effects of the solar and magnetic activities on the electromagnetic wave propagation through the ionosphere.

In 2003 and 2004 he participated in the COST-289 action: "Spectrum and Power Efficient Broadband Communications" funded by the European Union. The main objective of the Action was to increase the capacity of communication systems within a specified transmission bandwidth with minimum available transmitter power, bearing in mind the cost effectiveness and the practical implementation of the system. The research topics developed by the DCTS were related to SDR and peak to average power ratio (PAPR) reduction. He contributed with the implementation of some parts of a radio modem in an FPGA.

In September 2006 he joined a second *Antarctic project*: CGL2006-12437-C02-01 "Monitoring of the geomagnetic and ionospheric variability at the Livingston Island. Advanced techniques for its characterization and data transmission in the HF band." funded by the Ministry of Science and Innovation from the Spanish Government. This project started from a wide knowledge of the hourly, monthly and annual variability of frequency availability and channel parameters such as attenuation, SNR, Doppler and delay spread, gathered and computed along the previous project. This project was focused on designing a complete communication system, minimizing power consumption and increasing bit rate as much as possible. Historical series of vertical and oblique soundings were carried on, with the aim to find a relationship between them in to predict the oblique channel conditions from the vertical soundings. Another goal of the project was to go further with the study of the geomagnetic field, updating the geomagnetic station, making it compatible with the INTERMAGNET network and using automatic learning techniques (neural networks and wavelets) for automatic magnetic storm detection.

In September 2009 he joined a third *Antarctic project*: CTM2009-13843-C02-02 "The Geophysical Observatory on Livingston Island: Installation of a permanent seismic station, improving data transmission system by HF and continuing the collection of historical series of data" funded by the Ministry of Science and Innovation from the Spanish Government. This project represented another challenge with the aim of

transforming the Spanish Antarctic Base Juan Carlos I into a Geophysical Observatory with data transmission in almost real time using a low power system independent of the satellite. Evidently, another objective of the project was the continuity of the historical data series of the geomagnetic observatory, the vertical ionospheric sounder and the trans-equatorial oblique sounding.

From 2008 to 2010 he participated in the project "Broadband Carrier Wave" funded by ENDESA Network Factory S.L. Previous work with Endesa Network Factory S.L. (WPLC-Viability) showed that the high voltage power line channel (3-30 MHz) can be exploited in a more efficient way as it is done nowadays. These improvements were basically based on multicarrier modulations and cognitive radio techniques, i.e., on one hand, improving the system robustness against multipath and the highly selective noise scenario and, on the other hand, the use of friendly and unlicensed band that ranges from 500 kHz and beyond. The main goal of this project was the implementation of a real time version of the proposed physical layer. This project showed the real performance of the proposed system when adaptive techniques were deployed. Two multiprocessor SDR platforms were used to implement the application. The main tasks the author developed in this project were related to the physical layer of the communication protocol developed on FPGAs and DSPs.

1.2 Motivation

In this section we explain some historic issues related to the development of radio technology and specially HF communications. Then, we make a short review of the standardization process of the link layer of HF protocols. Finally, we review the standardization process of the physical layer of several HF standards; as well as other digital techniques approached in the literature to implement an HF digital link.

Historic radio beginnings In the first decade of the 20^{th} century several radio pioneers and developers (e.g., Marconi, Telefunken, United Wireless, Lodge-Muirhead) were developing long wave transmitters to reach ships at sea from the shore [2]. They believed they could compete with transatlantic cables deployed during the previous century. However, it was almost by coincidence that amateur operators discovered the features of shorter wavelength (less than 200 meters):

- Higher range may be achieved with less power due to the existence of the ionosphere.

- Lower atmospheric noise at HF than at the lower frequency band.

- Smaller antennas for wavelengths of tens of meters than for kilometer wavelength.

The Titanic's sinking in 1912 represented a milestone that demonstrated that first radio technology was useful but needed to be improved. These words from Marconi explained the situation just after the tragedy [10]:

It is worthwhile to have lived to have made it possible for these people to have been saved. Just now all the world is thinking of this greatest of sea disasters, I feel that I must speak of it, but I do it reluctantly. I know you will understand me if I say that all those who have been working with me, entertain a true feeling of gratitude that wireless telegraphy has again helped to save human lives. I also want to express my thanks to the press for the hearty approval it has given my invention.
I am proud, but I see many things that will have to be done if wireless is to be of the fullest utility. It will be necessary to compel all ships to carry to operators, so that one may be on duty at all times.
Some of the ships failed to hear the Titanic's call for help because they were receiving news bulletins from Cape Cod. With two operators, one could be working the news, the other—on any ship equipped properly—could be listening for distress signals, which would not interfere with long distance news messages.

Latter he added the following suggestions [10]:

Wireless, however, should not be regulated to death, as it easily could be. But, it simply must be governed in some manner, and the one body fit to the regulating would be an international board. It's a bigger job than any one nation could handle. All must be considered and must join in the proceedings.

HF link layer standardization Although it was clear, already from the second decade of 20^{th} century, that wireless systems should be regulated, it was not since the 80's, with the advent of the microprocessor and the integration improvement of ASICs, that appeared the first proprietary systems. Microprocessor should be powerful enough to run ionospheric prediction programs in personal computers. Even more interesting was to embed the microprocessor in the HF radio to seek for the best working frequency. These systems implemented a number of solutions that alleviated the job of radio operators:

- Scanning a previously configured set of frequencies

- Listening for call signs

However, these first-generation of digital HF radios did not provide interoperability among equipment from different manufactures. This was the main reason why in 1986 appeared a second-generation of automatic link establishment (ALE) proposed in FED-STD-1045 [15] and adopted by the military community as the standard MIL-STD-188-141A [8]. The key functions of this data link layer standard can be summarized as:

- Selective calling and handshake

- Scanning a set of frequencies listening for calls

- Sounding to determinate which frequencies are working

- Polling to test frequencies

- Connectivity exchange for relaying or routing protocols

- Link quality analysis and channel selection

- Automatic message exchange

- Message store and forward to work around link interruptions

- Network coordination and management

In the mid-1990s the major concern was not interoperability among HF radios but the scarce HF spectrum worldwide. Moreover, the second generation of ALE systems worsened this issue (e.g., long scanning calls, long establishment calls, long and numerous answer calls and high SNR needed to establish the link), which constrained the traffic level on second generation ALE systems. These reasons explained why industry and academic communities started to develop a new ALE standard seeking the following goals [29]:

- Decrease the SNR needed to set up an HF link

- Increase the number of HF stations that could use the network

- Increase spectrum efficiency

Which lead to integrate the following capabilities:

- A new connection management function (link set up and automatic link maintenance function)

- A new traffic management system which plays a role after link set up and decides the communication protocol to be used to harmonize traffic.

- A set of new packet-oriented data link protocols (high throughput and low latency data links)

- Circuit link management to coordinate circuit-based links

- A set of PSK burst waveforms

A wide range of applications is covered with this 3G HF system ranging from analog and digital voice to circuit and packet-based data. This HF system also describes how information is exchanged between nodes by radio and the non-HF interface which allow external users to interact with the subnetwork and with each other over the subnetwork. This subnetwork interface is similar to that described in the protocol standard STANAG 5066, which was promulgated on January 2004 (first draft on July 2000) [33].

These first, second and third generation ALE systems covered the major layers of the OSI model. Obviously, they all implemented a physical layer to counteract the HF channel impairments: from a simple 16 tone waveform in the late 1950s to sophisticated burst waveforms in the beginning of 2000.

HF physical layer standardization The work developed in this thesis is focused on several candidates for the physical layer of a long-haul HF link, as it is explained in the next section. Therefore, we now summarize the physical layer proposals appeared in the standards to check whether they fit a 4-5 hops [37], trans-equatorial HF link.

The physical layer of the link undertakes all the functions to combat the short-term effects of the HF channel (i.e., noise, interference and short fades), whereas the intermediate and long-term effects are addressed in the upper layers of the stack with the help of automatic repeat request (ARQ) and ALE systems. First wireless operators, by the beginning of the 20^{th} century, used spark gap transmitters that were substituted by continuous wave transmitters which, in turn, were substituted by complex M-ary FSK modems (e.g., 16-tone Kineplex [20]). These initial HF modems performed well under good channel characteristics but could not recover from severe SNR fluctuations, ISI and frequency dispersion.

It was not until the 70^{th} and 80^{th} decade of the last century that military research designed a single-carrier PSK waveform, which was finally included in STANAG 4285 [34] in 1989 and a similar performance waveform was included in US MIL-STD-188-110A [8] in 1991.

STANAG 4285 modulates a single carrier waveform within a 3 kHz bandwidth. BPSK, QPSK and 8-PSK modulations (which are scrambled to prevent the modulated signal from degenerating to a tone when constant inputs are mapped) achieve a coded data throughput of 1200, 2400 and 3600 bps, respectively, though lower rates are also possible. Data transmission is divided in 256 segments, in each of which a preamble composed of 80 symbol (31 chip m-sequence) and four blocs of 32 data symbols intercalated with 3 blocs of 16 training symbols are transmitted. Data demodulation is performed recursively by means of a least mean squares-decision feedback equalizer (LMS-DFE) [39] to estimate and to equalize the channel impulse response. Data symbols are mapped to bits with Gray coded modulation. Afterward, a convolutional decoder (code rate 1/2, constraint length=7) [21] decodes channel codification and a

convolutional deinterleaver breaks bursts of errors with two possible depths: 0.8 s and 10.24 s.

MIL-STD-188-110A is similar to STANAG 4285 but includes characteristics that improves STANAG 4285 performance: longer preamble provides more robustness in poor scenarios, it includes embedded information to be used by the receiver and it automatically detects the baud rate. Moreover, due to a different block structure, it is able to cope with worse delay and Doppler spread; however, it performs worse than STANAG 4285 on long fading channels. MIL-STD-188-110A has better throughput efficiency for the highest data rates (i.e., 2400 bps and 3600 bps), which avoids the use of a punctured convolutional encoder.

In MIL-STD-188-110A, robust transmission is achieved at 75 bps by means of Walsh modulation [11]. This modulation technique is also used by the robust standard STANAG 4415 [35]. Walsh modulation uses the bits, in groups of two, coming from the coder and the block interleaver structure to select one of four orthogonal Walsh functions of length four. Then, these Walsh functions are repeated eight times, resulting in a 32-symbol 8-PSK sequence. The interleaved data also decides which of the four Walsh functions is used to rotate $180\,^\circ$ (in case of 1) or $0\,^\circ$ (in case of 0) each of the 8-PSK symbols of the underlying PN sequence. Finally, the scrambled PN sequence is mapped to the inphase and quadrature components of the carrier signal (1800 Hz) at a rate of 2400 symbols per second. The minimum required performance of STANAG 4415 is defined as follows [35] (modem operating in long interleaving mode (4.8 seconds) and with a convolutional encoder (code rate=1/2, constraint length=7)):

- In a single path and non-fading channel, the modem shall achieve BER$< 10^{-3}$ at -9.00 dB SNR (3 kHz) in an additive white Gaussian noise environment.

- In a dual path channel, with multipath delay spread equal to 10.0 ms the modem shall achieve BER$< 10^{-4}$ with a Doppler spread ranging from 0.5 Hz to 50.0 Hz, in both paths, and SNR between -1.00 dB and 0.00 dB (3 kHz).

- The modem shall be capable of achieving synchronization and providing BER$< 10^{-5}$ for multipath delay spreads up to 10.0 ms in a 0 dB SNR (3 kHz) channel with Doppler spreads of 2 Hz and 20 Hz.

- The modem shall be able to cope with a signal to interference ratio (SIR) of -6 dB, -25 dB and -40 dB, while maintaining BER$< 10^4$ with SNR=+10 dB, for the following types of interference: self interference, SSB voice and swept CW.

As previously explained, the concern in the mid 1990s was not interoperability of HF systems but spectral efficiency. Therefore, international standard efforts were made to include in the ARQ standard STANAG 5066 a new waveform that achieved higher bit rates than those (i.e., 1200, 2400 and 3600 bps) offered by previous standards (i.e., STANAG 4285 and MIL-STD-188-100A). The issue was to use more complex constellations (i.e., QPSK, 8-PSK, 16QAM, 32QAM and 64QAM) to achieve bit rates

Standard	Publication year	Bandwidth and code rate	Modulation	Bit rate [bps]
STANAG 4285	1989	2400 baud/s, 1/2	BPSK, QPSK, 8-PSK	1200/2400/3600
MIL-STD-188-110A (serial tone)	1991	2400 baud/s, 1/2, 1/4, 1/8	Walsh, BPSK, QPSK, 8-PSK	75/150-600/1200/2400
STANG 4415	2000	2400 baud/s, 1/2	Walsh	75
MIL-STD-188-110B (appendix C)	2000	2400 baud/s, 3/4	4,8-PSK, 16,32,64-QAM	3200-12800
STANAG 4539	2000	2400 baud/s, 3/4	4,8-PSK, 16,32,64-QAM	3200-12800

Table 1.1: Characteristics of the main HF physical standards.

up to 12800 bps. The new waveform is described in the STANAG 4539 and in the appendix C of MIL-STD-188-110B [42]. The main features of this waveform are:

- A 184 symbol preamble composed of PN sequences with good correlation properties to detect the signal, plus 103 symbols which include modulated sequences with information for the receiver (e.g., code rate and interleaving settings).

- Data blocks of 256 symbols are alternated with known data blocks of 31 symbols with a total efficiency of 7/8.

- Star quadrature amplitude modulation (QAM) achieving a user data rate of 6400 bps, 8000 bps, 9600 bps and 12800 bps (no coded). Star QAM maximizes signal space distance, minimizes peak to average ratio [3] and since it is Gray coded reduces bit error rate.

- Channel estimation is based on known data rather than on equalization of data symbols as previous standards did.

- A tail-biting convolutional encoder which avoids the rate loss incurred by zero-tail termination at the expense of a more complex decoder [27]. This characteristic is very useful for slotted transmissions and to optimize ARQ.

- A bloc interleaver with 6 different depths (from 120 ms to 8.64 s) to fit both low latency and broadcast applications.

In table 1.1 we summarize the main characteristics of the HF physical standards that we have just described.

HF radio modems based on single carrier waveforms rather than multicarrier waveforms have been chosen by military authorities (i.e., US Department of Defense and NATO) as the waveform to be implemented in many standards over many years (e.g., STANAG 4285 and STANAG 4539) and more recently also used in the new 3G standard-STANAG 4538 (uses Walsh functions for robust transmissions, while PSK for higher throughput data links) [29]. Although the huge complexity of single carrier demodulation carried out by a maximum likelihood sequence estimation (MLSE) approach or even the reasonably complexity of adaptive equalization, authorities have always decided to choose single carrier solutions (with a few exceptions, e.g., the 39-tone waveform defined in appendix B of MIL-STD-188B and the 16-tone waveform defined in MIL-STD-188A). The decision is due to the slightly better performance compared

with OFDM, claimed by Harris Corporation in [31] and [30] (Harris Corporation proposed the waveform finally adopted in STANAG 4539) and due to the availability of commercial off-the-shelf products (also according to Harris Corporation).

Multcarrier modulation, concretely OFDM, is high bandwidth efficient and has low computational complexity [45]. In the HF field, OFDM has been studied in terms of robustness against impulsive noise, PAPR, synchronization and other parameters [6] [20]. In a time and frequency dispersive environment, OFDM is combined with channel coding and interleaver to benefit from time and frequency diversity. Long interleavers introduce latency, which is an important downside for systems that employ ARQ or for interactive applications; however, it does not represent a serious problem for broadcast applications. OFDM and spread spectrum (SS) can work together by means of a MC-CDMA scheme [12], to benefit from frequency diversity without the need of long interleavers. This is a multiuser technique commonly used to multiplex several users in the same bandwidth. Instead of different users, different symbols, from the same user, may be multiplexed, what it leads to a synchronous system with no near/far problem (since all symbols are transmitted with the same power) and with a clear increase of the spectral efficiency. This technique enables to use very short interleavers and still reduce the degradation caused by frequency selective channels at the expense of a higher complexity receiver [36].

PAPR is a major constraint of OFDM waveforms because it increases bit error rate (BER) degradation and spectral outgrowth when signals pass through a non-linearity power amplifier. It requires to back-off the signal with the consequently reduction of the average transmitted power. This is the reason why an important research effort has been done to reduce envelope fluctuations in OFDM signals (e.g., tone reservation, active constellation extension, tone injection, selected mapping, ...). A different approach is to define a constant envelope OFDM waveform, as does [32]. It compares the performance of coded OFDM with constant envelope OFDM (CEOFDM) using pulse-amplitude modulation (PAM) in mid-latitude disturbed HF channels. It concludes that coded OFDM outperforms CEOFDM due to the poor performance of the linear equalizer and the fact that only pure real data can be mapped into the PAM and into each subcarrier. To overcome the PAPR problem on HF channels, [18] suggests a single carrier-frequency domain equalization (SC-FDE) scheme, which is a one user version of the single carrier-frequency domain multiple access (SC-FDMA) scheme (the uplink technique of the Long Term Evolution (LTE) standard [28]). Frequency domain equalization rather than time domain equalization is used and consequently a reduced implementation cost is achieved. Preliminary results seems to validate the use of SC-FDE scheme for long-haul HF links.

Another solution for HF waveforms is the continuous phase modulation (CPM) waveform because of the higher bandwidth efficiency compared with single carrier waveform. Its constant envelope characteristic eases the power amplifier linearity requirements. [31] sates that a CPM waveform (e.g., a GMSK waveform) on the HF

channel has a similar performance than a non constant envelope single carrier waveform at low bit rate (i.e., 1600 bps); whereas at high bit rate (i.e., 3200 bps) CPM performance worsens.

1.3 Goals

Sensors placed in remote areas of the Earth where satellite coverage is expensive, scarce or it does not exist at all can use the ionosphere as a communication channel for over-the-horizon communications. That is the case of the geomagnetic sensor placed at Livingston Island, South Shetlands archipelago, which daily transmits data to Spain by means of a geostationary satellite. The set up of the link is not always feasible due to problems of coverage.

The main goal of this project is to design and implement a skywave data link from the Spanish Antarctic Station (SAS) Juan Carlos I to Spain. The minimum requirements regarding the geomagnetic sensor data transmission from the SAS to Spain are:

- The system should support a data throughput of 5040 bits per hour. The system transmits an Intermagnet (the global network of observatories, monitoring the Earth's magnetic field) IMF v2.83 frame every 12 minutes. Each Intermagnet frame is 126 bytes long.

- The maximum delivery delay of the data should not exceed 24 hours.

The extreme conditions prevailing at the SAS impose a number of restrictions that affect the transmission system. We highlight the following ones:

- The transmission power should be minimal. It is noted the SAS is inhabited only during the austral summer, approximately from November to March. Throughout this period there is no limitation regarding the maximum power consumption. However, the transmission system is designed to continue operating during the austral winter, when energy is obtained entirely from batteries powered by wind generators and solar panels. Hence the power amplifier is set to a maximum of only 250 watts.

- Environmental regulations applicable at the transmission side advise against the installation of large structures that would be needed to install in case of using certain types of directive antennas or collocated antennas. Therefore, the transmitting antenna is a simple 7.5 meter monopole with a gain between -5 dB and 0 dB and approximately a 10 ° elevation angle (radiation pattern depends on the ground plane, which mainly depends on the 32 10-meter radials of the monopole).

It is a unidirectional skywave data link without neither ARQ system nor an ALE system to request for repetitions and to scan and establish the best available frequency as the HF standards, explained in section 1.2, do. Consequently, the system must choose the frequency with best availability by himself. This is the reason why we have been sounding the HF channel between the SAS and Spain since 2003. The goal is twofold: *i*) narrowband sounding to know the frequency with best availability as a function of time and *ii*) wideband sounding to know the multipath and Doppler spread figures, as well as the SNR, as a function of time and frequency, which all determine the physical layer of the data link.

Other HF channel characterization projects, such as DAMSON (Doppler and Multipath SOunding Network) [4], focused on studying the HF channel on high latitude paths. This project lasted from 1995 to 1999 and was focused on the following studies over the ionospheric channel between Svalbard (Norway), Oslo and Kiruna (Sweden): *i*) Absolut time of flight, *ii*) SNR, *iii*) Absolute signal strength, *iv*) Multipath spread, *v*) Doppler shift and spread. After four years of intermittent work they concluded that at frequencies between 2.8 MHz and 21.9 MHz: SNR at a 3 kHz bandwidth ranged from -20 dB to -5 dB, multipath spread ranged from 1 ms to 11 ms, and Doppler spread ranged from 2 Hz to 73 Hz.

Nonauroral path propagation generally has an upper limit of about 2 Hz of Doppler spread. The channel response exhibits a Rice distribution and a Rayleigh distribution, alternatively. Limited data relating to measurement of the correlation bandwidth indicate that it varies from about 100 Hz to 3000 Hz depending upon the channel turbulence. The time spread of arriving energy varies from less than 1 ms to about 4 ms. With good paths and proper operating frequencies the multipath spread can be lower than 1 ms. In contrast, on an auroral path, it is possible that Doppler spread may be as high as 25 Hz while the coherence bandwidth may be as narrow as 50 Hz. As it can be observed, ionospheric propagation via an auroral path is generally much more turbulent than nonauroral transmission [16].

In our scenario (a nonauroral trans-equatorial link) we should apply to the International Telecommunication Union (ITU), which is responsible for regulating the use of radio spectrum, for a temporal or experimental license for each of the frequencies we would like to use. Moreover, the signal travels through a number of countries and consequently, we should also apply for a license on each of them.

The ITU suggests the allocation of each frequency band to one or several services. When multiple services are attributed to the same frequency band in the same region, these fall into two categories, i.e., primary or secondary. Those that are classified as secondary services cannot cause interference to primary services; however, they can demand protection from interference from other secondary services attributed afterwards.

Given these considerations, the transmission system should fulfill the following re-

quirements:

- It cannot cause harmful interference to any other service station (primary or secondary)
- It cannot claim protection from interference from other services

To meet these requirements, we propose a system with some of the following characteristics:

- Reduced transmission power
- Low spectral density
- Robustness to interference
- Burst transmission
- Sporadic communications

Regarding the characteristics that we propose for this communication system, we note that:

- The standard modes (i.e., MIL-STD, FED-STD, STANAG) are designed for primary or secondary services. Therefore:
  - The bandwidth of the channels is standardized to a voice channel (3 kHz).
  - Interference reduction, i.e., minimize the output spectral density with other transmitting systems, is not considered.
  - Very few modes are considered based on short burst transfers to reduce interference with other users. Only the burst waveforms defined in the new 3G HF technology suite fulfill this requirement [29].
  - There are anti-jamming techniques (see MIL-STD-188-148) for additional application on a appropriate communication standard, but the proposals are not based on intrinsically robust to interference modulations.
- Robust configuration (e.g., [22] and [35]) require a minimum SNR of 0 dB on 3 kHz bandwidth, which is not common in this link under the specified conditions of transmitted power and antennas deployed at transmitter and receiver station.

We conclude that the configurations proposed by current standards do not meet the desirable characteristics for the type of communication that is required in this work, and consequently, a new proposal should be suggested. Therefore, we have approached the design from two different points of view:

- Design a communication system able to transmit low power spectral density to minimize the interference on other users at the expense of long transmitting periods, low data rate and wide bandwidth.

- Design a communication system able to transmit short data bursts with high data rate and narrow bandwidth at the expense of high power spectral density.

The waveform candidates we have chosen to implement these two approaches are DSSS and OFDM. On one hand, DSSS intrinsically minimizes spectral efficiency, hence reduces interference on other users by occupying a greater bandwidth than what it is really necessary [38]; then it matches the first of the above points. On the other hand, OFDM maximizes the spectral efficiency by transmitting high data rate data in narrow bandwidth [43], then it matches the second of the above points.

Chapter 2

The research work

The work presented in this thesis can be divided in two different blocks: *i*) oblique sounding of the channel and *ii*) transmission techniques to counteract the impairments of the channel and benefit from the diversity it offers. In this chapter we briefly explain the work undertaken by the author in these two fields.

2.1 Oblique sounding of the channel

Since 2003 the members of the GRECO have been sounding the channel with both narrowband and wideband signals. From the 2009/2010 antarctic campaign the hardware of the oblique sounder has been improved with a more powerful digital signal processing (DSP) unit, i.e., three FPGAs with higher number of slices and DSP cells and a high speed connection with a PC embedded. This new DSP unit has enabled to sound the whole HF band (2-30 MHz) during the whole day (0-24 h). It has enabled to improve the usable memory space, hence the size of the transmitted files has been increased and it has also improved the user interface. In chapter 5 we explain the methods used to sound the ionospheric channel between the Antarctica and Spain and the outcomes that we have obtained.

Regarding the narrowband sounding, a 10-second non modulated signal has been used to compute the narrowband SNR (10 Hz) and the availability factor. A number of windows (i.e., Hanning, Blackman, Flattop and Kaiser) have been considered to improve the detection of the signal, to lower the out-of-band signals and to reduce the transients generated by the rectangular window (used by the the previous oblique sounder [*Vilella et al.*(2008)]) at the receiver. We have divided the time interval where the signal was supposed to be into a number of segments to increase the robustness against narrowband interference signals of short duration. Two different SNR lower bounds have been set up (i.e., 3 dB and 6 dB) for each of the time intervals to increase the reliability of the availability factor and the SNR estimation.

Regarding the wideband sounding, the channel measurements have been computed by means of a pulse compression technique based on pseudo noise (PN) m-sequences

because of their good autocorrelation properties [17]. The m-sequences are 127 chips long, with 20 samples per chip. They occupy a bandwidth of $BW = 5\,kHz$ and hence each of them is $T_s = 25.4\,ms$ long. The channel has been sounded continuously during a period of 10 seconds. This technique and the characteristics of this PN sequence enable to sound any channel with an impulse response shorter than 25.4 ms (i.e., T_s). It provides a delay accuracy of 200 μs (i.e., $1/BW$). The maximum measurable Doppler frequency (shift or spread) is 19.58 Hz (i.e., $1/(2 \times T_s)$) and the Doppler accuracy is 0.1 Hz (i.e., $1/10\,s$).

The channel impulse response has been computed by correlating the received signal with a copy of the original PN sequence. The scattering function, the composite multipath and Doppler spread, the SNR, the propagation time and the Doppler frequency shift have all been derived from the channel impulse response. Composite multipath and Doppler spread have been computed in a frequency (i.e., (-4, 4) Hz) and time (i.e., (-3, 3) ms) window. All the noise outside these windows has been subtracted to improve the robustness of the estimation. The SNR has been computed by means of the scattering function and the frequency and time windows defined above. The signal power has been computed inside the windows, whereas the noise power outside.

The propagation time between transmitter and receiver has been computed by means of the correlation of several PN sequences with the transmitted PN sequence. The time difference between consecutive correlation peaks has determined the propagation time. The pulse per second (PPS) signal (with a $1\mu s$ of accuracy) of a global positioning system (GPS) receiver has been used at both the receiver and the transmitter for an accurate time reference.

In order to measure the Doppler shift introduced by the ionosphere —as long as the transmitter and receiver station are static—, a 10 MHz oven controlled crystal oscillator (OCXO) is used. The frequency stability in temperature of this oscillator is $\pm 0.1\,ppb$, which means, for instance, that a carrier frequency of 10 MHz may have a maximum frequency deviation of 0.001 Hz between remote oscillators in the range between 0 °C and 50 °C.

2.2 Transmission techniques

We explored several techniques as possible candidates for the physical layer (i.e., DSSS, DSSS plus signaling and OFDM) of the radiomodem of the link between Antarctica and Spain. As explained in previous sections, it is a low SNR, high interfered, frequency and time dispersive channel. Hence, symbol characteristics must be designed to counteract these impairments.

Direct sequence spread spectrum (DSSS) can be a good option because it shows good performance in low SNR links, it has intrinsic robustness against narrowband

interference and due to its wide bandwidth can benefit from frequency diversity in a frequency selective channel. Moreover, DSSS minimizes interference on other users due to its low power spectral density.

In chapter 6 we show the experiments that tested the performance of several DSSS symbol length and bandwidth. The goal was to find the lower bound of the PN sequence length, that is, which PN sequence showed insufficient process gain; which sequence had too wide bandwidth and consequently showed low SNR at the receiver; and which PN sequence were too long and too near to the coherence time of the channel.

The downside of DSSS is the wide bandwidth and the length of the PN sequence, which lead to low spectral efficiency. Although the bit rate achieved with DSSS is enough for our application (an Intermagnet frame is required to be transmitted every 12 minutes, which represents 5040 bits per hour), we have focused our research on other communication techniques that can improve data throughput. The issue is to increase the performance at the receiver by repeating the data to be transmitted as many times as possible to benefit from time diversity (we remind the reader that it is a simplex link with no ARQ). Then, we have focused on achieving higher spectral efficiency to shorten data bursts and reduce the interference on other users.

In order to increase the spectral efficiency we could increase the number of baseband symbols that are coded multiplexed within a symbol interval. This technique is known as direct sequence-code division multiple access (DS-CDMA), which sets the signal power to be proportional to the number of codes multiplexed (assuming that no multiple access interference occurs). In our system the transmitted power is constant, then the higher the multiplexed symbols the lower the SNR per symbol. When seeking higher spectral efficiency we could also decrease the process gain; however, the SNR would decrease as well. Therefore, we have proposed a technique called DSSS signaling [9] for this HF channel, which increases the number of bits per symbol without increasing the occupied bandwidth. This technique shows a good performance in low SNR scenarios at the expense of a more complex receiver. DSSS signaling consists on mapping m data bits into one of the $M = 2^m$ spreading codes of length 2^{m-1}. Consequently, we have chosen Gold sequences because of their good trade-off between cross-correlation and autocorrelation properties.

DSSS signaling demodulation is done by correlating the signal, after a root raised cosine (RRC) based matched filter, with the M spreading PN codes. Received bits are obtained by demaping the spreading code with maximum correlation value. Performance may be slightly increased if correlation is not only done at the maximum amplitude tap but at the nearest displacement of the received signal around the maximum amplitude tap [9]. This technique benefit from frequency diversity in a time dispersive channel. DSSS signaling does not need to estimate the channel response since PN sequences are not modulated. If we want to further increase the spectral efficiency we can modulate the PN sequence with n additional bits. Consequently,

channel estimation is mandatory to properly demodulate the received symbols.

DSSS signaling has been proposed to reduce the multiple access interference present in DS-CDMA systems. In [19] a performance evaluation of this system using Walsh M-ary orthogonal codes is shown. The advantages and downsides of this technique are:

- The spectral efficiency can be increased by hardly decreasing the SNR at the receiver. The higher the number of spreading codes (M) the higher the spectral efficiency.

- As long as PN sequences are not modulated, channel estimation is not required. Whereas accurate channel estimation is mandatory when using other physical layer techniques (e.g., DSSS and DS-CDMA), specially if a Rake receiver is used.

- Computational complexity is $\mathcal{O}(2^m)$.

In chapter 4 we review the basis of this technique and we briefly explain some of the results we have obtained from the experiments.

Another approach to increase the spectral efficiency has been to use a multicarrier technique. In wireless broadband multiple access systems (e.g., wireless local area networks, cellular mobile communication systems and bidirectional hybrid fiber coax (HFC)) the issue of achieving a throughput near the channel capacity has attracted a lot of research attention due to the increase of users and the scarcely available bandwidth. The theoretical solution for achieving the channel capacity for channels with Gaussian noise was presented in [14] and several practical implementations were shown more recently [41]. For multiple access channels, [5] found a generalization of the single user waterfilling theorem.

Owing to the fact that orthogonal frequency division multiplexing (OFDM) has an intrinsic robustness against frequency selective interference and multipath fading channel, many applications (e.g., DAB, DVB-T, Hiperlan/2, ADSL and 4G) uses a multicarrier technique to counteract the impairments of the channel. Frequency selectivity may be exploited by using a bitloading algorithm that determines, for each subcarrier, the power and the number of bits per symbol. If the channel is known at both the receiver and the transmitter, it can be shown that a multiple access multicarrier technique (i.e., OFDMA) with adaptive subcarrier allocation and adaptive modulation outperforms other multiuser techniques such as CDMA and TDMA.

Regarding the HF channel we are studying, no channel state information is available at the transmitter (except for the statistic information gathered by the oblique sounder in no real time) since it is a unidirectional link and therefore no adaptive algorithm can be used. Consequently, frequency diversity can be exploited by transmitting symbols with wider bandwidth than the coherence bandwidth of the channel and by using a forward error correction (FEC) code and an interleaver to avoid long bursts of

erroneous data. A combined MC and SS technique can also be used to benefit from frequency diversity. Since it is a broadcast application which is not sensible to the delays —introduced by an interleaving— we have decided to study a simple multicarrier system, such as OFDM, as a possible candidate for the physical layer of this data link.

A number of experiments concerning OFDM conducted throughout several antarctic campaigns (i.e., from 2006 to 2012) are explained in chapter 4, chapter 6 and appendix A, B, C and D. These experiments have been focused on finding which characteristics regarding OFDM symbols best solves or minimizes its inherent downsides, i.e., the peak to average power ratio (PAPR), time and frequency synchronization and the effects on performance of frequency selective channels. The tests have all been conducted on a channel that is indeed frequency and time selective, as it is the HF channel between Antarctica and Spain. Moreover, very low SNR is expected at the receiver station, which leads to design OFDM symbols with low number of subcarriers and low back-off.

PAPR The PAPR problem arises from the fact that OFDM symbols are a superposition of a number of modulated sub-channel signals and thus may exhibit a high signal peak with respect to the average signal level. Unless the transmitter's power amplifier shows an extremely high linearity across the whole input signal range, envelope fluctuations can produce out of band radiation signals and in band signal distortion which leads to BER degradation.

In the literature there are plenty of solutions to overcome this problem and it seems that three approaches have been taken: *i*) to improve the amplifier linearity, *ii*) to apply some post processing at the receiver and *iii*) to reduce the envelope fluctuations at the transmitter. Regarding this last issue, [40], for instance, suggested the use of codification schemes prior to modulation, [26] studied the effects of clipping the envelope signal on BER degradation and spectral outgrowth, [23] proposed that some of the outer signal constellations points should be extended beyond the constellation limits such that the OFDM symbols within a given block experienced an envelope fluctuation reduction and [24] studied the effect of reserve a few tones, known as correcting tones, within the transmitted bandwidth to reduce envelope fluctuations.

In this project, we have approached this issue (see chapter 4 and 6) by using a soft-limiter algorithm, which has clipped the signal envelope to a desired input back-off (IBO) (i.e., the range from the input mean power to the input saturation power). We have transmitted several blocks of symbols with different IBOs (i.e., 1, 3, 5, 7, 9, 10 and 11 dB) to check whether the PAPR issue is a real problem in our scenario. Due to the distortion introduced by this envelope clipping technique and the low SNR expected at the receiver, only simple constellations (i.e., BPSK and QPSK) have been used. Moreover, OFDM symbols have been over sampled with factors 125, 250 and 500.

Synchronization OFDM systems are very sensitive to frequency mismatch between transmitter and receiver local oscillator and it is also crucial to identify the start of the OFDM symbol. In case of not performing frequency and time synchronization tasks, the orthogonality between subcarriers can be partially lost and intersymbol interference (ISI) and intercarrier interference (ICI) arise.

In order to avoid ISI between consecutive symbols, a guard interval has been appended at the beginning of each OFDM symbol of all experiments. As the channel impulse response is almost always shorter than 3 ms (see chapter 5) the guard interval equals 3 ms. In order to see the effective part of the received symbol as a cyclic convolution between the transmitted symbol and the channel impulse response, the guard interval is a copy of the last samples of the OFDM symbol.

In this data link the coarse timming synchronization has been performed by means of a global positioning system (GPS) receiver and its pulse per second (PPS) signal, which has an accuracy of $1\,\mu s$. The fine timming synchronization has been performed by means of a preamble composed of a set of 20 maximal length PN sequences of 255 chips and a bandwidth within the range between 5 kHz and 10 kHz.

Before the 2009-2010 antarctic campaign the modem used a low performance oscillator with a frequency stability of 10 ppm. This clock variability caused a maximum frequency mismatch of 60 Hz between remote oscillators and a timing offset of $\pm$ 0.0127 samples after 5 OFDM symbols with a time symbol (T_s) of 50 ms. In this scenario we built a frame structure composed of one M-sequence and 5 OFDM symbols ($T_s \in [30, 50]ms$). This frame duration (i.e., $5 \times T_s$) was shorter than the coherence time of the channel, then if the largest correlation peak was chosen as the acquisition point, the system would demodulate the data signals provided by the strongest path. Therefore, a timing tracking algorithm was not needed if an offset lower than one sample was introduced in the direction of the cyclic prefix, from the estimated FFT window position (see appendix A).

Frequency mismatch (i.e., a maximum up to 60 Hz) was estimated by means of the discret Fourier transform (DFT) of a 5 seconds long non modulated carrier. This estimation method had an uncertainty error lower than 1% of the subcarrier space, which ranged between 33.3 Hz and 20 Hz for symbol lengths between 30 ms and 50 ms.

During the 2009-2010 antarctic campaign the modem hardware was upgraded and two OCXO were installed at the transmitter and receiver side. The high stability features ($0.1ppb/^{\circ}C$) of these oscillators have lead to much longer data blocks, performing data acquisition only at the beginning of each block (i.e., every 12 second, on average). The fast Fourier transform (FFT) time synchronization error induces a progressive phase rotation among adjacent subcarriers, which is detected by the channel estimation algorithm and is corrected by the subsequent equalization stage, as long as

coherent detection has been utilized. With these news OCXO, cumulative windowing offset has been almost neglected and no ICI effects have been shown due to frequency oscillators mismatch. Consequently, only the Doppler spreading of the channel (a maximum spread of 2 Hz) has been present on the received symbols.

Channel estimation In multicarrier systems, channel estimation is required to fetch the data contained in the received signal constellations since the receiver needs a phase and amplitude reference to properly detect the transmitted symbols. Consequently, channel detection and tracking are mandatory in a frequency and time dispersive channel. Differential detection can alternatively be used, in which case the detection is made without any reference but by comparing phases and amplitudes of symbols transmitted on consecutive OFDM symbols or an adjacent subcarriers. However, a 3dB disadvantage of SNR exists for the differential channel estimation method because two noise processes with equal variance are present, the noise of the channel estimation and the noise of the data symbol to be detected.

In this study, coherent modulation is used and channel is estimated by means of a pilot symbol aided technique. The downside of this method is the loss of spectral efficiency due to the fact that several subcarriers are occupied with known pilot symbols. The channel is estimated by means of the least square technique, due to its simple implementation, and cubic spline interpolation is used in two dimensions (i.e., time and frequency) to estimate the channel at data subcarriers position. Finally, assuming a flat fading channel in each subcarrier a simple one coefficient channel equalization is performed.

In pilot symbol assisted channel estimation techniques the selection of the pilot frequency-time pattern is very important. In that regard, an experiment with a rectangular and hexagonal pilot pattern with different pilot density in time and frequency direction has been done (see appendix A). A major concern on multipath and time variant channels is the trade-off between efficiency and the minimum number of pilot symbols to estimate the channel transfer function at the receiver—as the Nyquist criterion dictates. In appendix B we have studied the trade-off between performance and efficiency by means of real measurements of noise an interference.

Correspondingly, other experiments (see chapter 4 and chapter 6) have studied the best symbol time (from 10 ms to 90 ms) and hence the best subcarrier frequency space. The number of subcarriers, as the transmitted power is constant, depends on the available SNR at the receiver. In a multipath channel the occupied bandwidth need to be wider than the coherence bandwidth of the channel to benefit from frequency diversity. In a low SNR and multipath scenario, as the number of subcarriers need to be low, the subcarrier space need to be carefully studied as well.

Other issues Other experiments (see appendix D) have studied the fact of using a time interleaving plus a convolutional encoder prior to the OFDM modulator. Time interleaving has been applied in the time direction for each subcarrier. The size —also known as depth— of a block interleaver is generally lower bounded by the time coherence of the channel and upper bounded by the memory capacity of the modem. In our case, the memory capacity is quite reduced (these experiments were conducted before the upgrade of the 2009/2010 campaign) and almost equals the coherence time of the channel. In that sense, time interleaving depths from only 131 ms to 295 ms have been tested. As stated in [1] (see chapter 4), Doppler spread depends on frequency and time of day, ranging from 0.5 Hz to 2.5 Hz. Therefore, a sufficient time interleaving depth for a certain frequency at a certain hour may be insufficient for the same or other frequencies at a different hour of day. Appendix D shows that long time interleaving depths perform slightly better than short ones in high Doppler scenarios; however, they were clearly useless in low Doppler scenarios, as there was little time diversity to exploit.

In appendix A we have estimated the HF channel for a wide bandwidth. Due to the low SNR expected at the receiver, the HF channel has been estimated in subchannels of narrower bandwidth to increase the SNR per subcarrier. The aim has been to study a 5 kHz bandwidth by consecutively transmitting 5 OFDM symbols of 1 kHz bandwidth. The number of subcarriers of each OFDM symbol is 16, the useful symbol time is 48 ms and thus the intercarrier spacing is 20.83 Hz. In each OFDM symbol 2 virtual subcarriers (zero padded) have been inserted between each active subcarrier to increase the bandwidth of the symbol up to 1 kHz (i.e., 16 subcarriers $\times$ 3 $\times$ 20.83 Hz) and preserving the same power per subcarrier than non padding symbols. We have designed a block composed of one PN sequence for synchronization purposes, followed by 5 OFDM symbols of 1 kHz bandwidth. Consecutive OFDM symbols have shifted the subcarrier position in order to estimate a total bandwidth of 5 kHz. Two pilot patterns have been compared (i.e., rectangular and hexagonal) and several pilot densities have also been studied. Preliminary results have showed the feasibility of using OFDM as a communication technique in this HF link. As expected, hexagonal pilot patterns has outperformed rectangular patterns and the higher the pilot density the better the BER performance, at the expense of lower spectral efficiency.

In appendix B we have studied the robustness of multicarrier modulation against interference from the experience we got from the paper in appendix A. In the HF channel, the level of interference is an important limiting factor. In this work we have simulated the performance of OFDM in a real noise and interference scenario recorded at the receiver station. Interference in the HF channel is usually slow variant [25], consequently, interference could be avoided if a feedback channel existed. Since it is a simplex link, interference existence is unknown by the transmitter, and thus frequency diversity can be a good option to guarantee the best average performance of the link. In this work we have compared the performance of OFDM symbols in a multipath channel under three different noise conditions: AWGN, recorded noise plus interference in average conditions, and recorded noise plus interference in worst conditions. Narrow-

band interference that affect a single subcarrier can be combated with FEC codes and interleaving. However, if OFDM bandwidth equals the interference bandwidth then the receiver sees a global decrease of the available SNR. A simplex long haul HF link can use a mixed frequency-hoping multicarrier modulation approach to counteract this situation. In this work we have compared the performance of static symbols with OFDM symbols that have been shifted 1 kHz every 1, 7 and 31 symbols. Results have showed that frequency-hoping have improved the performance of the worst condition scenario and almost have become equivalent to the average condition scenario.

In appendix C we have taken another approach to neutralize the interference of the HF channel, we have called it OFDM signaling. The idea has been to divide the available bandwidth (approximately 8500 kHz) in M slots of 266 Hz each, in which N Golay sequences could be transmitted. Therefore, each OFDM symbol has coded $log_2(M)$ bits, which has selected the occupied frequency slot, and $log_2(N)$ bits, which have selected the Golay sequence to be transmitted within a family of length N. Symbol subcarriers have not been mapped with modulated symbols but with 8 and 16 chip Golay sequences that have assured a PAPR lower or equal than 3 dB [7]. The demodulator has included a maximum likelihood detector to decide which of the M slots has been occupied with an OFDM symbol. The decision process has been aided with a minimum phase detector which has decided which of the N possible sequences had been transmitted. The outcomes from data gathered at the receiver station have showed that longer Golay sequences have outperformed shorter ones, due to the higher frequency diversity.

Chapter 3

Outcomes

Oblique sounding Regarding the narrowband sounding of the channel, windowing techniques have been used to increase the estimation process performance as well as reducing the out of band and in band generation of spurious signals at the receiver. More robustness against short narrowband interference signals has been achieved by dividing the available signal period in small frames. The availability results have shown the following two periods:

- Diurnal activity: from 18 UTC to dawn of the following next day the highest availability has been shown at frequencies from 3 MHz to 18 MHz.

- Nocturnal activity: from dawn to 18 UTC the highest availability has been shown at frequencies from 10 MHz to 23 MHz.

The availability results agree with those that appeared in [44] at night; however, a diurnal availability period has been recorded at frequencies from 10 MHz to 23 MHz. This diurnal period has not been studied before because the previous oblique sounder was not able work on this frequency range.

Regarding the wideband sounding of the channel, we have found a clear difference between day and night. During the night and just after dawn, we have gathered the highest delay and Doppler spreads (i.e., 3.1 ms and 2.4 Hz); whereas throughout the day the lowest values have been recorded (i.e., 0.2 ms and 0.1 Hz).

Propagation time from Antarctica to Spain ranges from 45 ms to 51 ms, which is slightly higher than what was expected. Doppler shift varies from -4 Hz to 1.2 Hz during daytime and from -0.5 Hz to 1.2 Hz during nighttime. The sudden change of Doppler shift at dawn may be attributable to the appearance of D layer and the fact that F layer splits into F_1 and F_2 layers.

Data transmission DSSS results have been computed by means of DEVM and BER figures. Since the number of available symbols is not high (148 blocks of 25 symbols for each DSSS experiment and 33 blocks of 120 symbols for each OFDM experiment)

the results have not been plotted against SNR. Instead, we have used the cumulative distribution function (CDF) to compare the performance of different experiments.

The best results regarding DSSS transmissions have been achieved with Gold PN sequences of 31 and 63 chips whose bandwidth ranged from 250 Hz to 1 kHz:

- In 50% of the received symbols, the 31 chip sequences with a bandwidth of 250 Hz have achieved a BER lower than 9×10^{-2}.

- In 50% of the received symbols, the 63 chip sequences with a bandwidth of 500 Hz and 1 kHz have achieved a BER lower than 1.3×10^{-1}.

Wide bandwidth (i.e., 2 kHz, 5 kHz, 10 kHz and 20 kHz) have always showed worse performance than narrow bandwidth (i.e., 250 Hz, 500 Hz and 1 kHz) for PN sequence length of 31 and 63 chips. However, for sequences of length 127 chips the best performance has been shown by PN sequences with a bandwidth of 2 kHz. Note that in all these best cases the symbol length ranges from 62 ms to 126 ms. The shortest symbol length suffer from low SNR, whereas the longest symbol length reach the coherence time of the channel. The bit rate that achieves the middle length symbol ranges from 7.94 bps to 16.3 bps.

OFDM results have always shown better performance when using BPSK rather than when using QPSK due to the 3 dB penalty of SNR. The best results with 8 subcarriers have been shown by 50 ms symbols ($EVM \leq 1$ in 64% of cases), with 16 subcarriers have been shown by 70 ms symbols ($EVM \leq 1$ in 56% of cases) and with 32 subcarriers have been shown by 90 ms symbols ($EVM \leq 1$ in 46% of cases). The bit rate achieved by these 3 best cases ranged from 125 bps to 286 bps.

On low number of subcarrier symbols (i.e., 8 subcarriers) short symbols have not performed well due to the high subcarrier spacing. Long symbols have not performed well either, due to the narrow bandwidth occupied (narrower than the coherence bandwidth of the channel). On medium and high number of subcarrier symbols (i.e., 16 and 32 subcarriers) longer symbols (i.e., 70 ms and 90 ms) have performed better due to the higher occupied bandwidth and hence the higher frequency diversity.

Regarding the issue of PAPR, the best results have been achieved when applying a softlimiter to OFDM symbols with an intermediate value of IBO (i.e., 7 dB). From the results it can be derived that higher IBOs reduce the power efficiency and the average transmitted power, whereas lower IBOs increase the in band distortion.

Part II

Contributions

Chapter 4

Remote Sensing and Skywave Digital Communication from Antarctica

Pau Bergadà[1], Marc Deumal[1], Carles Vilella[1], Joan R. Regué[1], David Altadill[2] and Santi Marsal[2]
[1] LA SALLE, Universitat Ramon Llull, Passeig Bonanova 8, 08022 Barcelona, Spain
[2] Grup de Geofísica, Observatorio del Ebro, Universitat Ramon Llul-CSIC, Horta Alta 38, 43529 Roquetes, Spain

OPEN ACCESS
sensors
ISSN 1424-8220
www.mdpi.com/journal/sensors

Sensors 2009, 9, pp. 10136-10157; doi:10.3390/s91210136
Received: 16 October 2009;in revised form: 30 November 2009/ Accepted: 7 December 2009/ Published: 14 December 2009

This paper presents an overview of the research activities undertaken by La Salle and the Ebro Observatory in the field of remote sensing. On 2003 we started a research project with two main objectives: implement a long-haul oblique ionospheric sounder and transmit the data from remote sensors located at the Spanish Antarctic station Juan Carlos I to Spain. The paper focuses on a study of feasibility of two possible physical layer candidates for the skywave link between both points. A DS-SS based solution and an OFDM based solution are considered to achieve a reliable low-power low-rate communication system between Antarctica and Spain.

Keywords: Antarctica; remote sensing; ionosphere; geomagnetism; oblique sounding; skywave communications; DS-SS; OFDM

4.1 Introduction

Antarctica is a remote and an isolated continent of large interest for the scientific community. Many research stations and remote sensors are scattered across the continent to conduct experiments related to different disciplines such as geology and physics that cannot be reproduced anywhere else on The Earth. The Research Group in Electromagnetism and Communications from LA SALLE, together with the Ebro Observatory (EO), both belonging to the Ramon Llull University, are partners of a research project for remote sensing and skywave digital communication from Antarctica. The project was born in 2003 with a double objective: transmit the data from remote sensors located at the Spanish Antarctic Station Juan Carlos I (referred to as SAS in the remainder) directly to the EO in Spain, and implement a long-haul oblique ionospheric sounder. Even though the SAS is only manned during the Austral summer, collection of scientific data is never stopped. While the station is left unmanned, the continuous set of data is stored in memory devices that will not be downloaded until the next Antarctic campaign. The information that has to be analyzed in almost real-time is transmitted to the EO in Spain through a satellite link. The skywave digital communication system is intended to transmit the information from the Antarctic sensors as a backup or even an alternative to the satellite. The oblique ionospheric sounder is a low power high frequency (HF) transceiver that monitors the ionospheric channel between the Antarctica and Spain. The sounder is fully configurable and can analyze different parameters from the ionospheric link at any frequency in the HF band. The oblique sounder is not the only sensor available at the SAS. In 1996 the EO deployed a geomagnetic observatory. The observatory is composed of two independent variometers, an Overhauser magnetometer deployed in dual axis Helmholtz coils in a $\delta D/\delta I$ configuration, and a suspended tri-axial fluxgate magnetometer, along with sampling hardware and data logging software. Later, in 2004, a vertical-incidence low-power pulse-compressed ionosonde with a double delta loop antenna was also installed. The large amount of information gathered from the oblique sounding surveys is analyzed for both physics and communication purposes. One of our topics of research is to use the oblique sounding information to complement the ionospheric models obtained from the vertical sounding. From the communications point of view, the oblique sounding is used to obtain models of long-haul ionospheric channels. Parameters such as link availability, power delay profile and Doppler spread are analyzed and considered in the design of the physical layer of the skywave communication system. Currently, we have proposed two different physical layer solutions which are based on direct-sequence spread spectrum (DS-SS) signaling and orthogonal frequency division multiplexing (OFDM). Preliminary transmissions suggest that both solutions can achieve reliable low-power low-rate communications between Antarctica and Spain.

4.2 SAS Research Activity

The SAS is placed in Livingston Island (62.7 °S, 299.6 °E; geomagnetic latitude 52.6 °S) in the South Shetlands archipelago. It was inaugurated in 1988 and it is managed by the Spanish National Research Council (CSIC), which belongs to the Spanish Ministry of Science and Innovation (MICINN). Spain endorsed the Antarctic Treaty System in 1982, by which only scientific and technological issues can be developed in the Antarctica. It is MICINN who is in charge of the scientific research developed at the SAS and awards research groups grants to undertake research activities there.

The Spanish research activities in Antarctica are focused on the study of the biological and geological environment as well as the physical geography in Livingston and Deception islands and some places in the Antarctic Peninsula. Some examples of this research activities include: (i) tracking the changes in the temperature of permafrost to model the weather behaviour; (ii) study the geomorphology and movement of Johnsons-Hurd glaciers, which show a large sensitivity to temperature changes as they are very close to the melting point; (iii) study the variation of the magnetic field at Livingston Island to complete the map of the Earth's magnetic field and (iv) study the layers of the ionosphere and their relationship with the Sun activity. Many of these research projects collect data of temperature, position, magnetic field, height, etc. that are stored in data loggers. Also some of the data are transmitted to research laboratories in Spain.

In this project, we work on the design of a system for oblique ionospheric sounding and to transmit the data from remote sensors located at the SAS to Spain. The situation faced in this research project is similar to other situations where communication is scarcely possible due to economic or coverage problems. Therefore, the solutions and conclusions presented in this work may be adopted in other situations such as communications in developing countries or communications in the middle of the ocean.

4.3 Remote Sensors at the SAS

In this section we describe the main sensors located at the SAS, including a geomagnetic sensor, a vertical incidence ionosonde and a oblique incidence ionosonde. The geomagnetic sensor and the vertical incidence ionosonde are commercial solutions from third parties independent of this project. The oblique incidence ionosonde, which is used to sound the ionosperic channel between Antarctica and Spain, was developed by LA SALLE within the framework of this project.

4.3.1 Geomagnetic Sensor

Ground-based geomagnetic observatories are intended to provide a time series of accurate measurements of the natural magnetic field vector in a particular location on the Earth's surface. The data from the worldwide network of observatories are used for several scientific and practical purposes, some examples being (i) the synthesis and updates of the global magnetic field models [1]; (ii) the study of the solar-terrestrial

relationships and the Earth's space environment, framed in the modern discipline of Space Weather [2]; and (iii) the support for other types of geophysical studies in a more regional or even local framework, such as mineral exploration, plate tectonics studies [3], or risk mitigation [4].

The geomagnetic observatory at the SAS in Livingston Island participates in the global network of geomagnetic observatories [5]. It was deployed in December 1996 and it was given the three letter code LIV by the International Association of Geomagnetism and Aeronomy (IAGA). Data collection and management is driven by the EO institute. Although the Spanish station is manned only during summer season, roughly from November to February, the instruments are left recording during the whole year, which implies the equipment is unattended during more than 8 months per year.

From 1996 to 2008 the SAS observatory consisted of three huts: one houses the absolute instrument, the so-called D/I fluxgate theodolite, which permits a manual measurement of the Declination and Inclination angles of the vector magnetic field in *absolute* terms (for a discussion of the uncertainties made with this instrument see [6]). This instrument consists of a fluxgate magnetometer bar mounted on the telescope of a non-magnetic theodolite. A second hut houses a variometer of the type $\delta D/\delta I$ vector magnetometer [7], which automatically measures the variations of the magnetic field vector once per minute. This instrument consists of two perpendicular pairs of Helmholtz coils, the polarization of which allows measuring the Declination and Inclination variations by means of a Proton magnetometer located at their center (see [8] for an assessment of this instrument). The Proton magnetometer, in turn, measures the total field intensity, F, when the coils are not polarized. Finally, the electronic system controlling this automatic instrument is placed in a third hut. From 2008 onward, a new variometer has been added up to the old instrumentation. The new magnetometer is a three-axis fluxgate, and allows automatically measuring the magnetic field variations from an analogue output, which is currently sampled at both, 1 and 0.1 Hz by the corresponding analog to digital converter (ADC).

Once the raw observatory data are processed, the definitive data set is sent to the World Data Centres, where the worldwide scientific community can access them. This process may well take several months; however, for several scientific and practical purposes it is convenient to have real-time access to the data, especially for those unattended and/or remote observatories such as LIV. The INTErnational Real-time MAGnetic observatory NETwork (INTERMAGNET) provides means to access the data in near real-time through a satellite link. The data are thus packed and sent to the geostationary satellites, and afterwards collected by the so-called Geomagnetic Information Nodes (GINs), where the information is freely accessible. However, almost ten years of experience with satellite transmissions have shown us that the satellite link is not 100 % reliable, and therefore it is suitable to have an alternative mean to retrieve the geomagnetic data. The skywave digital communication system between Antarctica and Spain designed within the research project between LA SALLE and the EO is intended to provide this backup/alternative to the satellite link. There are two major motivations to design a backup system by skywave. One one hand, visibility problems appear when trying to reach geostationary satellites from polar latitudes, which can be

overcome with a skywave link due to its higher angle of departure. On the other hand, in a not 100 % reliable scenario, end-to-end reliability can be significantly increased by transmitting each frame repeatedly throughout the day, that is by using time diversity. In opposite to satellite, using time diversity in skywave does not represent an extra cost as no extra time-slots must be reserved. Moreover, in skywave the time diversity can be exploited at the physical layer by employing similar techniques to those considered in space time coding (STC). This results in larger performance improvement than if diversity is employed at the information bit level.

4.3.2 Ionosonde: Vertical incidence soundings of the ionosphere

In order to have a sensor providing ionospheric monitoring in this remote region, a vertical incidence ionospheric sounder (VIS) was installed at the SAS during 2004-2005 Antarctic survey. This ionosonde is nowadays also being used to provide information for the HF radio link employed for data transmission from the SAS to Spain. A brief description of the HF radio link and of the results obtained from it will follow after the current discussion. The VIS operating at the SAS is the Advanced Ionospheric Sounder (AIS) developed by the *Istituto Nazionale di Geofisica e Vulcanologia* (INGV) of Rome, Italy. Details of the sounder are available in [9]. Data provided by the VIS serve for conducting ionospheric research at that remote region, mainly to characterize the climatology of the ionospheric characteristics and to investigate the ionospheric effects caused under geomagnetically disturbed periods (e.g., [10, 11]). The typical pattern of the summer behavior of the ionospheric F2 characteristics and of their variability was evaluated for different Spanish Antarctic surveys, and the differences of the above patterns from survey to survey was related to the different solar activity. Such a pattern at mid-high latitudes of the SAS was also compared with the summer behavior at other mid-latitude stations and it was noticed a larger post-sunset electron density enhancement at the SAS than that recorded in other regions. The significant decrease of the critical frequency of the F2 region, foF2, and their strong uplift as observed by the significant increase in the virtual height, h'F2, for the geomagnetically disturbed period of 18 February 2005 was also investigated and explained in terms of response of the ionosphere to the geomagnetic storms [12, 14]. In addition, the data recorded with the VIS, especially the maximum usable frequency for a single hop transmission at 3000 km reflected at the F2 layer MUF(3000), has been correlated with data extracted from the HF radio link established between the SAS and Spain [11]. The above correlations were obtained for a chain of available VIS located nearby the radio path, resulting that the frequency with the largest availability of the ionospheric channel seem to be limited by the lowest of the MUF(3000) recorded along the path and that the ionospheric conditions close to the receiver have the larger influence on the daily behaviour of the channel availability for most of the time under the investigated seasonal conditions. In [11] it is also stated that frequencies of HF radio link delivered at the receiver suffer a significant drop of power for those frequencies larger than the MUF(3000) as recorded at the receiver compared to those frequencies lower than the

MUF(3000).

The above results obtained with the ionospheric sensors installed at the remote region of the SAS fit with current ionospheric research carried out by other teams for regions nearby the Antarctic latitudes and other latitudes of the globe. As a brief summary and just focusing in the more recent works, we would like to highlight the following examples which are organized according to climatological studies, meteorological events and radio HF investigations. [13, 15] discussed about the spatial correlation of the ionospheric measurements and of their implications on global ionospheric models. [16] stressed the need for long-term climatological observations of solar-terrestrial phenomena to benefit the science and applications. [17] highlighted the role of the geomagnetic activity in the secular change of the ionosphere and confirms the latitudinal dependence of the trends. [18] tracked a complete night-time Weddell Sea Anomaly (WSA) - the WSA in the ionosphere is characterized by higher plasma densities at night than during the day in the region near the Weddell Sea - and strong horizontal plasma flows that registered the high-conductivity regions of the South Atlantic Magnetic Anomaly (SAMA), and revealed that the strong east-west hemispherical difference was due to the SAMA. [19] showed that the WSA occurs only in the southern summer hemisphere for low solar activity but the WSA occurs in all seasons except for winter when solar activity is high, being most prominent during the December solstice and still strong during both equinoxes, and they conclude that WSA appears to be an extreme manifestation of the longitudinal variations. [20] also reported these anomalous diurnal variations of the ionospheric peak density NmF2 related to the WSA but not found in the diurnal variations of the ionospheric peak height hmF2. [21] showed experimental evidence that the traveling atmospheric disturbances (TADs) play significant role in the ionospheric daytime effects of geomagnetic storms and demonstrate a systematic uplifting of the ionosphere during storms. [22] found changes in the critical frequency (foF2), density (NmF2), and height (hmF2) occurring after the onset of magnetospheric convection associated with high-speed solar wind streams (HSSs) arrival at the Earth's magnetosphere. [23] suggested that impulsive Joule heating of the polar thermosphere, which was accompanied by the generation of the large-scale gravity wave packet that propagated to mid latitudes, was the most probable such source for large-scale ionospheric inhomogeneities, vertical winds monotonously increasing with increasing altitude, and upward plasma transfer. [24] presented an HF selection tool (EDAM533) that has been implemented thanks to the MUF(3000) predictions generated by real-time assimilative electron density model. Also [15] have developed an HF propagation program that takes advantage of the availability of a real-time global model of the ionosphere to specify in real time the range of frequencies that would be supported on a given HF communications circuit which favorably validates against several months of oblique propagation observations on mid latitude circuits, although its day-to-day variability does not match the observations very well, and it tends to underestimate the MUFs.

The future ionospheric research at the SAS would benefit with installation of new sensors, as a high sampling rate receiver of Global Navigation Satellite System (GNSS) signals. This type of sensor would provide information about the wave front distortion

of a GNSS signal caused by electron density irregularities, which giving rise to highly transient and a random amplitude and phase modulation of the GNSS signal. Such systems have been adopted by several groups for both scientific purposes and space weather applications (e.g., [17, 25]).

4.3.3 Oblique ionosonde

The aim of the oblique ionosonde [26] is to obtain the useful parameters to model the HF radiolink between the SAS and the EO. These parameters include link availability, the power delay profile of the channel and the frequency dispersion. The system performs soundings during the austral summer, coinciding with the period when the SAS is open. The sounder includes a transmitter, placed in the premises of the SAS and a receiver placed at the EO. A photography of the transmitter antenna is shown in Figure 4.1. Both transmitter and receiver are specifically designed to fulfill the requirements of this particular oblique sounder and the data transmitter explained in section 4.4 The block diagram of the oblique sounder is shown in Figure 4.2.

Figure 4.1: Antenna of the oblique ionosonde transmitter placed at the SAS.

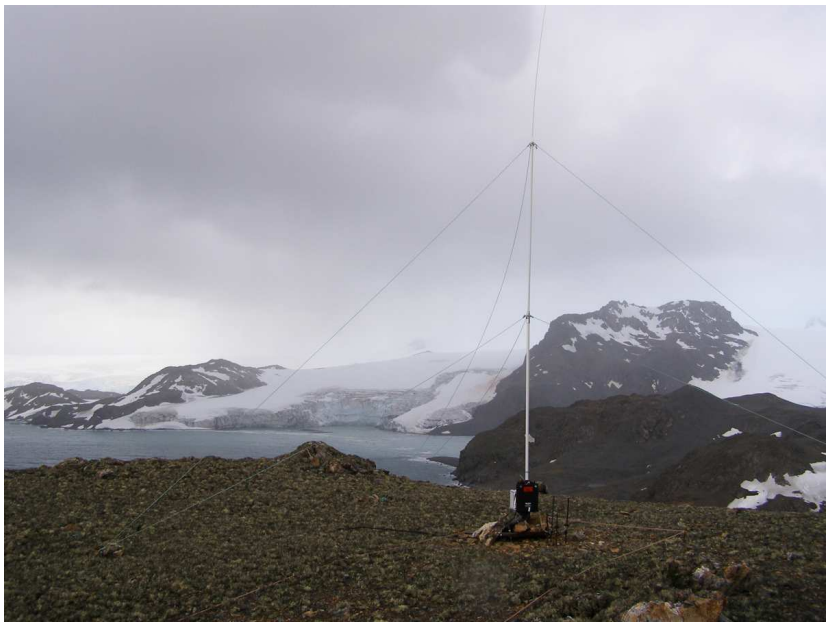

The most relevant interest of this oblique sounder is that the link is difficult to establish. Firstly, for the distance of the link (12700 km), which requires at least four hops to reach the receiver. And secondly, for the fact that the path crosses the equator and four different time zones.

The sounder analyzes the ionospheric radiolink each hour within a frequency band that ranges from 4.5 MHz to 16.5 MHz, with a frequency step of 500 kHz. Each sounding is divided into three intervals. The first one, with a length of 5 seconds, is used to tune the antenna. In the second one, a single tone (CW) at the frequency of interest is

transmitted during 5 seconds in order to perform a narrow band sounding. And finally, during the third interval a pseudo-random noise sequence is transmitted to perform a wideband sounding. The narrowband sounding is mainly used to determine the link availability. The wideband sounding can be used to extract the parameters related with time dispersion (power delay profile) and with frequency dispersion (Doppler spread and Doppler shift). The results of this oblique soundings performed during the 2006/07 austral summer are presented in [26]. The main conclusions about link availability can be summarized as follows. (i) Between 21 UTC and 04 UTC availability is greater than 95 % at frequencies in the range 8-10 MHz,(ii) between 07 UTC and 08 UTC availability is greater than 95 % at frequencies in the range of 11-12 MHz and (iii) between 08 UTC and 09 UTC availability is greater than 95 % at frequencies in the range of 14-15 MHz. Whereas, between 10 UTC and 19 UTC availability scarcely reaches values of 20 % at any frequency. In addition, the data extracted from these oblique soundings has been correlated with the data recorded with the VIS, especially the maximum usable frequency for a single hop transmission at 3000 km reflected at the F2 layer (MUF(3000)) [11]. The above correlations were obtained from a chain of available VIS located nearby the radio path, resulting that the frequency with the best availability of the ionospheric channel seem to be limited by the lowest of the MUF(3000) recorded along the path. Moreover, the ionospheric conditions close to the receiver have a high influence on the daily behaviour of the channel availability for most of the time under the investigated seasonal conditions. In [11] it is also stated that the received signals suffer a significant drop of power for those frequencies larger than the MUF(3000) when compared with those frequencies lower than the MUF(3000).

4.4 Data Transmission

The sensors placed at the SAS premises are only manned during austral summer but they are active during summer and winter. Hence, in order to process the data in close to real time, they have to be send to the research laboratories in Spain. Since 1998, the data from the geomagnetic sensor have been transmitted by means of a geostationary satellite link from the SAS to the INTERMAGNET GIN in Edinburgh. During 2007-2008 Antarctic campaign, the new geomagnetic sensor transmitted the data to a GIN placed in Ottawa, with high reliability. The aim of this research project is to establish a low-rate low-power skywave link between Antarctica and Spain that serves as a backup or even an alternative to the satellite link.

The skywave radio link between the Antarctica and Spain has a set of characteristics and impairments that have to be taken into account to properly design the analog front-end and the digital signal processing (DSP) modules:

- The Antarctic Treaty System regulates international relations with respect to the Antarctica. Among others, it regulates the environmental laws, including aesthetic factors, and restricts the deployment of big structures because of the environmental impact. Hence, high gain antennas that would need reinforce concrete underpinning are discouraged.

- Frequency availability of this HF link is highly time dependent [26]. Therefore, the transceiver must be able to reconfigure the oscillators frequency and the antennas must cover a wide HF frequency range.

- Low transmission power is required not only to fulfill the International Telecommunication Union (ITU) recommendations but also because during austral winter, the power consumption at the SAS is restricted as it is only served by batteries charged by wind and solar power.

- The ground path between the SAS and EO is approximately 12700 km, which corresponds to a minimum of 4 hops. A one-hop link is considered to be less than 4000 km [27].

- The attenuation of a transmitted signal at 10 MHz is of 135 dB only due to free space path loss.

- The noise and interference levels at the receiver are very high. e.g. the signal to interference level at the antenna output at frequencies between 4.5 MHz and 9 MHz can be as low as -75 dB [28].

- The ionospheric channel is a multipath channel since reflections occur at different layers of the ionosphere. Also, since the ionization level of each layer varies in time, the channel is time variant.

- A simplex ionospheric link is considered. Thus no channel state information exists at the transmitter site and no automatic repeat-request (ARQ) error control method can be implemented.

The HF band serves a wide range of applications and purposes: broadcasting, surveillance, monitoring, etc., and might have a wide range of coverage. Potentially, global coverage may be reached by taking advantage of the two modes of propagation: surface wave and sky-wave propagation. So, a global organism must take care and coordinate the access to the ionospheric medium.

ITU is the leading United Nations Agency for information and communication technology issues. Since mid nineteenth century, the ITU Radiocommunication Sector (ITU-R) has coordinated the shared global use of the radio-frequency spectrum. The primary objective of the ITU-R is to ensure interference free operations of radiocommunication systems. Consequently, the world has been divided into three different regions. Region 1 comprises Europe and Africa, region 2 comprises Asia and Oceania and America forms region 3. In each region, the ITU-R suggests the attribution of a

frequency band to one or several services, such as fixed, maritime mobile, aeronautic mobile, broadcasting, etc. When more than one service merge into the same frequency band then they are categorized into primary and secondary services. The secondary services: (i) are not allowed to interfere primary services, (ii) are not allowed to complain against primary services interferences and (iii) are not allowed to complain against previously attributed secondary services interferences. Moreover, each country has an organization to clarify ITU-R suggestions and to authorize to permanently, temporary or experimentally operate at a certain frequency.

The radio link we are dealing with, ranges through two ITU-R regions and crosses several countries. Hence a frequency spectrum request should be applied in each country, and of course it should be the same in all of them. Moreover, since the channel frequency availability is time dependent, not just one but several frequency bands along the whole HF frequency band should be requested for operation. As applying for such an international reservation of multiple frequency bands is not a feasible solution, our goal was instead to implement a communication system that should not interfere any other primary or secondary service with permanent, temporary or experimental operation authorization. To achieve it, the communication system should: (i) employ a low transmitting power, (ii) have a low power spectral density and (iii) operate with sporadic and short time transmitting periods. Also it should have a good robustness against noise, interference and time-variant multipath fading.

Several HF standards proposed by the NATO, the USA Department of Defense and the Institute for Telecomunications Science that depends on the USA Department of Commerce have been revised and we conclude that none of them satisfies the requirements of this HF link. As a result, a new physical layer solution must be proposed to match the strict requirements of the communication system considered in this project. In the following sections two preliminary physical layer proposals will be addressed.

4.4.1 System description

In this section, the transceiver used in the Antarctica to Spain HF link is described. HF receivers are typically implemented by means of several super-heterodyne conversions. Multiple intermediate frequency stages are used because of the complexity to achieve high selectivity and gain to any single frequency. However, high quality synthesizers are required and local oscillators should have to be phased locked to a reference frequency. Moreover, high quality automatic gain control systems are required in each stage to preserve the receiver performance. The aim of the transceiver architecture used in this research project is to place the ADC as close to the receiver antenna as possible, digitize the whole HF band and then, in the digital domain, select and downsample the channel of interest to baseband. This is only possible due to the development of high performance ADCs and digital signal processing (DSP) technology.

The HF transceiver developed and used in this HF link is based on a digital platform with a Field Programmable Gate Array (FPGA) from Xilinx plus a high speed digital to analog converter (DAC) and an ADC [26]. The signal is fully processed in the digital domain and therefore only amplification and some filtering are performed in

the analog domain. This architecture benefits from the advantages of Software Defined Radio technology [29] and thus it allows us to implement any communication system by just introducing changes to the software. The transmitter platform, see Figure 4.2.a, upsamples the sampling frequency by means of a digital upconverter (DUC), filters and upconverts the baseband signal to the proper frequency that maximizes link availability. The upsampled analog signal feeds a low pass filter (LPF), then it is amplified up to 250 watts and finally delivered to a 7.5 meter monopole. In the receiver site, see Figure 4.2.b, the incoming signal is received with a 7.5 meter monopole, amplified with a low noise amplifier (LNA), filtered by a tunable bank of band pass filters (BPF), amplified with a variable gain amplifier (VGA) that adjusts the received power level 6 dB below the full scale range of the ADC and finally it is low pass filtered to reduce aliasing components. In the digital domain, the same FPGA digital platform used in the transmitter site mixes the received signal to baseband, filters it and decimates the sampling frequency by means of a digital down converter (DDC). Eventually, data demodulation are obtained in non real time mode after DSP.

Figure 4.2: Transmitter (a) and receiver (b) system architecture based on Software Defined Radio Technology.

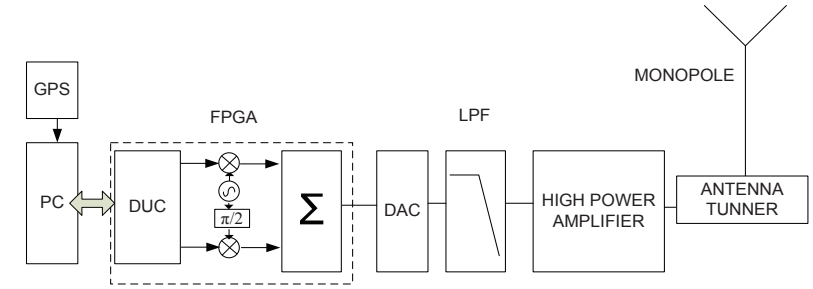

(a)

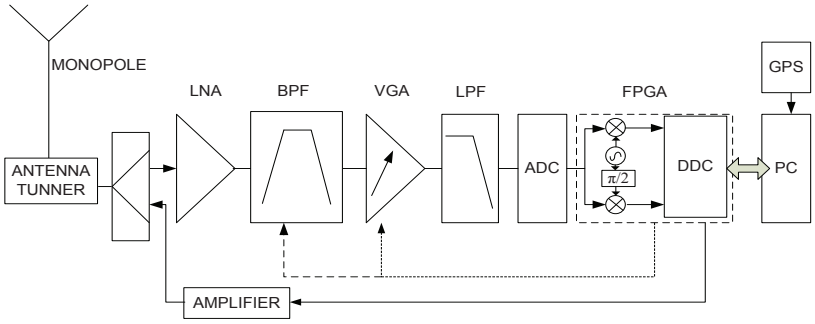

(b)

Prior to transmit the data from the sensors, a preamble, depicted in Figure 4.3, must be transmitted for tuning and synchronization. Since the wide range of frequencies that

Figure 4.3: Transmitted frame.

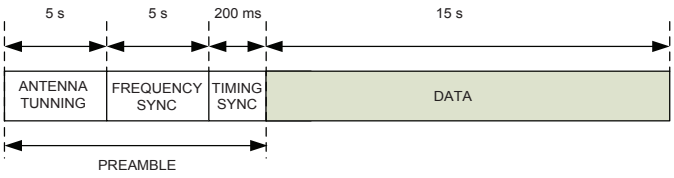

maximize availability of the ionospheric link between the SAS and EO, transmit and receive antennas must have a wide frequency range of acceptable performance. Furthermore, they must be tuned to match its impedance with the transmitting and receiving elements at each different frequency. Approximately, 5 seconds are needed for antenna tuning. Clock frequency mismatch between transmitter and receiver oscillators due to time and temperature drifts must be fixed, otherwise they may have severe effects on data demodulation. During 5 seconds, a non modulated tone is transmitted and used at the receiver site to estimate the frequency deviation between transmitter and receiver clocks. This non modulated tone is also used to determine frequency availability and signal to noise ratio (SNR) statistics. The Global Positioning System (GPS) provides coarse timing synchronization between transmitter and receiver. Fine timing synchronization is acquired by means of a number of Maximal Length pseudo noise sequences of 255 chips each, transmitted at chip rate of $\frac{1}{T_c} = 5.4$ kcps, approximately during 200 ms. The good autocorrelation properties of these sequences assure an accurate timing synchronization.

In the following sections, two proposals to implement the physical layer of this HF radio link will be addressed. One solution is based on DS-SS signaling, the other is based on OFDM.

4.4.2 DS-SS proposal

This section is divided in three parts: (i) an introduction where DS-SS theoretic features are revised, (ii) a second one called DS-SS signaling technique where the method of modulation and demodulation used in this part of the paper is explained and compared with other techniques and finally (iii) a third one called System description and results, where the emitter and the receiver used in this experiment are described as well as the results obtained with this technique.

Introduction. On the basis of the sounding results described in [26], the most relevant characteristics of the long-haul ionospheric link between the SAS and Spain are: (i) negative SNR at the receiver site for a signal bandwidth of 3 kHz and the system architecture described in Section 4.4.1, (ii) dispersion both in time and frequency, (iii) interference. We note that spread spectrum (SS) techniques and more specifically DS-SS are a good alternative to deal with this impairments [30]. SS techniques were first

developed in the military field in the middle XXth century. Nowadays it is a principal technology in wireless and mobile communications [31–33]. The application of SS techniques in ionospheric communications has also been proposed in many papers (see, for example, [35]).

DS-SS [34] is a transmission system where the signal uses a bandwidth much larger than the minimum required to send the information. Spreading is achieved by means of a code. At the receiver, a synchronized replica of that code is used to recover the data. Bit rate can be increased by using several spreading codes to transmit different baseband symbols at the same time and frequency. This technique is known as direct sequence code division multiple access (DS-CDMA). In order to maintain the SNR per symbol constant, conventional DS-CDMA systems set the transmit power to be proportional to the number of codes that are multiplexed (assuming that no multiple access interference occurs). However, as previously described the transmission power in our system is fixed. Hence, the more symbols are code multiplexed the less their SNR will be. In general, in a fix-power point-to-point DS-SS based system, the SNR per symbol after despreading can be expressed as

$$\mathrm{SNR_d} = \mathrm{SNR_{rx}} + 10\log(\frac{G_p}{N_s})\ [\mathrm{dB}], \tag{4.1}$$

where G_p is the process gain of the spreading code, N_s is the number of spreading codes that are transmitted within a symbol interval and $\mathrm{SNR_{rx}}$ is the SNR at the input of the receiver. Note that $N_s = 1$ in DS-SS and $N_s > 1$ in DS-CDMA, and that (4.1) is defined assuming that no multiple access interference occurs, that is, the cross-correlation between all spreading codes is zero. The spectral efficiency can be expressed as

$$\eta = k \cdot \frac{N_s}{G_p}\ [\mathrm{bits/sec/Hz}], \tag{4.2}$$

where k is the number of bits per symbol and the transmission bandwidth is assumed to be equal to the chip rate, i.e., spectral outgrowth due to upsampling is not taken into account. It is interesting to notice that when the transmitted power is fixed both DS-SS and DS-CDMA have the same performance, that is, if a certain $\mathrm{SNR_d}$ is desired both systems achieve the same spectral efficiency.

From Equations (4.1) and (4.2) it can be observed that an increase in the spectral efficiency can only be achieved at expenses of reducing the SNR per symbol after despreading. This is in fact a major drawback for employing DS-SS/DS-CDMA in low-power skywave communication systems. Note that in such systems the SNR at the input of the receiver is very low (typically negative), therefore to achieve low bit error rate (BER), the spectral efficiency must be low.

DS-SS signaling technique. In the Antarctica to Spain HF link, when a transmission bandwidth of 3 kHz is used, the typical SNR at the receiver is $\mathrm{SNR_{rx}} = -5$ dB [26]. Preliminary transmissions in [36] suggested that BPSK and $G_p \geq 127$ should be used. Then, assuming a 3 kHz bandwidth the maximum achievable uncoded bit rate is 23.6 bits-per-second (bps). To overcome this problem we propose a physical layer based

on DS-SS signaling. DS-SS signaling consists in mapping m data bits into one of the $M = (2^m)$ spreading codes. At the receiver, the transmitted bits are obtained by correlating the received time-frequency synchronized signal with the M spreading codes. Maximum correlation value determines the most probable transmitted spreading code, *i.e.*, the most probable transmitted group of m bits. This technique was proposed to reduce the multiple access interference in DS-CDMA systems, in [37] a performance evaluation of this system employing Walsh M-ary orthogonal signaling is done. The advantages of this technique are that the spectral efficiency can be increased by hardly decreasing the SNR and that accurate channel estimation is not required. Other physical layer candidates such as conventional DS-SS and DS-CDMA require accurate channel estimation in order to avoid large performance degradation, specially if a RAKE receiver is used. The downside is that the computational complexity of the receiver is high, of order $\mathcal{O}(2^m)$. It is important to notice that DS-SS and DS-CDMA achieve higher spectral efficiency by scarcely increasing the complexity at the expenses of suffering from a large degradation of the BER performance. On the other hand, DS-SS signaling achieves higher spectral efficiency by scarcely increasing the BER at the expenses of a large increase of the system complexity.

To further increase the spectral efficiency of DS-SS signaling one can modulate the spreading code by using n more data bits. In that sense the number of bits per spreading code is increased from m (DS-SS signaling) to $m + n$ (DS-SS signaling plus modulation). The m bits corresponding to DS-SS signaling are obtained at the receiver as described previously, the n bits corresponding to the modulation are obtained as in conventional DS-SS systems assuming the spreading code estimated from the DS-SS signaling detection. Note that to detect the n modulation bits it is required to have an estimate of the channel response.

System description and results

Emitter. The emitter block diagram is depicted in Figure 4.4.a. First an interleaver and a rate 1/3 turbo coder is applied to the raw data. The coded data is then divided in two blocks: one block of bits of length multiple of n is BPSK or QPSK modulated, the other block of bits of length multiple of m is used to determine the spreading code. In pure DS-SS signaling no modulation is done, i.e., $n = 0$. The transmitted frames consist of a preamble followed by the spread data multiplexed with channel estimation M-sequences. Let us recall that in pure DS-SS signaling no modulation is done, i.e., $n = 0$, therefore channel estimation is not required. Finally, the signal is filtered using a root raised cosine and delivered to the up-converters.

Receiver. The receiver block diagram is depicted in Figure 4.4.b. As previously described, fine frequency synchronization is achieved by using the preamble information. Then an impulsive noise limiter is used to improve the receiver performance. Channel estimation is obtained by means of correlation of the input signal and a replica of the M-sequences multiplexed in the frame. Then the signal is despread,

Figure 4.4: DS-SS signaling emitter (a) and receiver (b) block diagram.

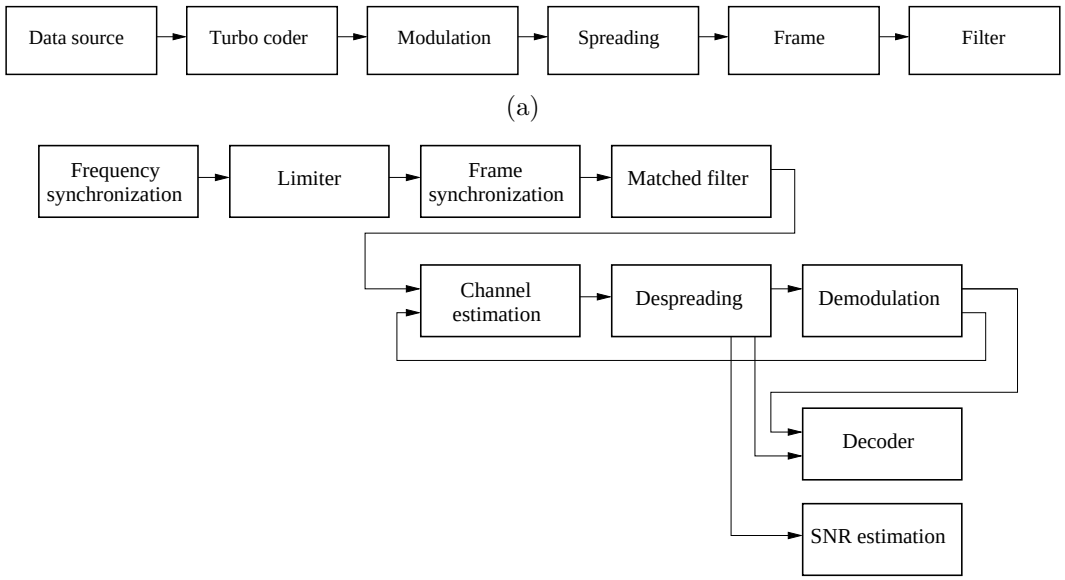

demodulated and decoded to obtain the information data. The SNR is estimated from this data in order to evaluate the performance of the configuration under test.

Results. An example of the experimental results is depicted in Figure 4.5, where the scatterplot of the BER measured in a 972 coded bits frame (BER$'$) versus the estimated SNR is shown. Every cross corresponds to the demodulation of a single frame. For the configuration under test, if the receiver was only limited by Gaussian noise all the crosses should lay between the two continuous lines with a 90 % probability. However, most of the crosses are located outside that region, shifted to higher SNR. As expected, the implemented receiver exhibits lower performance due to mutlipath fading, nonlinear amplification, etc. Although the improvement of the receiver algorithms could increase the performance of the reception, a 3 dB loss of SNR is a realistic assumption when dealing with this ionospheric channel.

Many different configurations have been compared, depending on the occupied bandwidth, the sequence length (processing gain) and the modulation, and a scatterplot has been obtained for each configuration under test. On the basis of these results, we concluded that DS-SS techniques are a successful choice for data transmission in very long distance ionospheric links. We showed that a 150 bps transmission can be achieved in a 3 kHz channel bandwidth with a signal to noise ratio of -5 dB. In those conditions, more than 90 % of the packets were received without errors. This speed is sufficient for the transmission of low rate data from most of the remote sensors in the SAS.

Figure 4.5: Experimental results using the following configuration: BW = 3125 Hz, 64-ary DS-SS, QPSK and rate 1/3 turbo coding. Every cross corresponds to a demodulated frame. A 3 dB loss of SNR is observed when comparing experimental and theoretical results.

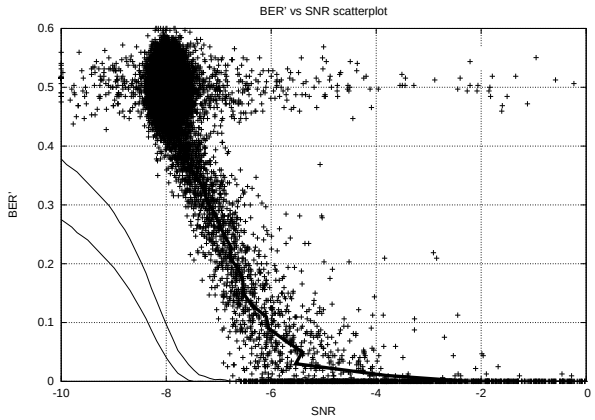

4.4.3 OFDM proposal

The principle of OFDM is to divide a high data rate stream onto several parallel streams with lower data rate such that each sub-stream is associated with a given subcarrier. The main advantage of this concept is that each of the data streams experiences a flat fading channel, even though the overall channel is frequency selective. This means that no complex equalization at the receiver is necessary. Another advantage is that intersymbol interference (ISI) can be easily avoided by just introducing a cyclic prefix before each OFDM symbol [38]. One of the major drawbacks of OFDM is that it suffers from large peak-to-average power ratio (PAPR), which might be a major inconvenience for low power communications in long-haul ionospheric links. In the reminder of this section we present some preliminary research outcomes that try to study the feasibility of using OFDM to implement the physical layer of this long-haul HF link. Table 4.1 summarizes the default OFDM parameters value used throughout the experiments.

Table 4.1: Default OFDM parameters value.

Useful symbol length	$T_U = 30$ ms
Cyclic prefix length	$T_{CP} = 2.8$ ms
Number of subcarriers	$N_C = 16$
Frequency pilot separation	$N_F = 8$
Time pilot separation	$N_T = 5$
Channel estimation method	Least squares
Interpolation method	Cubic splines
Input back off	3 dB
Modulation	Binary Phase Shift Keying (BPSK)
Error correction code	Convolutional (code rate = $\frac{1}{2}$, constraint length = 7)

OFDM symbol design. One of the first aspects to clarify when designing an OFDM system is the length of the OFDM symbol and the subcarrier spacing. Since the subcarrier spacing is the inverse of the useful part of the OFDM symbol, the shorter the symbol length is the wider each subcarrier will be. Consequently the probability that each subcarrier experiences a non-flat fading increases. On the other hand, making the subcarrier spacing small to assure flat fading results in long OFDM symbols. The multipath fading channel is not constant in time, thus having very large OFDM symbols is not desirable or otherwise the channel will not be constant within an OFDM symbol.

To correctly design the OFDM symbol, one must take into account the coherence time of the channel, delay spread and thus coherence bandwidth of the channel. In the following, a study of the OFDM symbol design in the system performance is presented. System performance is determined by means of the error vector magnitude (EVM) of the received symbols. EVM is defined as

$$EVM = \sqrt{\frac{P_{error}}{P_{reference}}}, \tag{4.3}$$

where P_{error} is the mean-squared error between the received constellation points and the ideally received constellation points, and $P_{reference}$ is the power of the outermost ideal constellation point. Figure 4.6 shows the cumulative density function (CDF) of EVM of real OFDM transmissions in the skywave link between the SAS and the OE. Bursts of OFDM symbols of length ranging from 10 ms to 60 ms were consecutively transmitted during several nights. As already expected, OFDM systems with too large (50, 60 ms) and too low (10 ms) symbol lengths, result in poor performance, while OFDM systems designed according to the channel characteristics (symbol lengths of 20, 30 and 40 ms) result in better performance.

Figure 4.6: CDF of the EVM of received symbols gathered from the SAS-OE HF link. OFDM signals were transmitted at frequencies between 4.4 MHz and 17.6 MHz from 21 UTC to 09 UTC, during the 2006-2007 Antarctic survey.

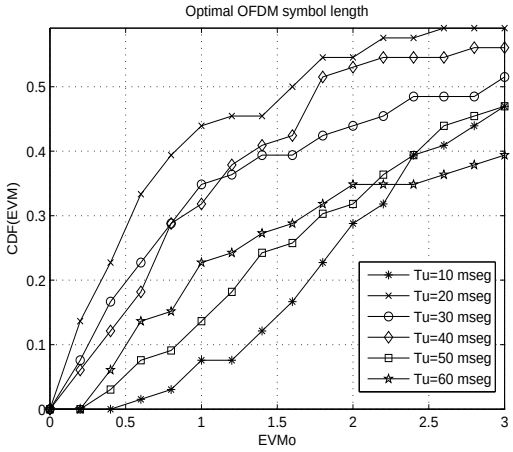

Channel estimation. The next aspect to determine is the pilot insertion pattern for channel estimation. A correct detection of coherent OFDM systems requires that the receiver knows the amplitude and phase distortions introduced by the channel at each subcarrier. To do so, the transmitter inserts known pilot symbols in the time-frequency lattice and the receiver estimates the channel at the scattered pilot positions and then interpolates the channel on the data symbol positions. To properly estimate the channel at the data symbol positions, the pilot spacing has to fulfill the Nyquist sampling theorem. This means that the pilot separation in time, N_T, and frequency, N_F, must fulfill

$$N_T \leq \left\lfloor \frac{1}{2 \cdot f_d \cdot T_S} \right\rfloor \quad \texttt{and} \quad N_F \leq \left\lfloor \frac{1}{2 \cdot \tau_{max} \cdot \Delta_F} \right\rfloor, \tag{4.4}$$

respectively. Where f_d is the Doppler frequency, τ_{max} is the maximum delay spread of the channel and T_S ($T_S = T_U + T_{CP}$) is the OFDM symbol time. According to [26], the maximum Doppler frequency expected for this channel is always lower than 1.5 Hz and the maximum delay spread expected is always lower than 2.1 ms. Note that, N_T and N_F can not be arbitrarily low because both power efficiency and throughput are reduced as the pilot density increases.

During the 2005-2006 Antarctic survey, the performance of OFDM systems employing different pilot densities ($N_T = 5;\ N_F = \{2, 4, 8\}$) and pilot distributions (rectangular and hexagonal) was evaluated. Table 4.2 shows the performance in terms of BER for the different experiments, the throughput for each experiment is also stated. As previously discussed, one can observe that BER can be reduced by increasing the pilot density at expenses of reducing the data throughput. Also one can observe that as stated in [39], hexagonal pilot distribution always outperforms rectangular pilot distribution.

Table 4.2: BER and data throughput with different distribution and pilot spacing in the frequency domain. In time domain, pilot spacing was constant, $N_T = 5$. Data was gathered from the SAS-OE skywave link during the 2005-2006 Antarctic survey.

Pilot distribution	Pilot density	BER without coding	Bit rate (bps)
Rectangular	N_F=8	$2.9e-2$	222.6
	N_F=4	$1.5e-2$	193.6
	N_F=2	$1.2e-2$	129.3
Hexagonal	N_F=8	$1.6e-2$	225.6
	N_F=4	$1.1e-2$	194.6
	N_F=2	$1.0e-2$	126.3

Envelope fluctuations and nonlinear amplification. One of the major drawbacks of OFDM is the sensitivity to nonlinear amplification. The OFDM signal is characterized by suffering from large envelope fluctuations, thus, when the time domain signal is fed through a non-linear device (such as the transmitter's power amplifier) a distortion term is introduced that results in out-of-band radiation and increased error probability. The spectral outgrowth is a limiting factor for regulated transmissions where the signal spectrum has to be located below a power spectral mask. However, our communication system is not restricted by any spectral mask and, therefore, only the BER degradation is of importance.

Figure 4.7: CDF of the BER of received symbols gathered from the SAS-OE HF link. OFDM signals were transmitted at frequencies between 4.4 MHz and 17.6 MHz from 21 UTC to 09 UTC, during the 2006-2007 Antarctic survey.

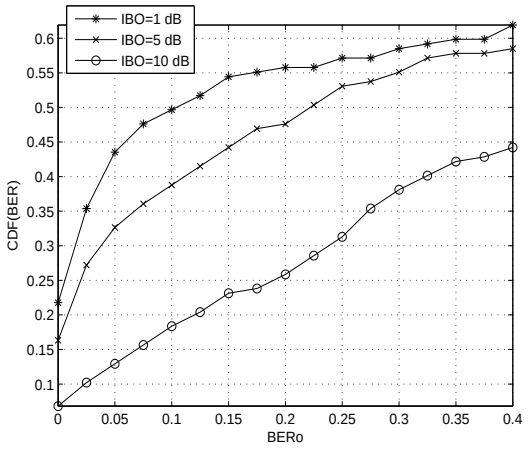

To reduce the nonlinear distortion introduced by the transmitter's power amplifier one can set its operating point far from saturation. In that sense the BER degradation caused by the amplifier is reduced as it is operating in a more linear region. However,

one should note that, for a given amplifier, setting the operating point far from saturation means reducing the power of the transmitted signal and, as a result, reducing the SNR at the receiver. During the 2006-2007 Antarctic survey several experiments were carried out to test the effects on the distortion introduced by the transmitter's power amplifier in the overall system performance. BPSK-modulated OFDM signals with an average power 1 dB, 5 dB and 10 dB below the input saturation power of the amplifier were transmitted. As it can be observed in Figure 4.7, employing larger input back off's (IBO's) in the transmitter's power amplifier results in poorer BER performance, even though less nonlinear distortion is introduced. The reason is that the BER degradation caused by a nonlinearity when BPSK mapping is used is very small, even if low IBO is used. As a result, it is much convenient to place the signal close to the saturation point of the amplifier to increase the SNR at the receiver. It is worth mentioning that large modulation schemes (16-QAM or 64-QAM) are much more sensitive to the nonlinear distortion and thus one should also consider the nonlinearty effects in case of employing a 16-QAM or 64-QAM modulated OFDM system. However, this is not the case for long-haul skyvawe communications.

Interferences from the primary and secondary services. Interferences in the HF band are usually slow variant and have a bandwidth similar to that of our skywave communication system. As a result, if a primary or a secondary service operating at almost the same carrier frequency is present at the receiver site, the long-haul skywave communication system will be highly interfered and no communication will be possible. To avoid this one can employ a hopping pattern in the frequency domain so that the interference level is reduced.

Figure 4.8: BER simulation performance of an OFDM system under the worst, the average and no interference conditions. The performance of a FH-OFDM with different hopping rates operating at the worst interference conditions is also shown.

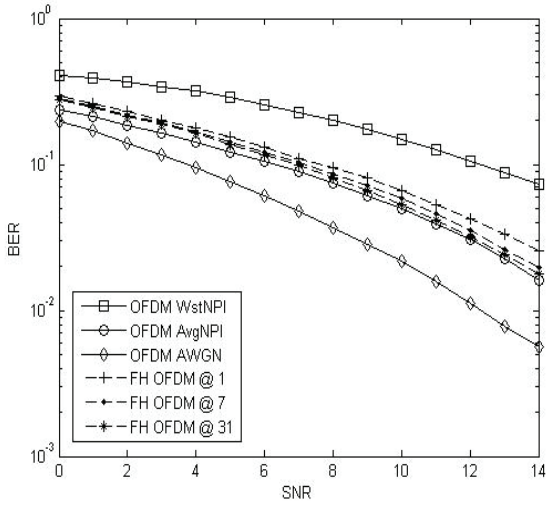

During the 2005-2006 Antarctic campaign, noise plus interferences at the receiver site were recorded and used to test system performance under real situations. Figure 4.8 shows the performance of an OFDM system in a AWGN channel when such interfering signals are present. Three type of interfering conditions are evaluated: worst interference conditions (OFDM WstNPI), average interference conditions (OFDM AvgNPI) and no interference (OFDM AWGN). The performance of an OFDM system employing frequency hopes of 1 kHz every 1, 7 and 31 OFDM symbols in the worst interference conditions is also shown. As it can be observed, interferences cause a serious impact on the system performance. But it can be reduced by introducing frequency hopping. For instance, as it can be observed an OFDM system employing frequency hopes of 1 kHz every 31 symbols operating in the worst interference conditions has almost the same performance as a conventional OFDM system operating at average interference conditions. When comparing the different hopping rates, we observe that a better performance is achieved for slow frequency hopes. The reason is that when the hopping rate increases, less pilots are used to interpolate the channel in each block, yielding to a larger channel interpolation error and, thus, poorer system performance.

4.5 Conclusions

In this paper the research work on remote sensors and data transmission undertaken by LA SALLE and the Ebro Observatory in the antarctic spanish station Juan Carlos I is revised. Three different sensors, shuch as (i) a geomagnetic sensor, (ii) a vertical

ionosonde and (iii) an oblique ionosonde, are described and conclusions about research outcomes are given. These three sensors have been generating data to study the earth magnetic field in this remote region as well as the behavior of the ionosphere from a physical and from a radio communications points of view.

Moreover a proposal to implement the physical layer of the skywave link between the Antarctica and Spain is studied. The main goal of this radio link is to transmit the remote data generated by the above sensors in almost real time. Research work has been focused in two possible modulation candidates:(i) OFDM and (ii) DS-SS. Both are able to cope with the channel impairments (low SNR and high level of interference at the receiver site, multipath and time variant channel,...) and link restrictions (long distance, low transmission power, non-directive antennas,...). Both modulations can achieve a data rate of 150 bits-per-second when the channel is available, which is enough for the amount of data to be transmitted from the remote sensors.

Acknowledgements

This work has been funded by the Spanish Government under the projects REN2003-08376-C02, CGL2006-12437-C02/ANT, CTM2008-03033-E/ANT and CTM2008-03236-E/ANT. LA SALLE and Observatorio del Ebro thank the *Comissionat per a Universitats i Recerca del DIUE de la Generalitat de Catalunya* for their support under the grants 2009SGR459 and 2009SGR507, respectively.

Bibliography

[1] Macmillan, S.; Maus, S. International geomagnetic reference field -the tenth generation. *Earth Planets Space* **2005**, *57*, 1135-1140.

[2] Prölss, G.W. *Physics of the Earth's Space Environment: An Introduction*; Springer: Berlin, Germany, 2004.

[3] Maldonado, A.; Balanyá, J.C.; Barnolas, A.; Galindo-Zaldívar, J.; Hernández, J.R.; Jabaloy, A.; Livermore, R.A.; Martínez-Martínez, J.M.; Rodríguez-Fernández, J.; Sanz de Galdeano, C.; Somoza, L.; Suriñach, E.; Viseras, C. Tectonics of an extinct ridge-transform intersection, Drake Passage (Antarctica). *Mar. Geophys. Res.* **2000**, *21*, 43-68.

[4] García, A.; Blanco, I.; Torta, J.M.; Astiz, M.; Ibañez, J.; Ortiz, R. A search for the volcanomagnetic signal at Deception volcano (South Shetland I., Antarctica). *Annali di Geofisica* **1997**, *XL*, 319-327.

[5] Torta, J.M.; Gaya-Piqué, L.R.; Riddick, J.C.; Turbit, C.W. A partly manned geomagnetic observatory in Antarctica provides a reliable data set, Contributions to Geophysics and Geodesy. *Geophys. Inst. Slov. Acad. Sci.* **2001**,*31*, 225-230.

[6] Marsal, S.; Torta, J.M. An evaluation of the uncertainty associated with the measurement of the geomagnetic field with a D/I fluxgate theodolite. *Measure. Sci.Technol.* **2007**, *18*, 2143-2156.

[7] Riddick, J.C.; Turbitt, C.W.; MCDONALD, J. *The BGS Proton Magnetometer ($\delta D/\delta I$) Observatory Mark II System, Installation Guide and Technical Manual*; British Geological Survey Technical report No. WM/95/32; BGS Geomagnetism Series: Edinburgh, UK, 1995.

[8] Marsal, S.; Torta, J.M.; Riddick, J.C. An assessment of the BGS $\delta D/\delta I$ vector magnetometer. *Publs. Inst. Geophys. Pol. Acad. Sci.* **2007**, *C-99*, 158-165.

[9] Zuccheretti, E.; Tutone, G.; Sciacca, U.; Bianchi,C.; Arokiasamy, B. J. The new AIS-INGV digital ionosonde. *Ann. Geophys.* **2003**, *46*, 647-659.

[10] Solé, J.G.; Alberca, L.F.; Altadill, D.; Apostolov, E.M.; Bianchi, C.; Blanch, E.; Curto, J.J.; De Santis, A.; Gaya, L.R.; Marsal, S.; Pijoan, J.L.; Torta, J.M. Ionospheric station at the Spanish Antarctic Base: Preliminary results (in Spanish).

In *Proceedings of the 5th Asamblea Hispano-Portuguesa de Geodesia y Geofísica*, Seville, Spain, January 30-February 03, 2006.

[11] Vilella, C.; Miralles, D.; Altadill, D.; Acosta, F.; Solé, J.G; Torta, J.M.; Pijoan, J.L. Vertical and oblique ionospheric soundings over a very long multihop HF radio link from polar to midlatitudes: Results and relationships. *Radio Sci.* **2009**, *44*, RS2014, doi:10.1029/2008RS004001.

[12] Prölss, G.W. On explaining the local time variation of ionospheric storm effects. *Ann. Geophys.* **1993**, *11*, pp. 1-9.

[13] McNamara, L.F.; Wilkinson, P.J. Spatial correlations of foF2 deviations and their implications for global ionospheric models: 1. Ionosondes in Australia and Papua New Guinea. *Radio Sci.* **2009**,*44*, RS2016, doi:10.1029/2008RS003955.

[14] Fuller-Rowell, T.J.; Codrescu, M.V.; Moffet, R.J.; Quegan, S. Response of the thermosphere and ionoshere to geomagnetic storms. *J. Geophys. Res* **1994**, *99*, 3093-3914.

[15] McNamara, L.F. Spatial correlations of foF2 deviations and their implications for global ionospheric models: 2. Digisondes in the United States, Europe, and South Africa. *Radio Sci.* **2009**,*44*, RS2017, doi:10.1029/2008RS003956.

[16] Lanzerotti, L.J. The need for long-term solar-terrestrial data series. *Space Weather* **2009**, *7*, S05006, doi:10.1029/2009SW000496.

[17] Alfonsi, L.; De Franceschi, G.; De Santis, A. Geomagnetic and ionospheric data analysis over Antarctica: a contribution to the long term trends investigation. *Ann. Geophys.* **2008**, *26*, 1173-1179.

[18] Horvath, I.; Lovell, B.C. Investigating the relationships among the South Atlantic Magnetic Anomaly, southern nighttime midlatitude trough, and nighttime Weddell Sea Anomaly during southern summer. *J. Geophys. Res.* **2009**, *114*, A02306, doi:10.1029/2008JA013719.

[19] Jee, G.; Burns, A.G.; Kim, Y.-H.; Wang, W. Seasonal and solar activity variations of the Weddell Sea Anomaly observed in the TOPEX total electron content measurements. *J. Geophys. Res.* **2009**, *114*, A04307, doi:10.1029/2008JA013801.

[20] Pavlov, A.V.; Pavlova, N.M. Anomalous variations of NmF2 over the Argentine Islands: a statistical study. *Ann. Geophys.***2009**,*27*, 1363-1375.

[21] Altadill, D.; Blanch, E.; Paznukhov, V. Ionosphere response against geomagnetic storms in mid latitudes (in Spanish). *Física de la Tierra* **2008**, *20*, 115-132.

[22] Denton, M.H.; Ulich, T.; Turunen, E. Modification of midlatitude ionospheric parameters in the F2 layer by persistent high-speed solar wind streams. *Space Weather* **2009**, *7*, S04006, doi: 10.1029/2008SW000443.

[23] Ignat'ev, V.M. Impulsive joule heating of the auroral thermosphere as a source of generation of large-scale gravity waves. *Geomagn. Aeron.* **2009**, *49*, 227-231.

[24] Angling, M.J.; Shaw, J.; Shukla, A.K.; Cannon, P.S. Development of an HF selection tool based on the Electron Density Assimilative Model near-real-time ionosphere. *Radio Sci.* **2009**, *44*, RS0A13, doi:10.1029/2008RS004022.

[25] De Franceschi, G.; Alfonsi, L.; Romano, V. ISACCO :an Italian project to monitor the high latitudes ionosphere by means of GPS receivers. *Eye on ionosphere. GPS Solutions* **2006**, doi:10.1007/s10291-006-0036-6.

[26] Vilella, C.; Miralles, D.; Pijoan, J.L. An Antarctica-to-Spain HF ionospheric radio link: Sounding results. *Radio Sci.* **2008**, *43*, RS4008, doi:10.1029/2007RS003812.

[27] Davis, K. *Ionospheric Radio*; Clarricoats, P.J.B., Rahmat-Samii, Y., Wait, J.R., Eds.; Peter Peregrinus: London, UK, 1990.

[28] Vilella, C.; Badia, D.; Pijoan, J.L.; Deumal, M.; Ribó, M.; Regué, J.R. On site receiver testing. Application to long distance HF links. In *Proceedings of the International Symposium on Electromagnetic Compatibility*, Barcelona, Spain, September 4–8, 2006.

[29] Mitola, J. The software radio architecture. *IEEE Commun. Mag.* **1995**, *33*, 26-38.

[30] Proakis, J.G. *Digital Communications*; McGraw-Hill: New York, NY, USA, 1995.

[31] 3rd Generation Partnership Project; Technical Specification Group Radio Access Network; Physical layer - General description (Release 1999), 3GPP TS 25.201.

[32] 3rd Generation Partnership Project; Technical Specification Group Radio Access Network; High Speed Downlink Packet Access: Physical Layer Aspects (Release 2005), 3GPP TR 25.858.

[33] 3rd Generation Partnership Project; Technical Specification Group Radio Access Network;FDD Enhanced Uplink; Physical Layer Aspects (Release 2006), 3GPP TR 25.808

[34] Pickholtz, R.L.; Schilling, D.L.; Milstein L.B. Theory of spread-spectrum communications - A tutorial. *IEEE Trans. Commun.* **1982**, *30*; 855-884.

[35] Enge, P.K.; Sarwate, D.V. Spread-spectrum multiple-access performance of orthogonal codes: linear receivers. *IEEE Trans. Commun.* **1987**, *35*; 1309-1319.

[36] Deumal, M.;Vilella, C.; Socoró, J.C.;Alsina, R.M.; Pijoan, J.L. A DS-SS signaling base system proposal for low SNR HF digital communications. In *Proceedings of the 10th IET International Conference on Ionospheric Radio Systems and Techniques*, London, UK, July 18-21, 2006.

[37] Hong, E.K; Kim, K.J.; Whang, K.C. Performance evaluation of (DS-CDMA) system with M-ary orthogonal signaling. *IEEE Trans. Vehicular Technol.* **1996**, *45*, 57-63.

[38] Peled, A.; Ruiz A. Frequency domain data transmission using reduced computational complexity algorithms. In *Proceedings of the IEEE International Conference on Acoustics, Speech, and Signal Processing* Denver, Colorado, USA, April, 1980; pp. 964-967.

[39] Fernández-Getino, M.J.; Zazo, S.; Páez-Borrallo, J.M. Pilot patterns for channel estimation in OFDM. *IEEE Electron. Lett.* **2000**, *36*, 1049-1050.

Chapter 5

A Comprehensive Sounding of the Ionospheric HF radio link from Antarctica to Spain

A.G. Ads[1], P. Bergadà[1], C. Vilella[1], J.R. Regué[1], J.L. Pijoan[1], R. Bardají[1], J. Mauricio[1]

[1] Grup de Recerca en Electromagnetisme i Communicacions (GRECO), La Salle, University of Ramon Llull, Barcelona, Spain.

Radio Science, Vol. 48, 1-12, doi:10.1029/2012RS005074, 2013

Received 16 July 2012; revised 16 October 2012; accepted 15 November 2012; published 24 January 2013.

Since 2003, our group has been investigating the performance of different transmission techniques for low-power low-interference High Frequency (HF) ionospheric communication systems. Specifically, we have focused on the link between the Spanish Antarctic Station (SAS) Juan Carlos I in Livingston Island and Ebro Observatory (OE) in Spain, in order to transmit the data gathered from some geomagnetic sensors. These transmission techniques require a valuable knowledge of the channel behavior, thus a comprehensive narrowband and wideband sounding of the ionospheric channel is needed. Some significant improvements both in the system and in the signal processing have been done to achieve this goal. The analysis time and the frequency band have been extended to 24 hours per day and to the whole HF band (2-30 MHz). Moreover, new measurements of the absolute propagation time and the Doppler frequency shift are introduced. In this paper, the sounding results obtained using the new system are presented.

5.1 Introduction

The ionospheric HF communications channel is a special case of slow fading multipath channel where both digital communications concepts and geophysical knowledge are required. The refraction of HF waves (2-30 MHz) in the ionized medium makes propagation over long distances possible up to 3000 km per reflection hop. HF communications are very useful for military purposes, fleet control and communications with remote areas, where no satellite coverage is available.

Communications from North and South poles underlines the importance of skywave propagation in the HF band since line of sight from geostationary satellite is not feasible. In that sense, our Research Group is developing a new communication system from the SAS to Spain in order to transmit the data from remote sensors installed in Livingston Island (South Shetland Islands), Antarctica to the OE in Roquetes, Spain.

The research project started in 2003 with three main objectives:

1. Channel sounding and modeling, taking into account the daily, annual, and solar cycle variations.

2. Design of the best digital modulation scheme for a low-power, low-interference communication system.

3. Implementation of robust hardware and software able to operate under hard environmental conditions.

A more detailed description of this project can be found in [*Bergadà et al.*(2009)].

Previous work, mainly in mid-latitudes and polar regions, is revised in [*Vilella et al.*(2008)]. [*Angling et al.*(1998), *Warrington et al.*(1998)] added important contributions for high-latitudes, [*Angling et al.*(1997), *Warrington et al.*(2003)] in mid-latitudes, and [*Houpis et al.*(1991), *Fitzgerald et al.*(1999)] introduced results for low-latitudes .

The first channel model, widely accepted for narrowband transmissions, was developed by [*Watterson et al.*(1970)]. [*Vogler et al.*(1993)] from Institute of Telecommunication Science (ITS) developed a wideband ionospheric HF channel model with non Gaussian statistics and delay spread parameters. [*Mastrangelo et al.*(1997)] provided an HF channel simulation system that is well operative with both narrowband and wideband HF channels model.

The hardware of the channel sounder and the radio modem has been updated several times since the 2003/2004 survey. Three main Software Defined Radio (SDR) platforms have been installed in both the transmitter and the receiver. The first one, Sounding System for Antarctic Digital Communications (SANDICOM) is described by [*Vilella et al.*(2005)].

During the 2005/2006 survey, the second generation SODIO started with a new digital platform using Field Programmable Gate Arrays (FPGA), and an Application Specific Integrated Circuits (ASIC) with high speed Digital to Analog Converter (DAC) as explained by [*Vilella et al.*(2006)]. The results obtained by the SODIO system have been introduced by [*Vilella et al.*(2008)]. The system had some limitations in both sounding time (00:00 UTC to 11:00 UTC and 18:00 UTC to 23:00 UTC), frequency

(4.5 MHz to 16.5 MHz), and also in the measurement capabilities. For these reasons, the daytime data, propagation time, and Doppler frequency shift could not be obtained. The limitation of the operating time of the system to 18 hours was due to the manual configuration of the system which carried out by the staff in the SAS. As well, these seven hours were considered having the worst propagation conditions according to the frequency band that have been employed during the 2006/2007 survey. However, this paper proves that such consideration was not completely precise in case of using the whole HF band.

Finally, in the 2009/2010 survey (November 2009 to February 2010), a third generation platform called POTASIO was installed in both the SAS and OE. The new system that is easier to handle and maintain than the previous, able to operate during 24 hours per day with an extended frequency range (2 MHz to 30 MHz). Therefore, the results presented in this paper represent a substantial improvement to the previous work.

First, a brief description of the link and the hardware is given. Next, the description of the narrowband and wideband analysis methodologies is provided. Finally, the results from both the narrowband, wideband sounding, propagation time, and Doppler frequency shift are presented.

5.2 Link Description

One of the main objectives of our work is to establish a permanent HF link between the SAS in Livingston Island (62.6S, 60.4W) and OE (40.8N, 0.5E). The distance between the SAS and OE is approximately 12700 km. Hence, according to [*Davies*(1990)], a minimum of four hops are needed. The coordinates of these hops are listed in [*Vilella et al.*(2008)]. The propagation conditions are strongly depend on sun radiation, so daily, seasonal, and solar cycle variations have to be studied. Furthermore, the equatorial anomaly, the auroral electrojet, and the variation of sunset time along the path influence on the channel behavior. Regarding interferences and multipath, a study of quiet frequencies has been made in order to avoid strong signals from broadcast stations, ionosondes, and other HF services.

In some subbands, echoes from different layers reflection, and even propagation throughout the long path, i.e., along the other side of the Earth, increase the time-delay spread of the channel, and so reducing the coherence bandwidth.

As there are few studies of such long-haul links, our group has been measuring all the significant channel parameters both in narrowband and wideband conditions since 2003 in order to have a complete historical series.

5.3 System Description

As previously mentioned, the hardware of the channel sounder and data transmission system has been updated in order to extend the frequency range and measuring capabilities and improve the frequency and time accuracy. Therefore, the whole transmission

system is totally redesigned and reequipped with faster and more reliable equipments during the 2009/2010 survey. Therefore, the resulted system is able to operate at higher bandwidth up to 40 kHz and more sampling rate (100 kHz). Throughout the development period of the project (2003 to 2012), several bandwidth has been deployed. However, 5 kHz is the usage bandwidth in the 2009/2010 survey. The main features of the transmitter and receiver hardware, as well as the data frame structure are summarized below.

5.3.1 Hardware of the Transmitter

The core of the system is a digital platform with an embedded PC with a Digital Signal Processing (DSP) unit inside, that performs the tasks of system control and parameter configuration. The main DSP unit (*XTremeDSP-IV*) from XILINX includes three FPGA. The first FPGA (*Virtex-II*) is responsible for configuring the clock. The main FPGA (*Virtex-4*) that designed by the user, within this device two 14-bit Analog to Digital Converter (ADC), two 14-bit DAC, and all the arithmetic and peripherals controls. A preconfigured FPGA (*Spartan-II*) which handles the interface between the PCI bus and the *Virtex-4*. A block diagram of the transmitter is shown in Figure 5.1.

A new GPS unit with the Pulse per Second (PPS) signal increases the time synchronization accuracy (1μs), making the measurement of the propagation time of the wave possible. In order to improve the frequency synchronization accuracy, a 100 MHz Oven Controlled Crystal Oscillator (OCXO) is installed in both the transmitter and the receiver side. Moreover, the transmitter power amplifier can be switched off in case of severe impedance mismatch by means of a wattmeter that controls the forward and reverse transmitted power.

All the transmitter hardware is deployed close to the antenna at the top of a hill near to the SAS. All the electronics are inside a watertight sealed box, which provides electromagnetic shielding and protection against hard weather conditions. The system is remotely accessed by using a Wireless Local Area Network (WLAN) from the laboratory in the SAS.

5.3.2 Hardware of the Receiver

The receiver, whose block diagram is shown in Figure 5.2, uses the same digital platform as the transmitter. Monopole and Yagi are the antennas used to receive the signal. The Yagi is only used around 15 MHz, whereas the monopole is used along the whole HF band.

As shown in Figure 5.4, the RF signal is passed through a Low Noise Amplifier (LNA) and two additional amplification stages. One of them is a digitally controlled Variable Gain Amplifier (VGA) with a variable gain range of -5 dB to + 40 dB. The first filter for the RF signal received from the monopole is a preselector of three tunable filters that cover the whole HF band, while it is a fixed 15 MHz Band Pass Filter for the signal received from the Yagi. A 32 MHz antialiasing filter is at the end of the filtering and amplification unit.

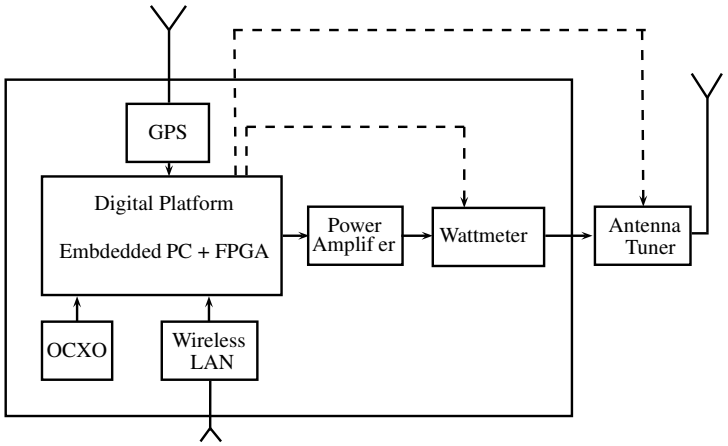

Figure 5.1: Block digram of the POTASIO transmitter side.

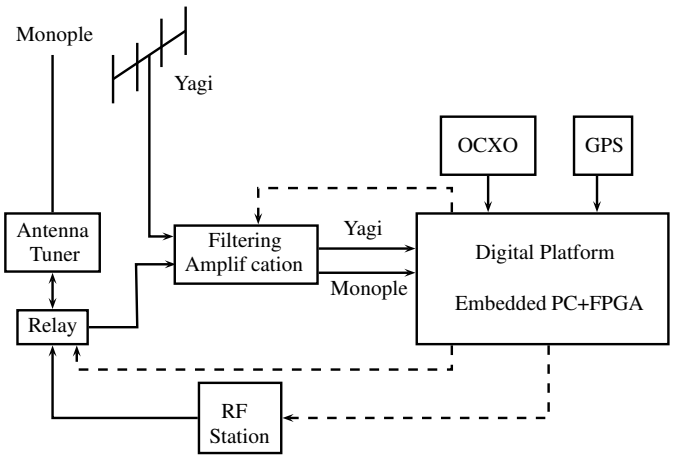

Figure 5.2: Block digram of the POTASIO receiver side.

A commercial RF station is used to transmit a low power signal during a short period of time in order to tune the antenna tuner of the monopole antenna.

5.3.3 Frame Structure

The signals to be transmitted are organized in a frame as shown in Figure 5.3. The waiting intervals are defined as W. After the antenna tunning period, a full power tone is transmitted during 10 seconds for narrowband sounding. This period is used for channel availability estimation and for computing the SNR statistics. After a 4 seconds waiting period, a pseudo random noise (PN) sequence (m-sequence) of variable length and with good autocorrelation properties, as discussed by [*Parsons*(2000)], is transmitted during 10 seconds for wideband sounding. The wideband channel parameters to be measured are wideband SNR, multipath spread, Doppler spread, propagation time, and Doppler shift.

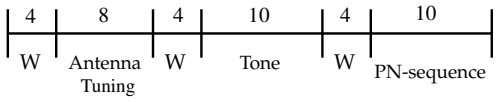

Figure 5.3: A simple transmitted frame.

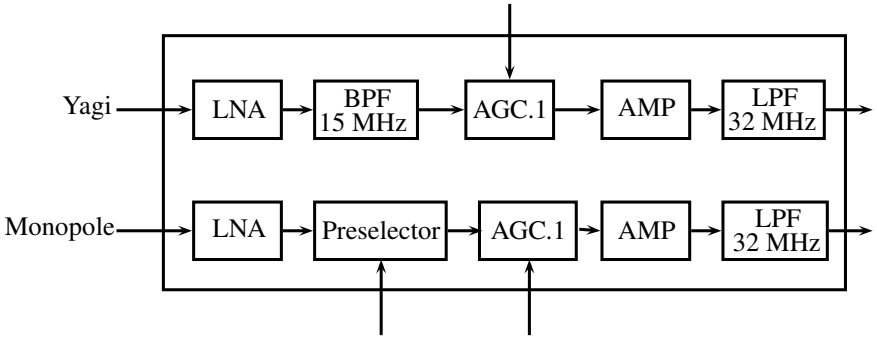

Figure 5.4: Filtering and amplification unit at the receiver side.

5.4 Narrowband Analysis

Narrowband analysis focuses on channel availability and SNR computation. The channel availability means the probability of a link to reach a minimum SNR value and hence achieve a certain quality of service as defined by [*Goodman et al.*(1997)]. According to [*Vilella et al.*(2008)] a minimum SNR value of 6 dB has been specified to estimate the channel availability in a bandwidth of 10 Hz. In this paper, we have improved the narrowband detection method by measuring the variation of the SNR along the received signal power profile. This is done by windowing and time framing the received signal in the time domain, as explained below. Such techniques improves the reliability of the detection system against noise and interference significantly.

SNR is computed by comparing the received power P_s measured during the tone interval to the noise power P_n measured during the waiting periods. The problem that we are facing is the false detections produced by interference signals present during the signal interval. A summary of the survey configuration parameters is shown in Table 5.1.

5.4.1 Windowing

In order to have a useful received signal power profile, the first step is to properly filter the received signal. In our case this is carried out in the frequency domain by multiplying the Fast Fourier Transform (FFT) of the received signal by the window frequency response. Such a filter has two main features:

1. It should eliminate signals at frequencies apart from the reception frequency.

2. It should have a good time response to avoid creating transients from the impulsive interferences that fall far away from the reception frequency.

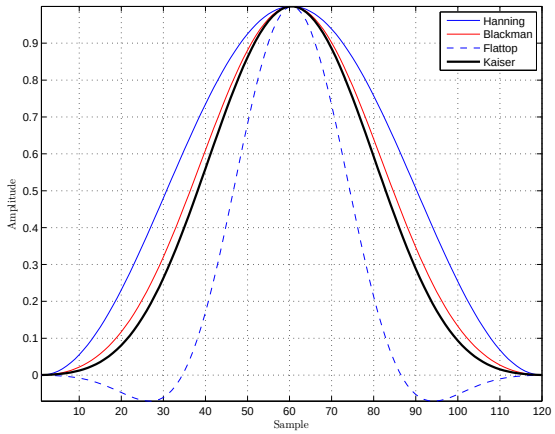

Figure 5.5: Time response of the four different window functions.

Table 5.1: Configuration setup for the narrowband sounding during the 2009/2010 survey.

	Configuration setup		
	1	2	
Sampling Frequency	100000		Hz
Time Interval	1–11	2–12	s
Guard Period	1		s
Window Filter	Kaiser		
Portion length	0.5		s
Threshold values	3, 6, 9, 15		dB

An example of a narrowband received signal filtered by an ideal rectangular window is shown in Figure 5.6, while a highly interfered one is shown in Figure 5.7. The window filter should deal with both cases. In the literature, several window function can be found. However for reasons of simplicity, we have just applied four windows which are Blackman ([*Blackman et al.*(1959)]), Hanning ([*Blackman et al.*(1959)]), Flattop ([*Oppenheim et al.*(1989)]), and Kaiser ([*Kaiser*(1974)]). A comparison between the four window functions is illustrated in Figure 5.5.

The four window functions are applied to an interfered narrowband signal and outcomes are compared in Figure 5.7. The results of applying those windows are much better than the ideal one that was used in previous works by [*Vilella et al.*(2008)]. Kaiser window has a slightly better and smooth response than the rest of the windows, and is the window used in the rest of the work.

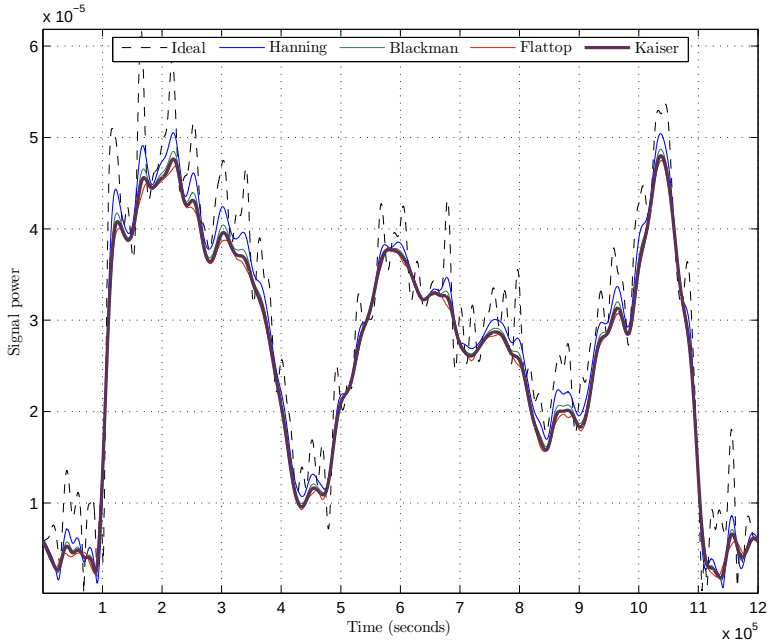

Figure 5.6: Narrowband signal filtered with the four different window functions with a carrier frequency of 15.5 MHz at 10:00 UTC.

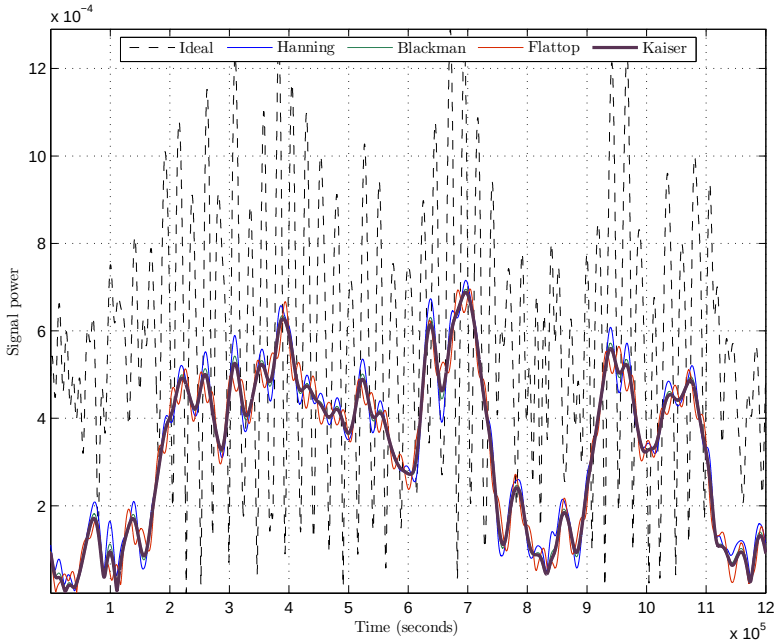

Figure 5.7: Ideal window compared with the other four window filters on a highly interfered narrowband signal with a carrier frequency of 20 MHz at 17:00 UTC.

5.4.2 Time Framing

SNR computation can be easily distorted by the presence of high-level interfering signals. As shown in Figure 5.8, an interfered signal present during some seconds of the analyzed interval can lead to false SNR calculations.

To overcome this problem, the whole received signal period was segmented into a certain number of periods, e.g., 10 periods in Figure 5.8. The SNR is computed as the ratio of the signal power on every segment over the noise power measured at the segments of the waiting period. So we have an evolution of the SNR along the observation interval. According to several experiments, two threshold values have been established, i.e., Th_{low} = 3dB and Th_{high} = 6dB. In order to have a high detection reliability, only measurements where SNR $\geq Th_{low}$ over 70% of the segments and SNR $\geq Th_{high}$ over 50% of the segments are considered to compute the availability and SNR estimations.

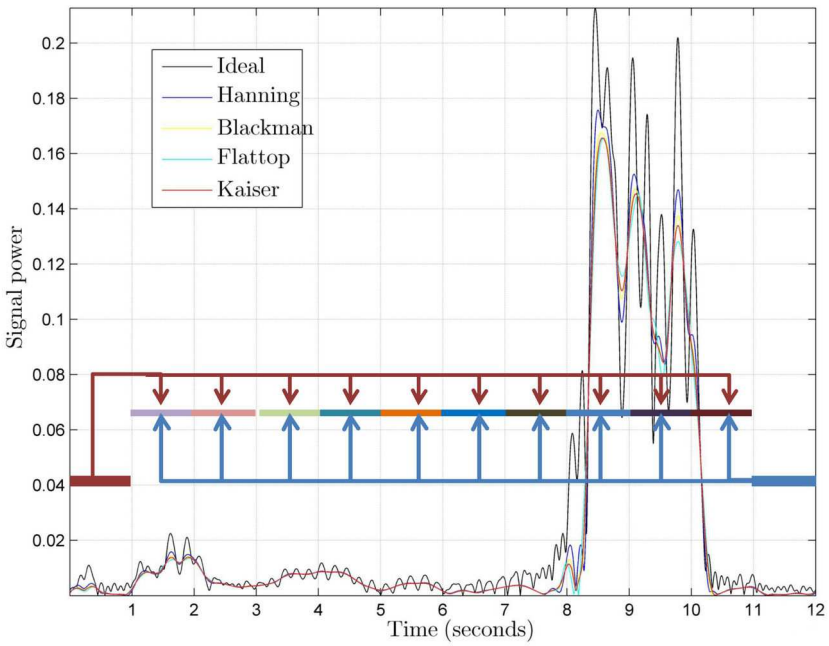

Figure 5.8: An example of high level interfered signal received during the tone period with a carrier frequency of 3 MHz at 00:00 UTC and the solution proposed to cancel its affect.

5.5 Wideband Analysis

The wideband analysis is useful to characterize time and frequency dispersion channels and not only those that are slow and frequency dispersive. Seeking this goal, some PN sequences of different time length and bandwidth are transmitted. The configuration parameters used in the 2009/2010 survey are listed in Table 5.2.

The received signal $r[n]$ is correlated with a copy of the original PN sequence S_e shaped by a raised cosine filter with a roll-off factor of 0.65 as illustrated in Figure 5.9. The correlation function $\phi_{r,S_e}[n]$ is calculated as:

$$\phi_{r,S_e}[n] = \sum_{k=0}^{N_e-1} r[n+k]S_e[k] \tag{5.1}$$

where N_e denotes the length of the PN sequence S_e. Therefore, the channel impulse response $h[n,\tau]$ can be expressed as:

$$\begin{aligned} h[n,\tau] &= \phi_{r,S_e}[nlN_c+\tau], \\ n &\in \big[0, \big[\frac{\Delta t F_m}{lN_c}\big] - 1\big], \\ \tau &\in [0, lN_c - 1] \end{aligned} \tag{5.2}$$

where τ is the delay variable, l is the number of chips, N_c denotes the number of the samples per chip, Δt is the interval of the wideband sounding and F_m is the sampling frequency.

From Equation 5.3, the following parameters are derived: scattering function, SNR, composite multipath spread, composite Doppler spread, propagation time, and Doppler frequency shift.

The scattering function $R_s[\tau,\nu]$ is calculated as the FFT of the channel impulse response as explained by [*Proakis*(2001)]:

$$R_s[\tau,\nu] = \sum_{\xi} R_h[\xi,\tau]e^{-j2\pi\xi\nu} \tag{5.3}$$

where ξ denotes the time variable, ν the Doppler frequency shift and

$$R_h[\xi,\tau] = \sum_{n} h^*[n,\tau]h[n+\xi,\tau] \tag{5.4}$$

The time spread and frequency spread observation windows have been defined in Table 5.2 according to the results obtained by [*Vilella et al.*(2008)]. The power delay profile $\phi[\tau]$ is expressed by refining $R_s[\tau,\nu]$ along the Doppler window $[\nu_1,\nu_2]$ as:

$$\phi[\tau] = \sum_{\nu=\nu_1}^{\nu_2} R_s[\tau,\nu] \tag{5.5}$$

In order to improve the robustness of the τ_c calculation, the power delay profile modified by subtracting the average value of the squared noise. It should be noted that, if the

observation window of multipath is well adjusted, $\phi[\tau]$ will contain the noise power outside the window. Therefore,

$$\tilde{\phi}[\tau] = \phi[\tau] - \frac{1}{T - (\tau_2 - \tau_1)} \sum_{m \notin [\tau_1, \tau_2]} \phi[m] \tag{5.6}$$

Then, calculate the integral function of $\tilde{\phi}[\tau]$ can be expressed as:

$$\Phi(\tau) = \sum_{m=\tau_1}^{\tau_2} \tilde{\phi}[m], \quad \tau \in [\tau_1, \tau_2] \tag{5.7}$$

So, the normalization of $\Phi(\tau)$ with respect to the maximum value defined as:

$$\bar{\Phi}(\tau) = \frac{\Phi(\tau)}{max(\Phi(\tau))} \tag{5.8}$$

Finally, we obtain the value of delay by which $\bar{\Phi}(\tau)$ ranges between 10% and 90% of the maximum value:

$$\tau_{min} = \overset{min}{\tau}\, \bar{\Phi}(\tau) \geq 0.1 \tag{5.9}$$

$$\tau_{max} = \overset{max}{\tau}\, \bar{\Phi}(\tau) \leq 0.9 \tag{5.10}$$

Hence, the composite multipath spread is expressed as:

$$\tau_c = \tau_{max} - \tau_{min} \tag{5.11}$$

In a similar way, the Doppler power profile $\phi[\nu]$ is calculated from $R_s[\tau, \nu]$, averaged along the multipath window $[\tau_1, \tau_2]$ as:

$$\phi[\nu] = \sum_{\tau=\tau_1}^{\tau_2} R_s[\tau, \nu] \tag{5.12}$$

By using the same algorithm used to calculate the composite multipath spread, the composite Doppler spread will be expressed as:

$$\nu_c = \nu_{max} - \nu_{min} \tag{5.13}$$

An estimation of the SNR is calculated as:

$$SNR = \frac{P|_{A_{sp}} - \rho_n A_{sp}}{\rho_n A_{sp}}, \quad \rho_n = \frac{P|_{\overline{A_{sp}}}}{\overline{A_{sp}}} \tag{5.14}$$

where A_{sp} represents the area spread factor which is the area of the scattering function over the multipath and Doppler spreads as expressed by [*Nissen et al.*(2003)], $P|_{A_{sp}}$ is the power in the area spread factor, $\overline{A_{sp}}$ is the area outside the area of spread factor, $P|_{\overline{A_{sp}}}$ represents the power in the area outside the spread factor area, and ρ_n is the noise power per unit of area in the scattering function.

Figure 5.10 shows an example of the correlated signal, channel impulse response and scattering function of 18.5 MHz sounding signal at 16:00 UTC. In order to get more practical plot, the axis of the channel impulse response and the scattering function in Figure 5.10 have been centred.

The high frequency stability of the OCXO unit gives the opportunity to calculate the Doppler frequency shift from the scattering function which is one of the new parameters presented in this paper. The synchronization between the transmitter and the receiver is done by means of the GPS unit. So the propagation time values can be measured from the correlated version of the received signal.

Table 5.2: Configuration setup for the wideband sounding during 2009/2010 survey.

Sampling Frequency	100000	Hz
Time Interval	1–11	s
Chip Frequency	5000	Hz
Sequence length	127	
Frequency spread window	(-4 4)	Hz
Time spread window	(-3 3)	ms
Minimum SNR threshold value	8	dB
Roll-off factor of the RCC filter	0.65	

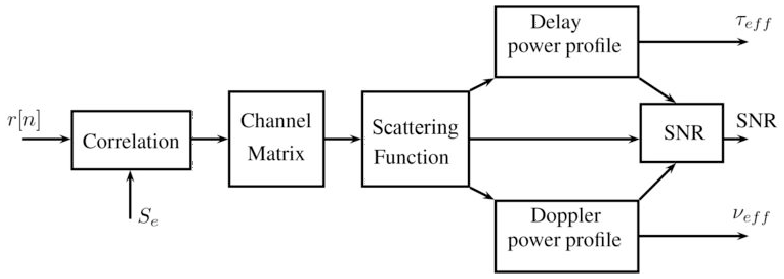

Figure 5.9: Block diagram of the algorithms applied in the wideband analysis.

5.6 Results

As previously stated , this paper is a step forward with respect to the previous soundings presented in [*Vilella et al.*(2008)]. In that work, a frequency range from 4.6 MHz to 16.6 MHz with an observation period from 18:00 UTC to 11:00 UTC was used. The results presented hereafter are based on measurements over the whole HF Band (2-30 MHz) and throughout 24 hour per day. Moreover, due to significant improvements on the hardware, new measurements of the propagation time and Doppler shift are introduced. All the results are referred to the 2009/2010 survey.

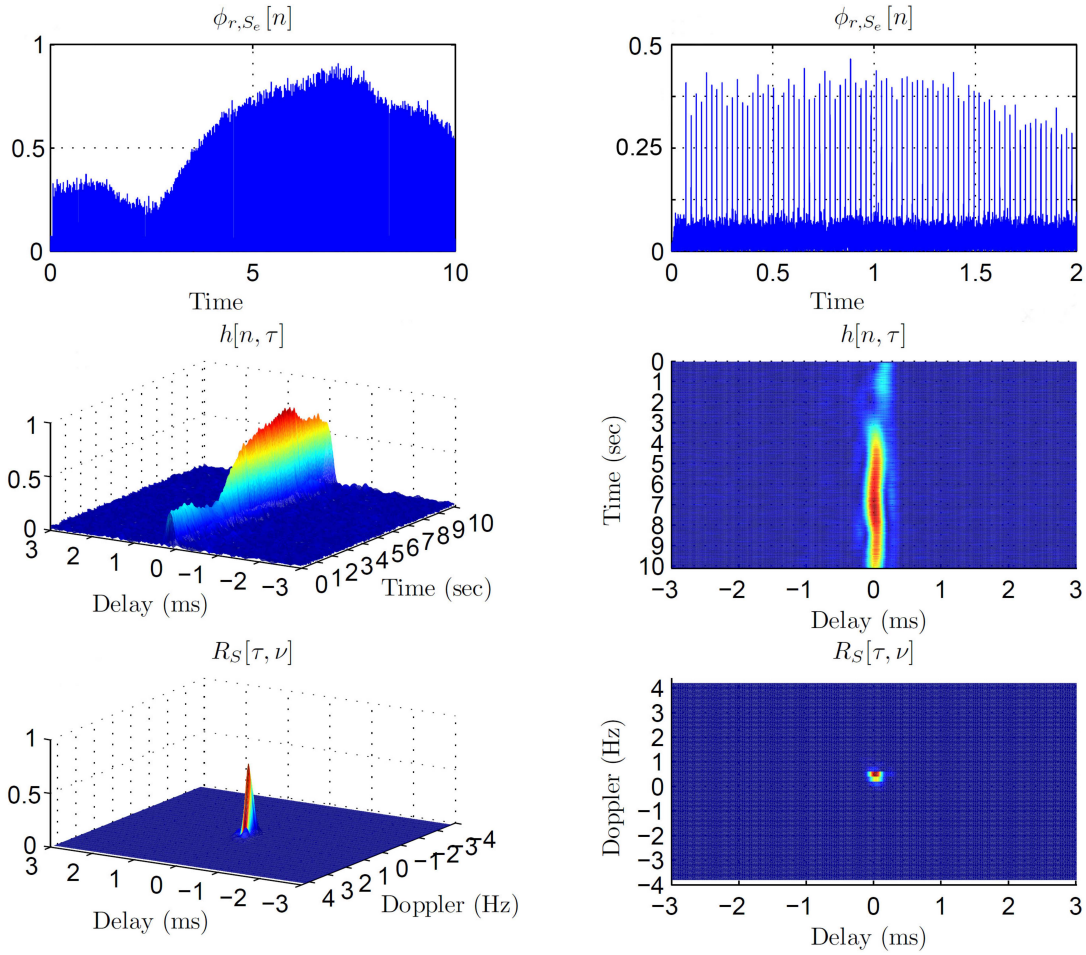

Figure 5.10: Sounding signal of 18.5 MHz at 16:00 UTC. A correlation of 10 seconds and 2 seconds of the received signal with the original sequence depicted at the top right and left frames respectively. At the middle right and left frame, channel impulse response in 3D and top-view. Scattering function in 3D and top-view are depicted at the bottom right and left frames respectively.

5.6.1 Narrowband Sounding

As explained in section 5.4, this analysis focuses on SNR estimation and channel availability, by means of new computing method based on windowing and time framing. Figure 5.11 is an example of the daily estimation of the SNR for every frequency and hour.

As stated in Section 5.4, the channel availability means the probability of a link to reach a minimum SNR value and consequently achieve a certain quality of service. Figure 5.12 represents the channel availability for every frequency and hour. In its first stage, we have considered the ionospheric channel available if 50% of the time frames show SNR higher than 6 dB. As it can be seen, there are some discontinuities that

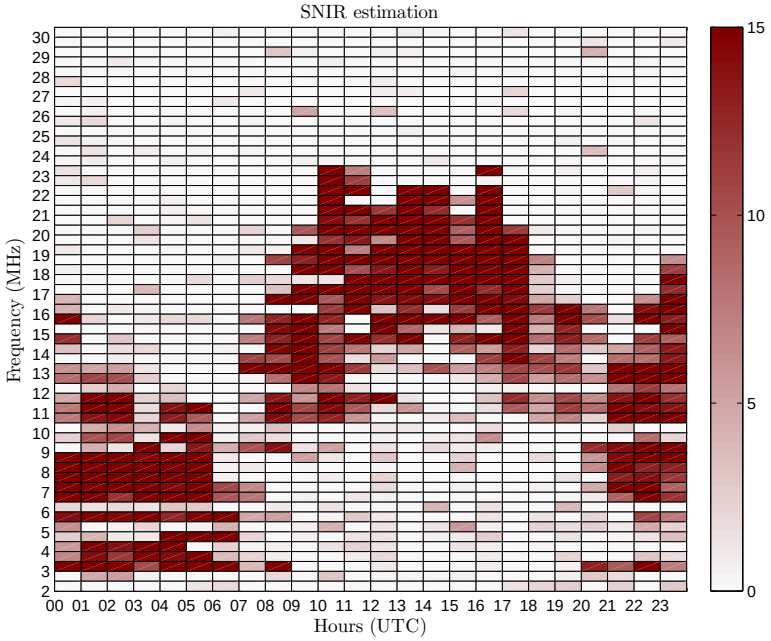

Figure 5.11: Narrowband SNR estimation as a function of the hour and the frequency of sounding.

cannot be attributed to the channel behavior.

To overcome this problem, and after further analysis of data, we suggest a new definition of channel availability, considering that the channel is available if 50% of the time frames show a SNR higher than 6 dB and 70% of the time frames show a SNR higher than 3 dB. The channel availability results with the time framing method are shown in Figure 5.13. The red slots mean that no signal could be detected due to the presence of other strong interfering signals. This fact may not be interpreted as a failure of the method since such signals could not be detected neither by time framing nor by any other technique. According to its position and well-known propagation theories, these red slots should be considered as points of potential availability of the channel. The blue slots mean that the channel is available, i.e., SNR $\geq$ 6dB the 50% of the time and SNR $\geq$ 3dB the 70% of the time. The position of the blue slots plus the red slots (global availability) is much more consistent than the availability estimated in previous works carried out by [*Vilella et al.*(2008)].

Finally we have a small amount of non-detected available slots (green ones), where the method failed to detect the presence of weak signals, and a single false alarm slot (black slot), where the method erroneously detected a good reception .

From Figures 5.11, 5.12, and 5.13, we can distinguish two propagation regions with the following characteristics:

1. The night region. It starts at sunset (around 17:00 UTC) and ends at sunrise (around 07:00 UTC). As sunset extends for four hours and half along the whole

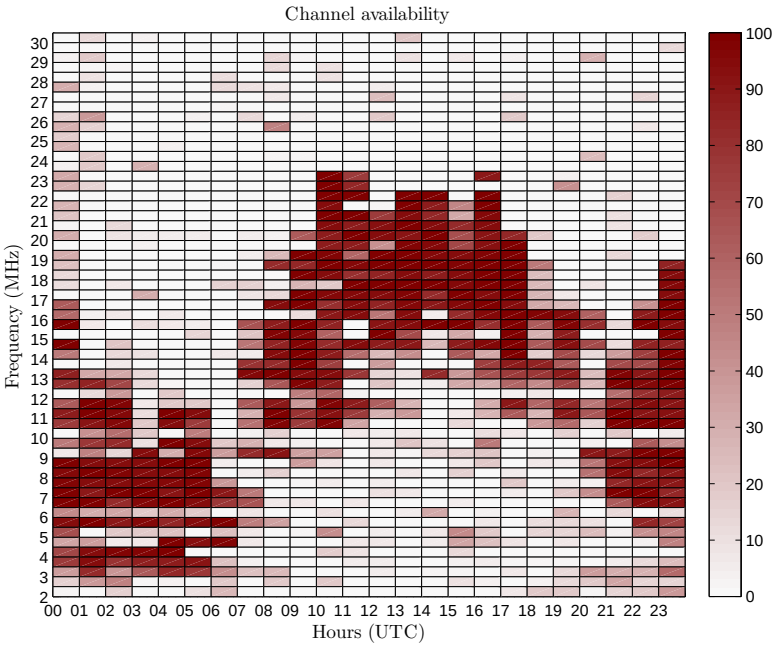

Figure 5.12: Channel availability which exceeds 6 dB as a function of the hour and the frequency of sounding.

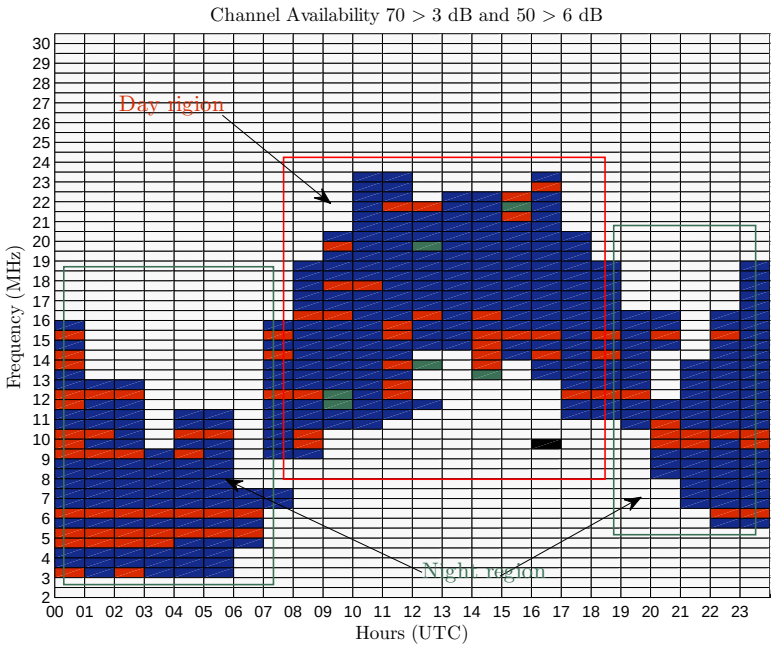

Figure 5.13: Channel availability with time framing method as a function of the hour and the sounding frequency.

path, good propagation conditions exist from 10.5 MHz to 16.5 MHz from 18:00 UTC to 20:00 UTC and it changes to the range from 6.5 MHz to 17.5 MHz from 21:00 UTC to 23:00 UTC. Due to the complete D-layer absence during the night, good propagation conditions exist from 3 MHz to 13 MHz from 0:00 UTC to 7:00 UTC, because all the ionic recombination have been done and the ionosphere is at a steady state. As the sunrise tends to be sudden, likewise is the change to the day region at 7:00 UTC.

2. The day region. It lasts from sunrise (7:00 UTC) to sunset (around 17:00 UTC). The absorption of the D-layer makes propagation of frequencies below 10 MHz impossible. High SNR values can be measured from 10 MHz to 17 MHz from 7:00 UTC to 11:00 UTC, and it changes from 13 MHz to 23.5 MHz from 11:00 UTC to 18:00 UTC. Such a daytime propagation is largely supported by the highly ionization conditions and hence the F2 layer existence.

A clear result is that high frequencies up to 23.5 MHz can be propagated during high solar radiation hours, whereas no data at higher frequencies were gathered during the whole survey.

5.6.2 Wideband Sounding

As explained in Section 5.5, this analysis focuses on estimation of scattering function, SNR, composite multipath spread, composite Doppler spread, propagation time, and Doppler frequency shift.

SNR Calculation

An estimation of the wideband SNR derived from the scattering function as computed in Equation 5.14, is depicted in Figure 5.14. As expected, there are no significant differences between the wideband and the narrowband SNR estimation of Figure 5.11.

Composite Multipath Spread

The composite multipath spread is calculated following Equation 5.11 and the results are shown in Figure 5.15. Each subfigure represents the multipath spread values obtained over 4 consecutive hours as a function of the sounding frequency. Looking at a summary of data in Table 5.3, we can state that multipath spread takes values from 3.1 ms to 0.2 ms, decreasing with increasing frequency. The maximum multipath spread values, ranging from 2.7 ms to 3.2 ms have been obtained:

1. In the frequency range from 6 MHz to 14 MHz from 20:00 UTC to 23:00 UTC.

2. In the frequency range from 3 MHz to 14.5 MHz from 00:00 UTC to 03:00 UTC.

3. In the frequency range from 8.5 MHz to 12 MHz at 8:00 UTC, just after sunrise.

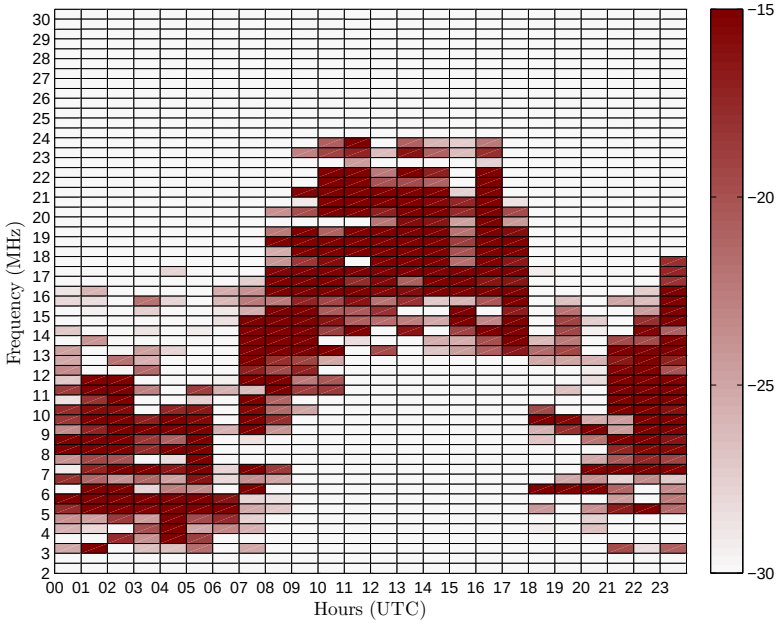

Figure 5.14: Wideband SNR estimation as a function of the hour and the frequency of sounding.

The minimum multipath spread of 0.25 ms occurred during the day from 12:00 UTC to 17:00 UTC, in a higher frequency range from 12.5 MHz to 23 MHz. The measurements from 18:00 UTC to 11:00 UTC and 4.5 MHz to 16.5 MHz agree with the results presented by [*Vilella et al.*(2008)].

Table 5.3: Degradation of the multipath spread values.

Hour (UTC)	Start F_c (MHz)	End F_c (MHz)	Max τ_{eff} (ms)	Min τ_{eff} (ms)
05:00	3.5	10.5	2.1	0.4
07:00	8	17	1.6	0.3
08:00	8.5	19.5	2.5	0.2
09:00	10.5	19.5	1.9	0.2
10:00	13.5	23.5	1.7	0.4
11:00	13.5	22.5	1.5	0.25
15:00	10.5	21	2.1	0.2
23:00	5	18.5	3.1	0.6

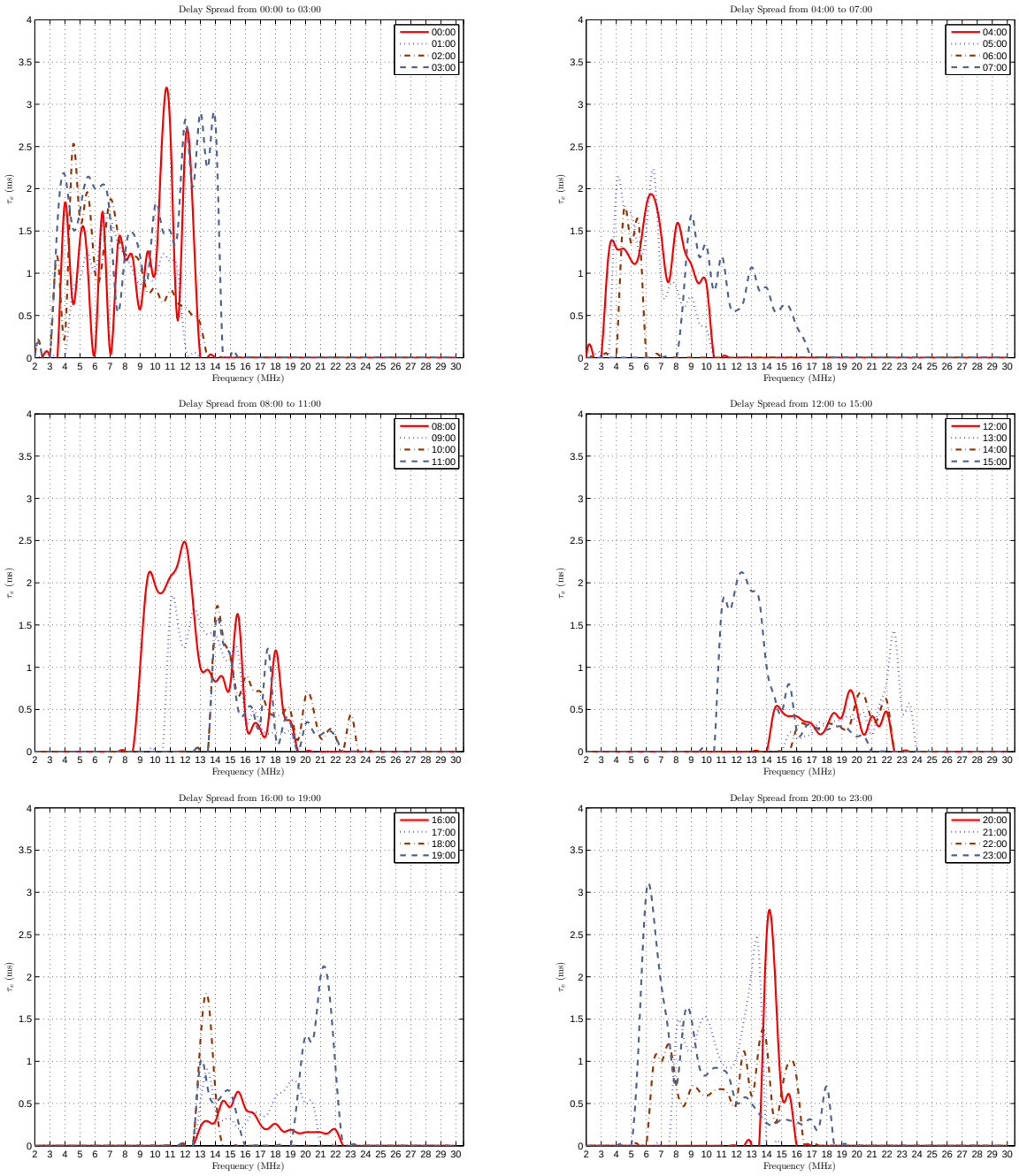

Figure 5.15: The multipath spread measurements as a function of the sounding frequency and hour.

Composite Doppler Spread

The composite Doppler spread is calculated as explained in Section 5.5 and the results are shown in Figure 5.16. Maximum Doppler spread values from 2 Hz to 2.4 Hz have

been measured in the frequency range from 3.5 MHz to 14 MHz from 00:00 UTC to 04:00 UTC.

The Doppler spread values decreased from 2.1 Hz to 0.6 Hz with increasing frequency form 8.5 MHz to 23 MHz, during the time period from 08:00 UTC to 11:00 UTC. As shown in Table 5.4, minimum Doppler spread values from 0.1 Hz to 0.24 Hz have been measured during the day from 10:00 UTC to 17:00 UTC, in a higher frequency range from 15 MHz to 22.5 MHz.

It is possible to have a better overview of the behavior of the channel looking at the scattering function, that combines information from both multipath spread and Doppler spread in a single graph. The scattering function for several sounding frequencies and hours is shown in Figure 5.17. As it has been previously mentioned, the ionospheric channel is wide spread both in time and frequency during the night at lower frequencies, while becomes narrow spread in both time and frequency during the day at higher frequencies.

Table 5.4: Minimum Doppler spread values.

Hour (UTC)	F_c (MHz)	Min ν_{eff} (Hz)
10:00	19.5	0.3
11:00	18	0.2
12:00	17.5	0.3
13:00	22.5	0.28
14:00	21	0.4
15:00	19	0.4
16:00	15	0.1
17:00	20	0.2

5.6.3 Propagation Time

The propagation time is the time it takes for the radio wave to travel from SAS to OE (12700 km). An initial approach, assuming a propagation speed equal to $3 * 10^8$ m/s (free space), is:

$$T = 12700/3 * 10^8 = 42.3\ ms \tag{5.15}$$

In practice, we should expect slightly lower propagation speeds, leading to higher propagation times. If we use VOACAP predictions as a first approach, we get propagation times ranging from 42.8 ms to 45.8 ms. In order to measure the propagation time, we have adapted the method mentioned by [*Davies*(1990)] for measuring the time delay of the first pulse of the received signal. As we are not transmitting RF pulses but PN modulated signals, the time delay of the first correlation peak has been measured. An accurate time reference is needed both in the transmitter and the receiver side, so a new GPS unit with a PPS signal with an accuracy of 1μs is used.

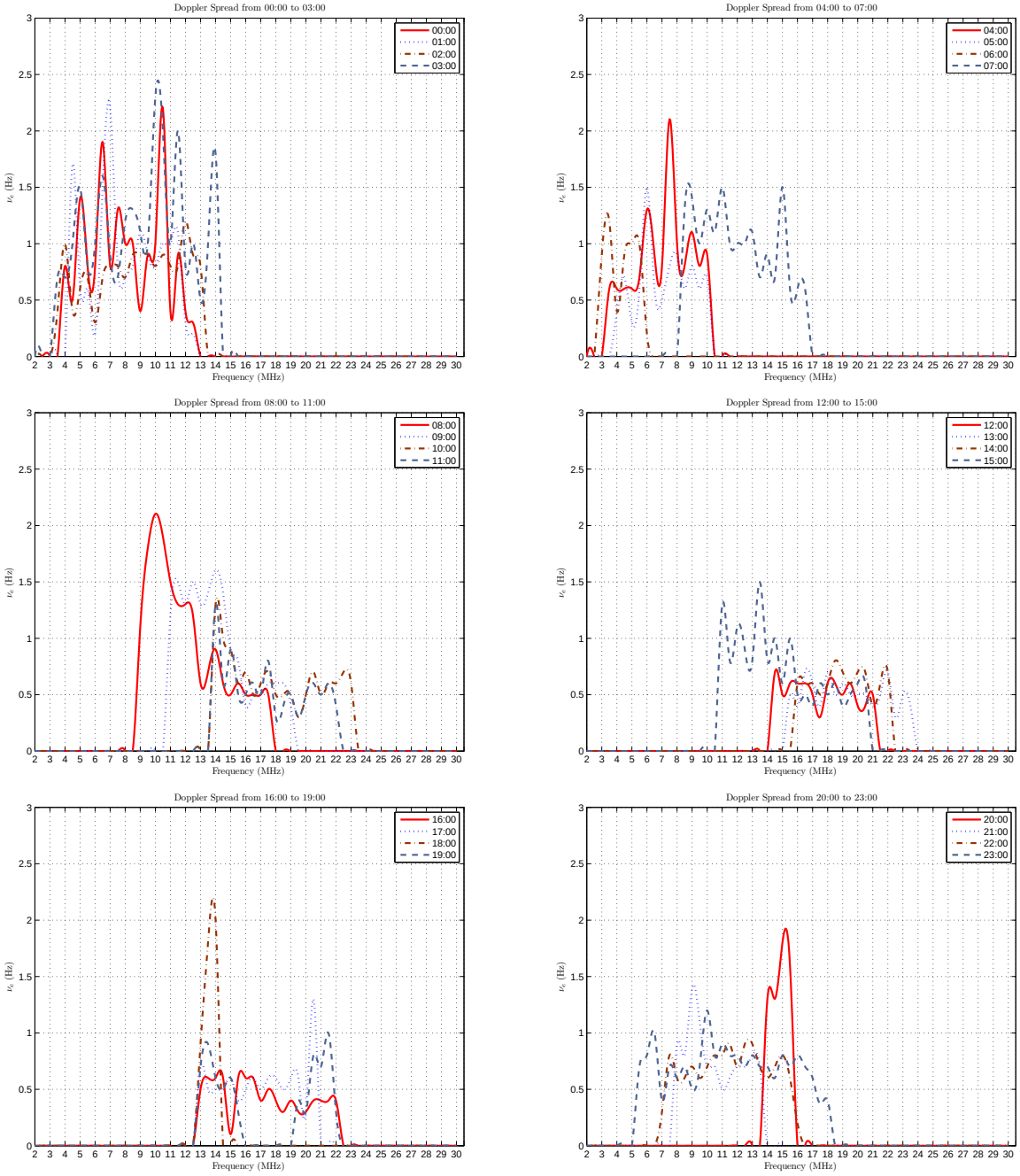

Figure 5.16: The Doppler spread measurements as a function of the sounding frequency and hour.

The average, maximum and minimum values of the propagation time as a function of frequency is shown in Figure 5.18. As expected, higher average values from 45 ms to 50 ms are obtained. The variation from minimum to maximum values at each frequency is due to the different reflection heights, propagation modes, e.g., four or five hops. In

all cases, the real transmission time is slightly higher than the VOACAP prediction.

5.6.4 Doppler Frequency Shift

Doppler frequency shift arises due to the mobility in the source or destination or any other objects in between that may change the length of the ray as mentioned by [*Clarke et al.*(1978)]. This can be formulated by a shift in the carrier frequency as follows:

$$f_D(t) = \frac{\nu_a(t)}{\lambda} \tag{5.16}$$

where $\nu_a(t)$ is the relative speed of the movement and λ is the wavelength. In our case both the transmitter and the receiver are static, while the reflective ionospheric layers are in continuous movement during the day.

In order to have enough accuracy in our measurement system, an OCXO with a frequency precision of $\pm 30.10^{-9}$ was installed during the 2009/2010 survey. The average Doppler frequency shift as a function of time of day is shown in Figure 5.19. As expected, the Doppler shift changes are directly related to the changes of ionization of the layers due to the solar radiation. Generally, larger ionization results in reflections at lower heights and shorter ray paths. During the day, Doppler shifts values increase from -4 Hz at 07:00 UTC to 1.2 Hz at 20:00 UTC. During the night, the values are ranging from -0.5 Hz to 1.2 Hz from 20:00 UTC to 06:00 UTC.

We would like to highlight the sudden Doppler shift variations at sunrise. As seen in Figure 19, Doppler shift values suddenly change from -0.5 Hz at 06:00 UTC to -4 Hz at 07:00 UTC, due to the fact that sunrise takes only 24 minutes along the 4 reflection hops as mentioned by [*Vilella et al.*(2008)]. On the contrary, the sunset takes 4 hours and 24 minutes along the 4 hops. That is the reason for the smooth changes from 17:00 UTC to 21:00 UTC.

5.7 Concluding Remarks

In this paper, a comprehensive analysis of the channel sounding data gathered from the 2009/2010 campaign between the Spanish Antarctic Station and Ebro Observatory has been presented. Both narrowband and wideband channel parameters have been estimated in the whole HF band, and 24 hours per day, and some new parameters such as the propagation time and the Doppler frequency shift have been included in the set of measurements.

1. Narrowband Sounding

   The windowing filtering techniques have proven to be a key issue in refining the received narrowband signals, being the Kaiser window the best option. We have also introduced a new method to estimate the channel availability, based on the time framing technique in order to mitigate the effect of interfering signals. Concerning the channel availability, two main time and frequency regions have

been observed. First, a relevant region of availability exists from 7:00 UTC to the sunset in a frequency range from 10 MHz to 23 MHz which had not been analyzed before. Second, during the night from 20:00 UTC to 06:00 UTC, the frequencies from 3.5 MHz to 16 MHz show the best degree of availability, in accordance with the results of [*Vilella et al.*(2008)].

2. Wideband Sounding

   The multipath spread values show clear differences between night and day. The maximum multipath spread values have been obtained from 20:00 UTC to 3:00 UTC and just after sunrise at frequencies lower than 14 MHz, while the minimum values were observed during the day from 12:00 UTC to 17:00 UTC, in a higher frequency range from 12.5 MHz to 23 MHz.

3. Propagation Time

   Average propagation time values ranging from 45 ms to 50 ms have been measured which is slightly higher than the theoretical one. The variation of the propagation time depend on the propagation path of the wave.

4. Doppler Frequency Shift

   The motion of the ionospheric layers causes a Doppler frequency shift, that varies from -4 Hz to 1.2 Hz during the day and from -0.5 Hz to 1.2 Hz during the night. It is remarkable the sudden change at 07:00 UTC due to the sunrise.

5.8 Acknowledgments

This work has been funded by the Spanish Government under the projects CGL2006-12437-C02-01, CTM2008-03536-E, CTM2009-13843-C02-02 and CTM2010-21312-C03-03. A. G. Ads has an FPI grant of BES-2008-00948 from the Spanish Government. The authors would like to thank D. Altadill for their important guidance.

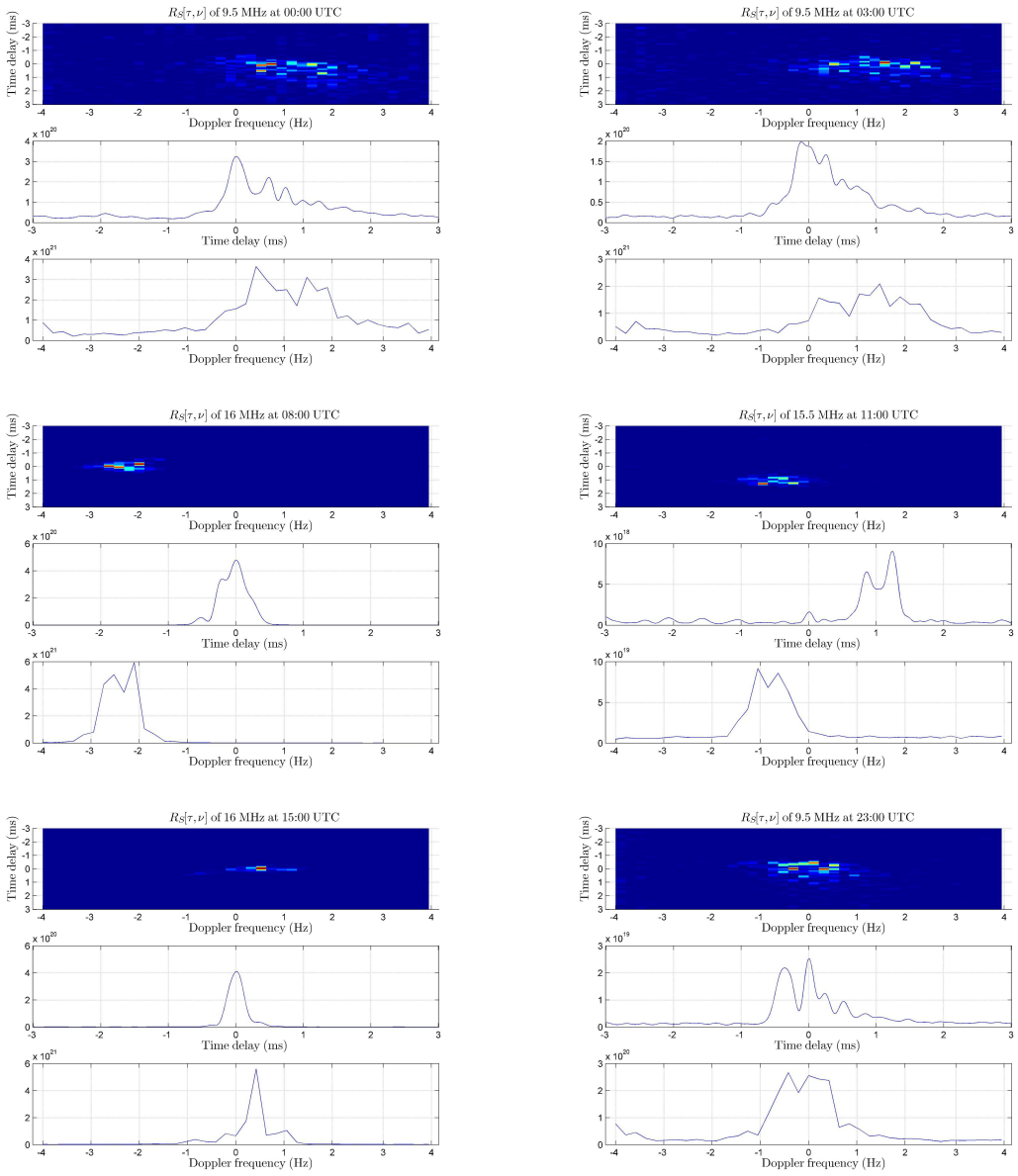

Figure 5.17: Scattering function and its corresponding delay time and Doppler frequency for different sounding frequencies and times.

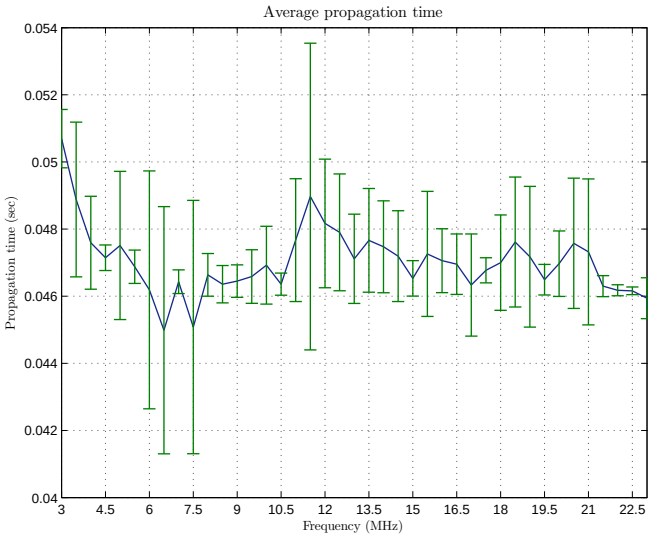

Figure 5.18: Average propagation time as a function of sounding frequencies.

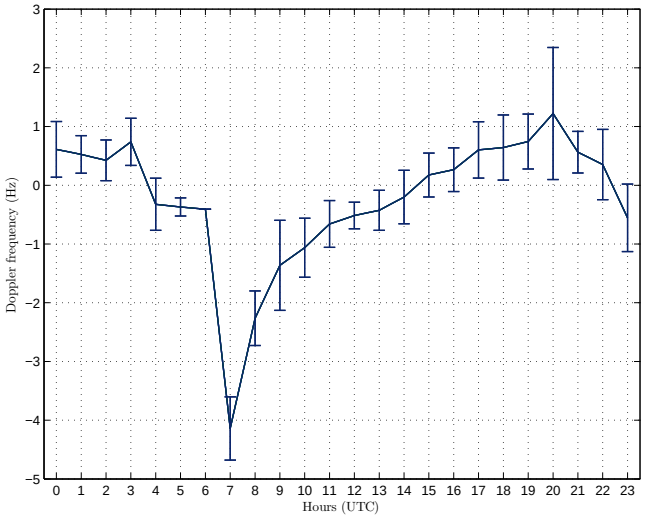

Figure 5.19: Average Doppler frequency shift during the 24 hours.

Bibliography

[*Angling et al.*(1997)] Angling, M. J., and N. C. Davies (1997), On an ionospheric channel simulator driven by measurements of multipath and Doppler spread, in *Proc. IEE Colloquium on, Propagation Characteristics and Related System Techniques for Beyond Line-of Sight Radio, 1997(390)*, pp. 4(1–6), doi: 10.1049/ic:19971351.

[*Angling et al.*(1998)] Angling, M., P. Cannon, N. Davies, T. Willink, V. Jodalen, and B. Lundborg (1998), Measurements of Doppler and Multipath spread on oblique high latitude HF paths and their use in characterizing data modem performance, *Radio Sci., 33(1)*, pp. 97–107, doi: 10.1029/97RS02206.

[*Bergadà et al.*(2009)] Bergadà, P., M. Deumal, C. Vilella, J. R. Regué, D. Altadill, and S. Marsal (2009), Remote Sensing and Skywave Digital Communication from Antarctica, *Sensors, 9*, pp. 10136–10157, 2009, doi: 10.3390/s91210136.

[*Blackman et al.*(1959)] Blackman, R. B., J. Tukey, and J. Wilder(1959), Particular Pairs of Windows, *The Measurement of Power Spectra, From the Point of View of Communications Engineering,* pp. 98–99, Dover Publications, New York, USA.

[*Clarke et al.*(1978)] Clarke, R. H., and D. V. Tibble (1978), Measurement of the elevation angles of arrival of multicomponent H.F. skywaves, in *Proc. Institution of Electrical Engineers, 125(1)*, pp. 17–24, January, 1978, doi: 10.1109/ICCSN.2009.55.

[*Davies*(1990)] Davies, K. (1990), *Ionoshperic Radio,* Peter Peregrines Ltd., London, UK.

[*Fitzgerald et al.*(1999)] Fitzgerald, J., P. Argo, and R. Carlos (1999), Equatorial spread F effects on an HF path: Doppler spread, spatial coherence, and frequency coherence, *Radio Sci., 34(1)*, pp. 167–178, doi: 10.1029/1998RS900013.

[*Goodman et al.*(1997)] Goodman, J., J. Ballard, and E. Sharp (1997), A long-term investigation of the HF communication channel over middle- and high-latitudes paths, *Radio Sci., 32(4)*, pp. 1705–1715, doi: 10.1029/97RS01194.

[*Houpis et al.*(1991)] Houpis, H., and L. Nickisch (1991), An ionospheric propagation prediction method for low latitudes and mid-latitudes, *Radio Sci., 26(4)*, pp. 1049–1057, doi: 10.1029/91RS00491.

[*Kaiser*(1974)] Kaiser, J. F. (1974), Nonrecursive Digital Filter Design Using the I_0 − sinh window function, in *Proc. IEEE International Sump. on, Circuits and Systems,* pp. 20–23, April, 1974.

[*Mastrangelo et al.*(1997)] Mastrangelo, J. F., J. J. Lemmon, L. E. Vogler, J. A. Hoffmeyer, L. E. Pratt, and C. J. Behm (1997), A New Wideband High Frequency Channel Simulation System, *IEEE Transactions on Communications, 45(1)*, pp. 26–34, doi: 10.1109/26.554283.

[*Nissen et al.*(2003)] Nissen, C. A., and P. A. Bello (2003), Measured channel parameters for the disturbed wide-bandwidth HF channel, *Radio Sci., 38(2)*, pp. 1023, doi: 1029/2002RS002746.

[*Oppenheim et al.*(1989)] Oppenheim, A. V., and R. W. Shafer (1989), *Discrete-time Signal Processing,* Prentice Hall, pp. 444–447, Upper Saddle River, New Jersey, USA.

[*Parsons*(2000)] Parsons, J. D. (2000), *Mobile Radio Propagation channel,* John Wiley and Sons, New York, USA.

[*Proakis*(2001)] Proakis, J. (2001), *Digital Communications,* pp. 807, McGraw-Hill.

[*Vilella et al.*(2005)] Vilella, C., D. Miralles, J. Socoró, L. Pijoan, and R. Aquilué (2005), A new sounding system for HF digital communications from Antarctica, in *Proc. International symposium on, Antennas and Propagation,* pp. 419–422, August, 2005, Seoul, South Korea.

[*Vilella et al.*(2006)] Vilella, C., P. Bergadà, M. Deumal, L. Pijoan, and R. Aquilué (2006), Transceiver architecture and Digital Down Converter design for long distance, low power HF ionospheric links, in *Proc. Ionospheric Radio Systems and Techniques,* pp. 95–99, London, 18- 21 July, doi: 10.1049/cp:20060311.

[*Vilella et al.*(2008)] Vilella, C., D. Miralles, and L. Pijoan (2008), An Antarctica-to-Spain HF ionospheric radio link: sounding results, *Radio Sci., 43*, RS4008, doi: 10.1029/2007RS003812.

[*Vogler et al.*(1993)] Vogler, L. E., and J. A. Hoffmeyer (1993), A model for wideband HF propagation channels, *Radio Sci., 28(6)*, pp. 1131–1142, doi: 10.1029/93RS01607.

[*Warrington et al.*(1998)] Warrington, E. M. (1998), Observations of the directional characteristics of ionospherically propagated HF radio channel sounding signals over two high latitude paths, *IEE Proceedings, Microwaves, Antennas and Propagation 145(5)*, pp. 379–385, October, 1998, doi: 10.1049/ip-map:19982068.

[*Warrington et al.*(2003)] Warrington, E. M., and A. J. Stocker (2003), Measurements of the Doppler and Multipath spread of the HF signals received over a path oriented along the midlatitude trough, *Radio Sci., 38(5)*, pp. 1080, doi: 10.1029/2002RS0028 15.

[*Watterson et al.*(1970)] Watterson, C. C., J. Juroshek, and W. D. Bensema (1970), Experimental configuration of an HF channel model, *IEEE Transactions on Communication Technology, 18(6)*, pp. 792–803, December, 1970, doi: 10.1109/TCOM.1970.-1090438.

Chapter 6

Digital transmission techniques for a long haul HF link: DSSS versus OFDM

P. Bergadà[1], R.M. Alsina-Pagés[1], J.L. Pijoan[1], M. Salvador[1], J.R. Regué[1], D.Badia[1] and S. Graells[1]
[1] GRECO-La Salle, Universitat Ramon Llull, Barcelona, Spain

Radio Science, Vol. 49, 1-13, doi:10.1002/2013RS005203, 2014
Received 22 November 2013; accepted 26 June 2014; accepted online 30 June 2014.

This paper presents two digital transmission techniques for long haul ionospheric links. Since 2003 we have studied the HF link between the Antarctic Spanish Base, Juan Carlos I, and Spain and we have described the link in terms of availability, signal to noise ratio (SNR) and delay and Doppler power profile. Based on these previous studies we have developed a test bed to investigate two digital transmission techniques, i.e. Direct Sequence Spread Spectrum and Orthogonal Frequency Division Multiplexing, which can provide a low power, low rate ionospheric data link from Antarctica. Symbol length, bandwidth and constellation are some of the features that are analyzed in this work. Data gathered from the link throughout the 2010/2011 and 2011/2012 Antarctic surveys show that spread spectrum techniques can be used to transmit data at low rate when the channel forecast is poor but when the channel forecast is good multicarrier techniques can be used to transmit sporadic bursts of data at higher rate.

6.1 Introduction

Much has been achieved during the last two decades to improve the spectral efficiency of new mobile communication services. Although there are many differences between the UHF and HF bands, skywave narrowband HF propagation can be modeled as a slow fading multipath channel [*Gherm et al.*(2005)]. Multiple paths arise from the refraction of HF waves in the different layers of the ionosphere and from multi-hop propagation. Moreover, within each path the wave splits into two modes, which are called ordinary (O) and extraordinary (X). These two phenomena cause frequency selectivity and degrade the signal to noise ratio, which can be combated with wideband signals plus coding and interleaving.

Many of the modulation and coding techniques applied to third and fourth generation mobile communications can be adapted to the HF band. Frequency Hopping (FH) [*Andersson*(1994)] and Direct-Sequence (DS) [*Wagner et al.*(1989)] were the first spread spectrum (SS) modulations proposed for the HF band. FHSS and DSSS are intrinsically designed to perform well against narrowband interference as well as to benefit from frequency diversity in frequency selective channels, which are key issues in the HF channel. Therefore, they have been adopted in the robust mode of several NATO standards [*NATO*(1999)].

Orthogonal Frequency Division Multiplexing (OFDM) is another successful technique that uses multicarrier transmission to overcome the problems of multipath channels. This includes new constant envelope OFDM modulation schemes, e.g. Single Carrier OFDM [*Myung and Goodman*(2008)] and Constant Envelope OFDM [*Nieto*(2008)], which are well adapted to HF channels.

Military research uses OFDM as a communication technique in the HF channel. MIL-STD-188-110A [US Department of Defense (1991)] describes a single tone, and two multitone (16-tone and 39-tone) OFDM based modem with a maximum bit rate of 2400 bps. In later improvements, [*M.C. Gill and Ball*(1995)] applied trellis-coded modulation to create redundant bits for error control purposes. The use of convolutional trellis codes combined with interleaving resulted in a 300 to 3600 bps modem that provided immunity to impulsive noise and narrowband interference.

High data rate HF systems typically need signal to noise ratios (SNR) greater than 20 dB to properly work in a 3-25 kHz channel. With a 25 dB SNR, bit rates up to 16 kbps for a BER=10^{-2} can be achieved [*Zhang et al.*(2005)]. Bandwidths up to 24 kHz have been standardized and bit rates up to 120 bps may be achieved in optimum conditions [*Furman et al.*(2012), *Johnson*(2009)], and greater bandwidths out of standardization are also being tested [*Dorazio et al.*(2007)]. Moreover, the use of several non-contiguous 3 kHz channels has also been investigated [*Smith et al*(2001)]. In contrast, NATO has standardized a serial-tone modem (STANAG 4415) for severely degraded HF radio links which is able to work at negative SNR in a 3 kHz bandwidth [*NATO*(1999)]. The penalty is a low bit rate. STANAG 4415 uses Walsh codes of length 32 achieving 75 bps in a 3 kHz bandwidth. It uses a 4.8 second interleaver combined with a rate $\frac{1}{2}$ convolutional encoder [*NATO*(1999)].

It is well-known that HF communication is a good option for very long radio links

where no other infrastructure (e.g. satellite) is available. In that regard, our research group has been investigating the HF channel (herein referred to the Antarctic channel) between the Spanish Antarctic Station (SAS) on Livingston Island (62.6° S, 60.4° W) and the Ebro Observatory (EO) in Roquetes (40.8° N, 0.5° E), Spain. We have sounded this channel throughout a whole solar cycle to characterize the availability, SNR, multipath and Doppler power profile [*Vilella et al.*(2008)], we have linked vertical soundings along the path with oblique soundings [*Vilella et al.*(2009)]; and we have developed a low power, adaptive communication system for data transmission from remote sensors.

Ours is a very long transmission path (12700 km, 4-5 hops [37]), which together with a transmitter power of only 200 W and very simple antennas at the transmission and reception sites, due to environmental restrictions. This results in very low or even negative SNR at the receiver [*Vilella et al.*(2008)].

Even the robust mode of STANAG 4415 would have problems to work in this scenario. STANAG 4415 is designed to work in severe scenarios of Doppler spread (i.e. up to 20 Hz) and delay spread (i.e. up to 10 ms) achieving a $BER < 10^{-4}$. However, STANAG 4415 requires SNRs above -1 dB to 0 dB (3 kHz) in a dual path channel. The Antarctic channel SNR is typically lower than -6 dB, with Doppler spreads up to 2 Hz and the maximum delay spread is 3 ms [*Ads et al.*(2012)]. Consequently, we have concluded that STANAG 4415 is not well matched to the Antarctic channel. To mitigate the channel STANAG 4415 would need to be modified and use longer symbols (or equivalently narrower frequency symbols) in order to cope with such a low SNR; however, then it would not perform well in fast fading channels.

Consequently, we have designed a physical layer adapted to low SNR, time and frequency dispersive channels and high interference occurrence, based on both DSSS [9] and OFDM [*Bergadà et al.*(2009)] techniques. Due to the distance, the low transmitted power and antenna constraints the received SNR is low. As a result, the transmitted bandwidth must be very narrow and only low bit rates can be achieved; hence the spectral efficiency is key. The challenge is to increase the efficiency of the link in the available bandwidth.

In this study we explore the use of DSSS and OFDM techniques for very long and power limited HF links, using various bandwidths and bit rates, taking into account the outcomes and impairments described in [*Vilella et al.*(2008)] and [*Ads et al.*(2012)].

6.2 Link and System Description

One of the main objectives of our work is to establish a permanent HF link between the SAS and the EO. The propagation conditions between both sites vary daily, seasonally and with the solar cycle. The first oblique soundings of the Antarctic channel were performed during the 2003/2004 survey, and since then, three software defined radio (SDR) hardware system upgrades have been installed at both the transmitter and the receiver sides.

The last generation platform was installed in the 2009/2010 survey and all the

results in this paper are based on this upgrade. The system is currently able to operate over the full HF band (from 3 MHz to 30 MHz), 24 hours a day. The system combines both channel sounding periods and data transmission periods. Each hour the whole HF band is sounded in narrowband and wideband mode for 40 minutes and data is transmitted for 10 minutes; see [*Ads et al.*(2012)] for a more detailed explanation of the system and the sounding process.

6.3 Test Design

In the design of an HF radio modem able to work on very long links with low transmission power, several important issues need to be considered. First, the selection of the best carrier frequency must consider the whole path, and satisfy the constraints of the most restrictive hop. Second, once the transmission power and the antenna are selected, the maximum bandwidth will be fixed by the required SNR at the receiver. If this bandwidth is higher than the coherence bandwidth of the channel (i.e. 150-500 Hz in our case [*Ads et al.*(2012)]) the use of wideband modulations that are robust against frequency selective channels may be considered. DSSS and OFDM are the most well-known schemes for slow fading, multipath channels such as the ionospheric channel [*Proakis*(2000)].

In this paper we compare the behavior of different transmission schemes based on DSSS and OFDM techniques and we present some conclusions that derive from the data gathered during the 2010/2011 and 2011/2012 Antarctic surveys. Previous results, [*Bergadà et al.*(2009)], showed preliminary conclusions supported on a reduced frequency and time range.

6.3.1 Direct Sequence Spread Spectrum

In this section we explore DSSS [*Proakis*(2000), *Peterson et al.*(1995)] as a possible solution to the frequency selectivity of the Antarctic channel.

When using DSSS techniques, the signal is spread over a wide bandwidth, proportional to a pseudo noise (PN) chip rate, which provides robustness against narrowband interfering signals. A drawback of DSSS is the low spectral efficiency symbols that may need to achieve good bit error rate (BER) performance. Its main advantage is that no channel estimation is needed.

We transmitted DSSS signals with different symbol lengths and bandwidths by changing the chip rate and the PN sequence length in order to determine which of the DSSS parameters best match the Antarctic channel. We have determined the maximum bit rate with an acceptable BER, assuming that no channel coding is used. Given that the channel is time varying, we have also determined the upper bound of the symbol period, this being limited by the coherence time of the channel.

DSSS Symbol Design

DSSS spreads a signal composed by symbols of length T by means of a PN sequence $c(t)$. The PN sequence is formed by L chips of length T_c with good autocorrelation and crosscorrelation properties, such that $L \cdot T_c = T$. L is known as the spreading factor and is the ratio between the spread bandwidth and the original signal bandwidth.

DSSS Test Details

The DSSS tests were conducted using various bandwidths, bit rates, sequence lengths and samples per xip (at fixed sample rate, i.e. 100 kHz). These four variables were modified according to previous knowledge of the channel [*Ads et al.*(2012)]:

- Bandwidth (BW): from 250 Hz to 20 kHz,
- Bit rate: from 1.97 bps to 645 bps,
- PN sequence length: 31, 63 and 127 chips,
- Samples per chip: 5, 10, 20, 50, 100, 200 and 400.

We used Gold spreading sequences [*Gold*(1968)] with length $2^n - 1$ and we chose a minimum sequence length of 31, because shorter sequences could not be detected in such a noisy scenario. Table 6.1 details DSSS tests, including bandwidth, symbol length T, bit rate and spectral efficiency. The outcomes are based on average of 148 blocks of data. Each block of data is composed of 21 experiments (see table 6.1) and for each experiment 25 DSSS symbols were transmitted. Figure 6.1 describes the data block design.

Previous work on this channel [*Ads et al.*(2012)], showed that the coherence time of the Antarctic channel ranges from 500 ms to 1 s depending on the time of day, so some of the combinations enumerated in table 6.1 (i.e. 400 samples per chip and 127 chips per sequence) go beyond the coherence time, and hence should show worse performance than other combinations with shorter T. Conversely, those codes with low samples per chip and a short sequence length (i.e. 5 samples per chip and 31 chips per sequence) exhibit a low probability of detection and hence a poor performance. Between these two points we should be able to show optimum combination of bandwidth and PN sequence length.

We note that none of the combinations provide a data throughput sufficient to support real time voice or image transmission but all are sufficient for our application [*Bergadà et al.*(2009)].

Timing Synchronization and Channel Estimation

Timing synchronization is a critical task in a DSSS receiver [*Proakis*(2000)]. The DSSS modulation described in this paper does not use any preamble but uses a number of sequences for synchronization purposes. The longest tests (i.e. PN sequence length of 127 chips and 400 samples per chip) are located at the beginning of the data stream,

PN seq. length	BW [kHz]	T [ms]	Bit rate [bps]	Spc. Eff. [bps/Hz]	CDF (10%)	CDF (30%)	CDF (50%)	CDF (70%)
31	20	1.5	645.16	0.032	0.2910	0.3330	0.3330	0.3740
31	10	3.1	322.58	0.032	0.2490	0.3330	0.3740	0.3740
31	5	6.2	161.29	0.032	0.2910	0.3330	0.3740	0.3740
31	2	15.5	64.52	0.032	0	0.0830	0.2490	0.3330
31	1	31.0	32.26	0.032	0	0	0.1240	0.2490
31	0.50	62.0	16.13	0.032	0	0	0.1240	0.2490
31	0.25	124.0	8.06	0.032	0	0	0.0830	0.2490
63	20	3.1	317.46	0.016	0.2910	0.3740	0.3740	0.3740
63	10	6.3	158.73	0.016	0.2910	0.3330	0.3740	0.3740
63	5	12.0	79.36	0.016	0	0.1660	0.2910	0.3330
63	2	31.0	31.75	0.016	0	0.0410	0.0830	0.2080
63	1	63.0	15.87	0.016	0	0.0410	0.1240	0.2910
63	0.50	126.0	7.94	0.016	0	0	0.1240	0.2490
63	0.25	252.0	3.97	0.016	0	0.1240	0.2490	0.3330
127	20	6.3	157.48	0.007	0.2910	0.3330	0.3330	0.3740
127	10	12.7	78.74	0.007	0.1660	0.2910	0.3330	0.3740
127	5	25.4	39.37	0.007	0	0.1240	0.2910	0.3330
127	2	63.0	15.75	0.007	0	0.0410	0.1660	0.2910
127	1	127.0	7.87	0.007	0	0.0830	0.2080	0.2910
127	0.50	254.0	3.94	0.007	0	0.1660	0.2490	0.2910
127	0.25	507.0	1.97	0.007	0.1240	0.2490	0.3330	0.3740

Table 6.1: Detail of the PN sequence length, bandwidth, corresponding bit rate, symbol time and spectral efficiency. The spectral efficiency is always the inverse proportion of the PN sequence length when a constant sampling frequency is used, and the bit rate is the inverse of the symbol time since differential binary phase shift keying (DBPSK) is used. The values of Cumulative Distribution Function of the BER are given for all the designed combinations.

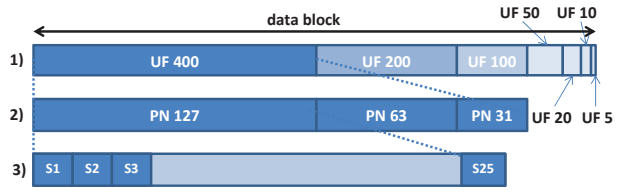

Figure 6.1: Graphic detail of the DSSS data block design. (row 1) The order depending on the bandwidth, which is a function of the number of samples per chip or Up Factor (UF). (row 2) The symbols are sorted considering the PN sequence length. (row 3) The detail of the 25 symbols used for each of the previously described combinations.

and fine time synchronization is performed by means of correlation [*Proakis*(2000)] over these symbols. The acquisition point is expanded to later PN sequences with higher bandwidth and shorter length of the same block. Tracking the channel performance and correcting the acquisition point are implemented when necessary while analyzing the data block.

The channel estimation and the demodulation process is performed by correlating the received signal by a delayed copy of the transmitted sequences, which is the best acquisition method in terms of BER outcomes [*Proakis*(2000)]. The downside of this method is the high computational cost at the receiver.

6.3.2 Orthogonal Frequency Division Multiplexing

We also explored OFDM because its spectral efficiency is higher than DSSS. The OFDM symbol must be adapted to the specific channel and its drawbacks of inter carrier interference (ICI) and peak to average power ratio (PAPR) must be carefully examined.

Our OFDM study transmitted symbols with different characteristics (i.e. time length, bandwidth, constellation and input back-off) over the 5 hop HF channel to find which OFDM design characteristics best fit the channel. In a frequency selective channel in our case with a coherence bandwidth $BW_c \in [150Hz, 500Hz]$ [*Ads et al.*(2012)] the OFDM bandwidth has to be wider than the BW_c to benefit from frequency diversity. However, this cannot be arbitrarily bigger because the larger the number of subcarriers the lower the SNR per subcarrier. Furthermore, intercarrier space cannot be arbitrarily wide because it must fulfill the Nyquist criterion to enable the equalizer to rebuild the channel. Moreover, the OFDM symbols also face a time variant channel (with coherence time $T_c \in [500ms, 1s]$ [*Vilella et al.*(2008)]) and hence when seeking high efficient symbols the length cannot be arbitrarily long, otherwise it may exceed the coherence time of the channel. Finally, the issue of saturation of the transmitter power amplifier has to be considered. This problem arises from the coherent addition of the OFDM signal components and is commonly dealt with reducing the drive to the transmitter.

OFDM Symbol Design

Orthogonal multicarrier modulation divides a single stream of symbols with length T into N_c streams with longer length N_cT. Let us define the OFDM symbol in the time domain, $x(t)$, as

$$x(t) = \frac{1}{\sqrt{N_c}} \sum_{k=0}^{N_c-1} X_k e^{j2\pi f_k t},\ -T_{cp} < t < N_cT, \tag{6.1}$$

where X_k are the frequency domain symbols that we allocate on each of the N_c subcarriers. The subcarriers are equally spaced $f_k = \frac{1}{N_cT}Hz$, which make them orthogonal. If we cyclically repeat $N_{cp} = T_{cp} \times f_{sampling}$ samples, [*Peled and Ruiz*(1980)], at the beginning of each OFDM symbol, it preserves orthogonality and immunity to time

dispersive channels whenever T_{cp}, which is the cyclic prefix guard time, exceeds the channel impulse response (τ_c). [*Ads et al.*(2012)] concluded that τ_c varies in time and frequency but it is always shorter than 3 ms in the Antarctic channel, hence the length of the cyclic prefix in all the multicarrier transmissions is fixed to 3 ms. The cyclic prefix appended to the start of each OFDM symbol reduces the spectral efficiency ($\rho_1 = \frac{N_c T}{N_c T + T_{cp}}$) of the system; however, a time symbol much longer than the cyclic prefix minimizes this drawback.

Frequency and Timing Synchronization

We have used two oven controlled crystal oscillators (OCXO) with high stability features ($\pm 0.1 ppb\,/^{\circ}\mathrm{C}$ and $\pm 30\,ppb$ versus aging per year), as well as ultra low jitter and phase noise features ($-125\,dBc/Hz|_{10Hz}@10MHz$). Consequently, no frequency synchronization techniques were necessary and no ICI effects were present, so only timing synchronization has been implemented. Due to the low SNR expected at the receiver, neither a technique based on pilot insertion in OFDM symbols [*Moose*(1994), *Schmidl and Cox*(1997)] nor a technique that exploits intrinsic redundancy based on the repetition of the N_{cp} samples of the cyclic prefix [*Tourtier et al.*(1993), *Sandell et al.*(1995)] is expected to work. Therefore, we designed a preamble composed of 40 maximal length pseudo noise sequences [*S. W. Golomb*(1967)], with good autocorrelation properties, 256 chips each and a bandwidth of $10\,kHz$. This preamble performs time acquisition at the beginning of the stream and time tracking every 12 seconds on average. It can also be used to estimate the channel impulse response, hence its wide bandwidth.

Clock deviation between transmitter and receiver causes a cumulative windowing position offset. However, the accumulated timing offset due to the tolerance of the clocks ($\pm 0.1\,ppb$) can be neglected because we transmit long symbols, with low number of subcarriers, and low complexity constellations.

Channel Estimation

In this OFDM study we coherently encoded the symbols of each subcarrier by means of a phase shift keying (PSK) modulation, although we could design a simpler and even a more efficient receiver without the pilot symbol overhead, as proposed by [*Engels and Rohling*(1995)] for Digital Audio Broadcasting. In extreme low SNR scenarios coherent modulation outperforms differential modulation since coherent decoding process includes channel state information [*Baum et al.*(1997)].

We defined a pilot pattern (see figure 6.2) to perform the channel estimation by means of the least squares algorithm and 2D cubic splines interpolation.

The pilot grid of the channel estimator must fulfill the two dimensional sampling theorem [*Hoeher et al.*(1997)] to properly track channel time and frequency variability. This means that pilot separation in frequency is upper bounded by:

$$N_F \leq \left\lfloor \frac{BW_c}{2\Delta f} \right\rfloor \tag{6.2}$$

and in time by:

$$N_T \leq \left\lfloor \frac{T_c}{2N_cT} \right\rfloor . \tag{6.3}$$

However, if we choose N_T and N_F close to 1 the efficiency of the system decreases and consequently decreases the SNR, as well as the throughput of the link. So, there is a trade-off between efficiency an performance that, taking into account previous studies on this channel [*Vilella et al.*(2008), *Ads et al.*(2012)], we have resolved as: *i*) $N_F = 1$ since the lower bound of the coherence bandwidth of the channel ($150Hz$) is similar to the subcarrier separation tested in this study, $\{11.0, 14.2, 20.0, 33.0, 100.0\}\,[Hz]$, and *ii*) $N_T = 6$ since the lower bound of the coherence time of the channel ($500\,ms$) is much higher than the length of the OFDM symbols, $\{10, 30, 50, 70, 90\}\,[ms]$. Consequently, the efficiency (ρ_2) and the loss of SNR ($1 - \rho_2$) can be computed as

$$\rho_2 = \frac{N_T \cdot N_F - 1}{N_T \cdot N_F}\Big|_{N_F=1, N_T=6} = 83.3\% \tag{6.4}$$

and the final efficiency of the system for each OFDM symbol length transmitted in this study (see table 6.2) is then:

$$\rho = \rho_2 \cdot \rho_1 \in [64.0,\ 80.6]\,\%. \tag{6.5}$$

Figure 6.2 depicts the pilot grid.

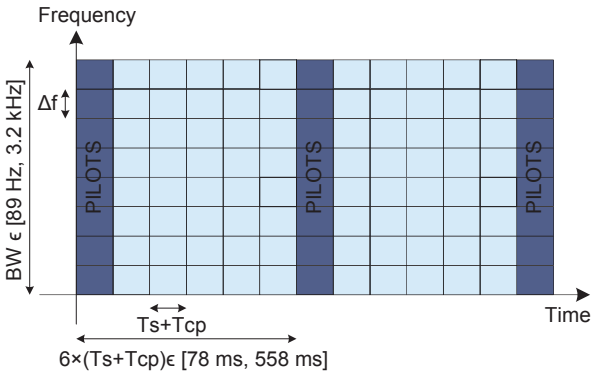

Figure 6.2: OFDM pilots lattice for channel estimation and equalization.

Peak to Average Power Ratio

It is well known that one of the most important drawbacks of multicarrier systems is the PAPR. The envelope variations cause the use of large back-off values in the amplifier, to avoid operating in the nonlinear region, and consequently reducing the mean transmitted power. In order to reduce the PAPR, we applied a soft limiter, which reduces the dynamic range of the signal at the expense of introducing both outband and inband distortion.

To reduce its effects we limited the number of subcarriers to less than 32 (i.e 8, 16, 32). Moreover, the constellations that we tested are simple (i.e. binary and quadrature phase shift keying (BPSK and QPSK)), which reduces the error probability introduced by the soft limiter. Finally, we oversampled each OFDM symbol to avoid aliasing by padding with zeros and taking longer inverse fast fourier transform (IFFT) windows. We gathered 33 blocks of OFDM symbols clipped at different values of Input Back-Off (IBO), i.e. the range from the mean power of the input signal to the clipping level, and we evaluated the distortion at the receiver by means of the Error Vector Magnitude (EVM) of the constellation. On each block we transmitted 120 symbols for each IBO value (i.e. 1, 3, 5, 7, 9 , 11 dB) with oversampling factors of 125, 250 and 500. It is worth noting that the lower the IBO the higher the in-band distortion and the higher the mean power of the transmitted signal. In a scenario with such a low SNR at the receiver side there is a trade-off between distortion and mean transmitted power. In other words, if we reduce the PAPR by applying a soft limiter with low IBOs we increase the in-band distortion and the mean transmitted power, whereas if we clip the signal at higher IBOs to reduce distortion we are at the same time reducing the mean transmitted power.

6.4 Test Results

The conclusions that we present in this section derive from the results gathered during the 2010/2011 and 2011/2012 Antarctic surveys. The carrier frequencies were spread across the whole HF band and transmissions were made over a wide range of hours. The figures of merit that we use in this paper are the Error Vector Magnitude (EVM) and the Differential Error Vector Magnitude (DEVM). EVM is defined in section 6.4.2 and DEVM represents the magnitude of the error between two received signals spaced one symbol apart in time:

$$DEVM_{rms} = \sqrt{|Actual| - |Ideal|}, \tag{6.6}$$

where *Actual* is the difference between two consecutive received symbols and *Ideal* is the difference between two ideal symbols. Due to the low number of received bits, these figures complement the information shown by the BER.

6.4.1 DSSS Outcomes

The DSSS modem was evaluated using the BER over the received data for every PN sequence length and bandwidth (see table 6.1). The DEVM is used to confirm the results already deduced from the BER. All BER and DEVM outcomes are computed using 148 blocks of 25 symbols for each experiment, as described in figure 6.1.

Bit Error Rate

The results concerning BER for all combinations of bandwidth and PN sequence length can be found in table 6.1. The results are shown by means of the cumulative distribution

function (CDF) of four probabilities of BER: 10%, 30%, 50% and 70%. The best configuration should expect a high probability value for a low BER. The best five combinations are the followings: *i)* Length 31 and $BW = 250\,Hz$, *ii)* Length 31 and $BW = 500\,Hz$, *iii)* Length 31 and $BW = 1000\,Hz$,*iv)* Length 63 and $BW = 500\,Hz$ and *v)* Length 63 and $BW = 1000\,Hz$.

All the results concerning length 127 show worse performance than these four combinations. These results are corroborated with the average BER (in %) evaluated over all tests and shown in figure 6.3 (left), as a function of the bit rate. The worst results in terms of average BER correspond to the widest bandwidths ($20\,kHz$ and $10\,kHz$) - related to high bit rates - and the longest possible symbol length (i.e. 400 samples per chip and 127 chips PN sequence). The best combinations (figure 6.3 (right)) correspond to: *i)* Length 31 and $BW = 250\,Hz$, *ii)* Length 31 and $BW = 500\,Hz$, *iii)* Length 63 and $BW = 500\,Hz$ and *iv)* Length 63 and $BW = 250\,Hz$ together with Length 63 and $BW = 2000\,Hz$.

The outcomes shown in table 6.1 and figure 6.3 agree on the best combinations of bandwidth and PN sequence length, which nearly have the lowest bit rate values. Moreover, figure 6.3 shows that when increasing the bit rate, the BER worsens nearly exponentially. Therefore, in order to increase the throughput of the link we think that a technique to increase the spectral efficiency ([9]) can be better than to decrease the symbol time.

In conclusion, the best results are achieved when combining a bandwidth of $250Hz$, $500Hz$ and $1000Hz$ with sequences of 31 and 63 chips. If we carefully study table 6.1 and figure 6.3 we see that the longest symbol period does not give the lowest BER. As a clear example, PN sequence length 127 and bandwidth $250\,Hz$ and $500\,Hz$ show the worst results. This is due to the long symbol time length, which exceeds the coherence time of the channel (ranging from 500 ms to 1 s with Gaussian distribution of probability [*Ads et al.*(2012)]) and leads to demodulation errors at the receiver. We have to take into account that one symbol time T can reach 500 ms when transmitting sequences with 127 chips and $250\,Hz$ of bandwidth, so high variations of the channel impulse response might occur while a single symbol is transmitted. Consequently, neither too short nor too long symbol length guarantee a good performance, hence the best results are given by intermediate symbol lengths.

Differential Error Vector Magnitude

In order to compare the results of all possible combinations of bandwidth and PN sequence length, the measure given is not EVM but DEVM. The DEVM, although based on the performance analysis of EVM, is independent of the entire symbol energy due to the differential evaluation.

On the left side of figure 6.4, we show the entire curve of CDF of DEVM of the nine best combinations obtained from BER analysis (see section 6.4.1). The best result is the curve that reaches the highest cumulative probability for a given value of DEVM. The best result is obtained with PN sequence length 31 and bandwidth $1000\,Hz$, followed by PN sequence length 31 and bandwidth $500\,Hz$ and the third best

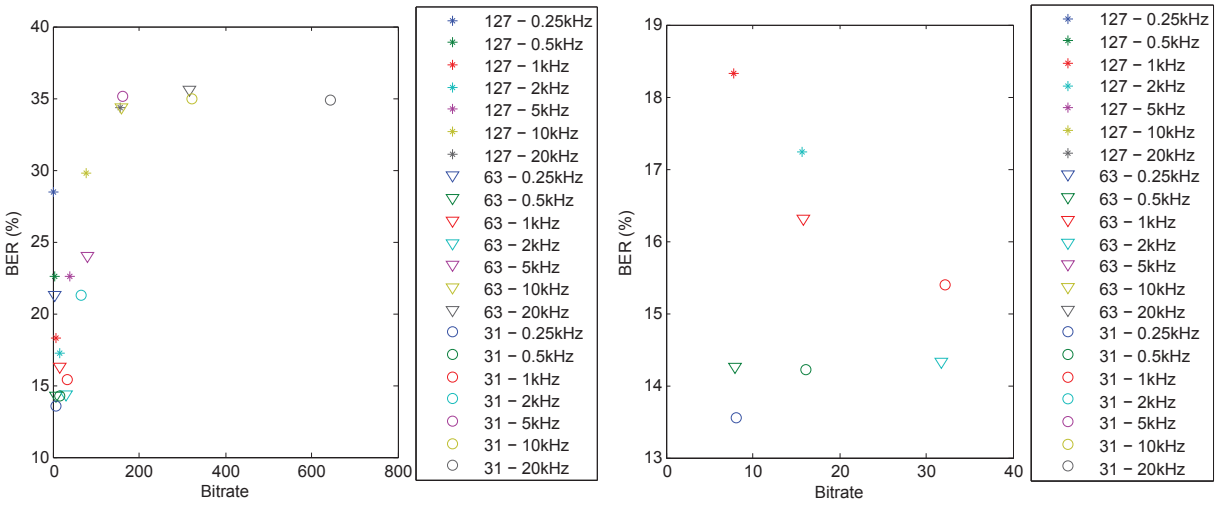

Figure 6.3: Average BER (in %) versus bit rate (in bps), for all the PN sequence lengths and bandwidth. On the left side the whole results, on the right side only the combinations showing the best BER results.

curve is PN sequence length 63 and bandwidth 500 Hz. So, the results of CDF of the DEVM corroborate the results obtained by means of BER in table 6.1, with minor variations.

6.4.2 OFDM Outcomes

The outcomes and conclusions related to OFDM tests are based on the reception of 33 blocks of 120 OFDM symbols for each experiment (i.e. symbol time length, number of subcarriers, constellation and IBO), which are all summarized in table 6.2.

Symbol Time Length

Concerning the symbol time length ($T_s = N_c T$) we tested 5 different values (see table 6.2). On one hand, we expect that shorter symbols have a poorer performance than longer symbols due to the loss of SNR (see equation 6.5) and also because the shorter the symbol length the wider the subcarrier separation and hence the worse the channel estimation. If we want to fulfill the Nyquist criterion in the frequency domain, when estimating the channel by means of OFDM pilot symbols (see section 6.3.2) at least two channel samples must be guaranteed inside the coherence bandwidth of the channel. We note that subcarrier separation in these tests ranges from 11 Hz to 100 Hz, which is inversely proportional to the symbol length ($T_s = \frac{1}{\Delta f}$), while the coherence bandwidth of the channel ranges from 150 Hz to 500 Hz. Moreover, the longest symbol lengths (i.e. 90 ms) must fulfill the Nyquist criterion in the time domain and guarantee at least two samples inside the time coherence of the channel, which ranges from 500 ms to 1 s. As depicted in figure 6.2 we estimate the channel every 6 symbols and hence

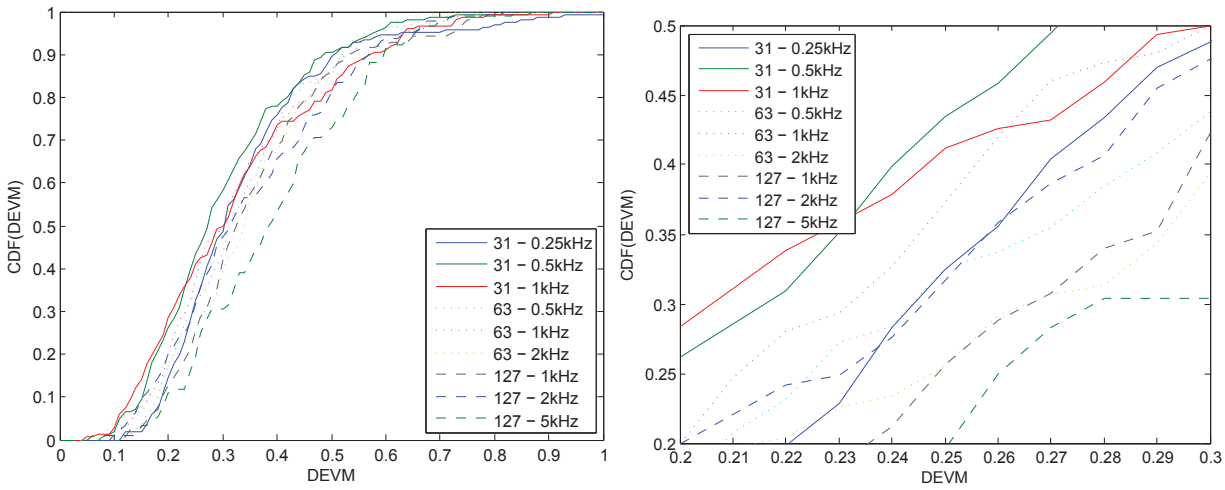

Figure 6.4: Cumulative Distribution Function of the DEVM, with the best combinations of the PN sequence lengths and bandwidth. On the left side the whole results for the nine best combinations, on the right side a detail of the evolution of the CDF(DEVM).

the sampling period of the channel ranges from 78 ms for the shortest symbols (10 ms) to 558 ms for the longest symbols (90 ms).

We present the outcomes of this section by means of the CDF of BER as well as by means of the root mean square of the EVM of the received symbols that can be defined as [*Forestier et al.*(2004)]

$$EVM_{rms} = \sqrt{\frac{\frac{1}{N}\sum_{r=1}^{N}|S_{ideal,r} - S_{meas,r}|^2}{\frac{1}{N}\sum_{r=1}^{N}|S_{ideal,r}|^2}}, \tag{6.7}$$

where $S_{ideal,r}$ is the ideal normalized point of the constellation for the r^{th} symbol, $S_{meas,r}$ is the normalized r^{th} symbol in the stream of measured symbols and N is the number of unique symbols in the constellation, in our case $N = 2$ for BPSK and $N = 4$ for QPSK.

Figure 6.5 (divided into a, b and c) show the results of CDF of the EVM for OFDM symbols with 8, 16 and 32 subcarriers, respectively. Each plot is divided in two halves, the left for the BPSK results and the right for the QPSK results. On each plot we depict the results of EVM of the 33×120 OFDM symbols that we received for each symbol length (i.e. $10, 30, 50, 70, 90\,ms$). It is clear that in all plots, for each OFDM symbol length, BPSK always performs better than QPSK. The reason is that QPSK symbols are twice more efficient than BPSK symbols and hence QPSK require a 3 dB higher SNR for the same $\frac{E_b}{N_0}$.

If we focus in BPSK figures, it is also clear that, given a symbol length, the higher the number of subcarriers the lower the power per subcarrier and hence the higher the EVM. We also remark the fact that shorter symbol lengths (i.e. 10 ms and 30 ms) always perform worse than longer ones due to the loss of SNR and the poor chan-

nel estimation explained in section 6.3.2. We note that the best symbol time length depends on the number of subcarriers and hence the bandwidth. For the case of 8 subcarriers, $T_s = 50\,ms$ obtains an $EVM \leq 1$ in 64% of cases, whereas for 16 subcarriers, $T_s = 70\,ms$ gets the best performance with an $EVM \leq 1$ in 56% of cases and for 32 subcarriers, $T_s = 90\,ms$ gets the best performance with an $EVM \leq 1$ in 41% of cases. This performance is due to the fact that those symbols that exceed the coherence bandwidth of the channel, on average perform better than those that occupy a lower bandwidth which may completely coincide with a fading of the channel or a narrowband interference. A multicarrier system takes advantage of frequency diversity as long as it applies forward error correction codes an interleaving; however, in our case we already see a better performance of wider bandwidths when transmitting long symbol lengths without applying channel codification techniques.

In table 6.2 we show the CDF of BER sampled at a probability of occurrence of $10\,\%, 30\,\%, 50\,\%$ and $70\,\%$. These values confirm the results obtained by means of the EVM: *i*) BPSK always outperforms QPSK, *ii*) the BER improves as the symbol length gets longer until $70\,ms$ and *iii*) the longest symbol length (i.e. $90\,ms$) outperforms all other lengths only when the occupied bandwidth exceeds the coherence bandwidth of the channel, which happens at 32 subcarriers ($BW_{OFDM} = 355.5\,Hz$).

Input Back-off

In order to study the effect of clipping the envelope of the OFDM symbol to reduce the PAPR, we transmitted 33×120 OFDM symbols for each value of IBO (see table 6.2). All symbols have the same length (i.e. $40\,ms$), 8, 16 and 32 subcarrriers and two types of constellations (BPSK and QPSK) were transmitted. We would like to remind the reader that high oversampling factors in the IFFT/FFT are implemented due the low number of subcarriers and the long symbol periods (see section 6.3.2).

As in previous experiments, the CDF of the EVM and the BER are used to find the best performance. When analyzing the EVM by means of figure 6.6 (a, b and c) we highlight the fact that neither the lowest nor the highest value of IBO but a medium value (i.e. 7 dB) outperforms the others. This is because lowest values of IBO produce high in-band distortion that degrade the EVM whereas high values of IBO reduce the mean transmitted power, which is a critical issue. If we focus on BPSK outcomes we note that as the number of subcarriers increases the majority of curves move from the one with IBO= 7 dB when $N_c = 8$ to the curve with IBO=1 dB when $N_c = 32$. This may be due to the fact that the probability of getting high PAPR symbols increases with the number of subcarriers and also increases the probability to clip the symbol. Therefore, those values of IBO that do not produce high values of distortion with low number of subcarriers, do increase in-band distortion with higher number of subcarriers.

T_s [ms]	N_c	BW [Hz]	Modulation	IBO [dB]	Bit rate [bps]	Spc. Eff. [bps/Hz]	CDF (10%)	CDF (30%)	CDF (50%)	CDF (70%)
10	8	800	BPSK	7	512	0.641	0.14	0.31	0.38	0.44
10	16	1600	BPSK	7	1025	0.641	0.12	0.36	0.45	0.47
10	32	3200	BPSK	7	2051	0.641	0.37	0.41	0.46	0.48
10	8	800	QPSK	7	1025	1.282	0.35	0.38	0.41	0.47
10	16	1600	QPSK	7	2051	1.282	0.37	0.44	0.45	0.47
10	32	3200	QPSK	7	4102	1.282	0.43	0.45	0.46	0.50
30	8	266	BPSK	7	202	0.757	0.06	0.19	0.22	0.33
30	16	533	BPSK	7	404	0.757	0.16	0.22	0.37	0.42
30	32	1066	BPSK	7	808	0.757	0.21	0.32	0.35	0.45
30	8	266	QPSK	7	404	1.515	0.21	0.29	0.35	0.40
30	16	533	QPSK	7	808	1.515	0.47	0.48	0.49	0.50
30	32	1066	QPSK	7	1616	1.515	0.31	0.40	0.45	0.49
50	8	160	BPSK	7	125	0.786	0.08	0.11	0.14	0.26
50	16	320	BPSK	7	251	0.786	0.17	0.20	0.23	0.36
50	32	640	BPSK	7	503	0.786	0.14	0.26	0.27	0.45
50	8	160	QPSK	7	251	1.572	0.09	0.26	0.32	0.47
50	16	320	QPSK	7	503	1.572	0.25	0.31	0.37	0.47
50	32	640	QPSK	7	1006	1.572	0.28	0.44	0.48	0.50
70	8	114	BPSK	7	91	0.799	0.04	0.11	0.12	0.28
70	16	228	BPSK	7	182	0.799	0.04	0.15	0.17	0.28
70	32	457	BPSK	7	365	0.799	0.07	0.22	0.23	0.45
70	8	114	QPSK	7	182	1.598	0.13	0.22	0.24	0.48
70	16	228	QPSK	7	365	1.598	0.16	0.27	0.34	0.48
70	32	457	QPSK	7	730	1.598	0.22	0.33	0.36	0.48
90	8	88	BPSK	7	71	0.806	0.08	0.10	0.13	0.34
90	16	177	BPSK	7	143	0.806	0.10	0.16	0.17	0.31
90	32	355	BPSK	7	286	0.806	0.06	0.21	0.24	0.37
90	8	88	QPSK	7	143	1.612	0.13	0.23	0.43	0.49
90	16	177	QPSK	7	286	1.612	0.23	0.31	0.46	0.47
90	32	355	QPSK	7	573	1.612	0.16	0.31	0.47	0.48
40	8	200	BPSK	1,3,5,7,9,11	155	0.775	-	-	-	-
40	16	400	BPSK	1,3,5,7,9,11	310	0.775	-	-	-	-
40	32	800	BPSK	1,3,5,7,9,11	620	0.775	-	-	-	-
40	8	200	QPSK	1,3,5,7,9,11	310	1.550	-	-	-	-
40	16	400	QPSK	1,3,5,7,9,11	620	1.550	-	-	-	-
40	32	800	QPSK	1,3,5,7,9,11	1240	1.550	-	-	-	-

Table 6.2: Summary of the characteristics of the OFDM symbols transmitted during the tests: symbol length (T_s), number of subcarriers (N_c), bandwidth (BW), modulation, input back-off (IBO), bit rate and spectral efficiency. The values of BER at several points of acumulated probability are given for the different values of OFDM length, number of carriers and modulation.

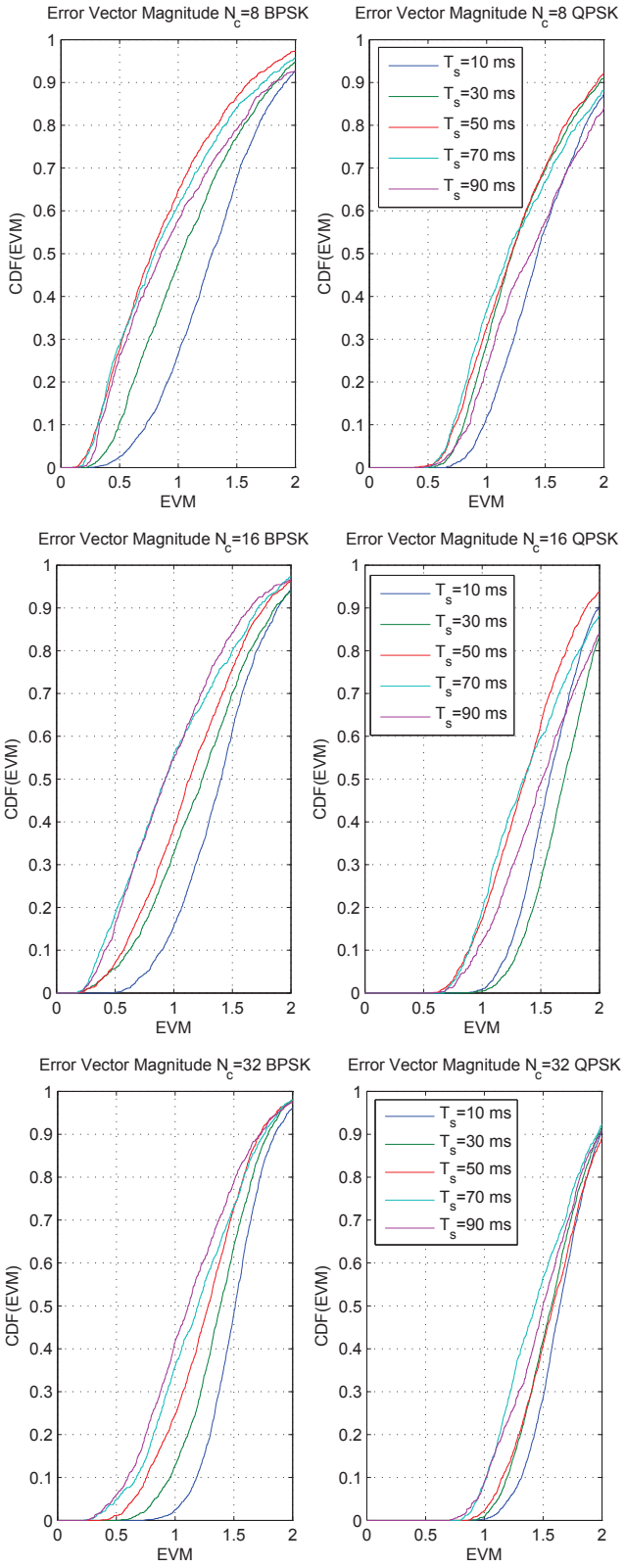

Figure 6.5: Cumulative Distribution Function of the EVM of all transmitted OFDM symbol lengths with 8 (up), 16 (middle) and 32 (down) subcarriers modulated with BPSK (left) and QPSK (right).

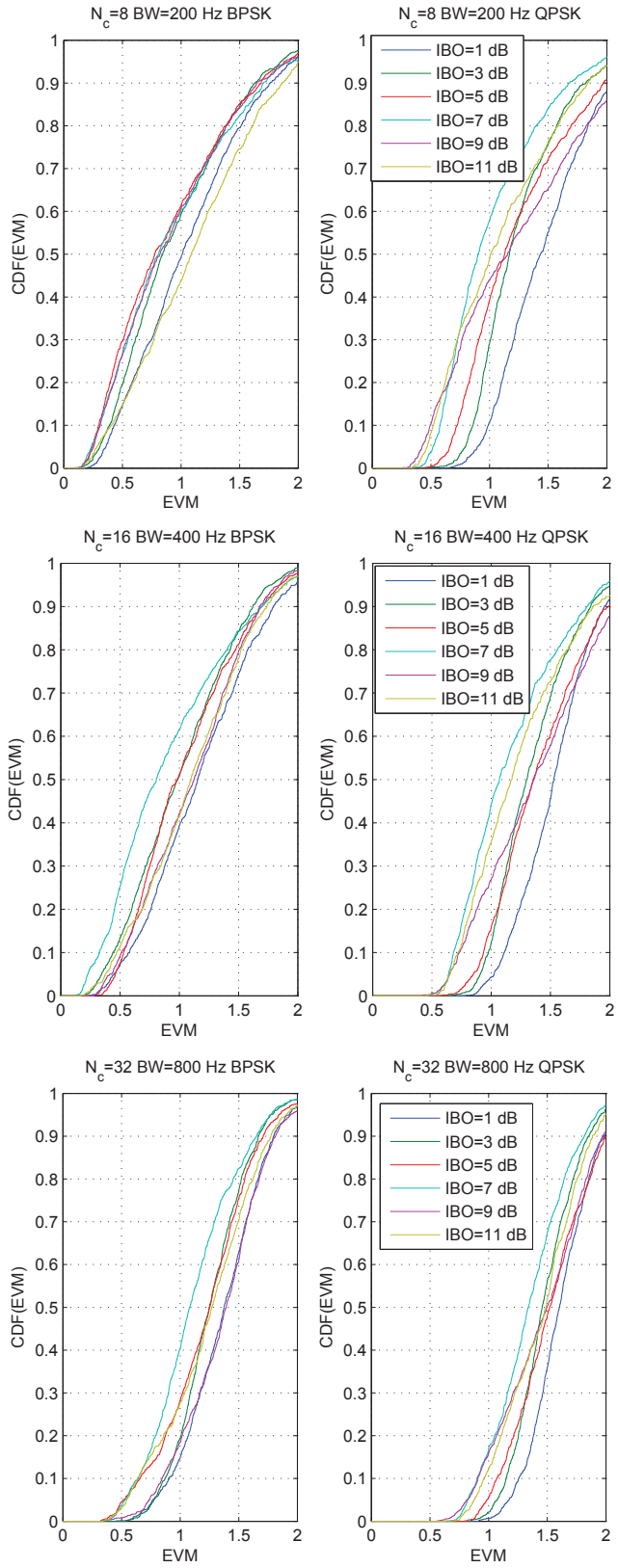

Figure 6.6: Cumulative Distribution Function of the EVM for different clipping levels applied to OFDM symbols with 8 (up), 16 (middle) and 32 (down) subcarriers modulated with BPSK (left) and QPSK (right).

6.5 Conclusions

In this paper we have analyzed a number of experiments on DSSS and OFDM data transmission over the HF channel between Antarctica and Spain. We gathered data from this ionospheric link during two Antarctic surveys to compare the performance of a low efficiency technique, which is far below the capacity of the channel, with a high efficiency technique, which transmits nearer the Shannon channel capacity upper bound [*Shannon*(1948)]. Table 6.3 summarizes the characteristics and performance of the best of both techniques.

The best DSSS results are obtained for time length between 62 ms and 126 ms (i.e. between 7.94 bps and 16.3 bps). Long DSSS symbols (i.e. 127 chips per symbol) always perform worse than short symbols (i.e. 31 chips per symbol) because long symbol lengths ($252\,ms \leq T \leq 508\,ms$) approximate the coherence time of the channel and hence experience high phase rotation within a symbol time, which is impossible to be tracked. For a fixed a bit rate, the best BER performance is given by the symbol with narrowest bandwidth. Although symbols with wide bandwidth (i.e. 2 kHz) may benefit from frequency diversity, in this low SNR and highly interfered scenario, symbols with narrow bandwidth prevail. Therefore, it seems that this data link will not benefit from frequency diversity unless symbols with wide bandwidth are combined with long PN sequences (i.e 511, 1023 and 2047 chips per sequence) to minimize interfering signals due to the higher process gain [*Peterson et al.*(1995)].

The best OFDM results are obtained for symbol time lengths ranging between 50 and 90 ms (i.e. 71 and 125 bps). The achieved raw BER for these configurations shows that it is mandatory to implement channel coding and interleaving techniques to reduce the BER. Frequency diversity is only reached when the number of subcarriers is maximum (i.e. 32), although the power per subcarrier is minimum. Those symbols clipped at large IBO (i.e. 9 and 11 dB) as well as those clipped at low IBO (i.e. 1 and 3 dB) always perform worse than those clipped at medium values (5 and 7 dB). This performance may be due to the fact that the first reach the receiver with mean power below the noise floor and the second leave the transmitter with in-band distortion higher than the energy per symbol.

OFDM spectral efficiency is between 20 and 40 times higher than DSSS spectral efficiency, which enables a 10 to 15 times higher bit rate in the same bandwidth. However, for a given BER the DSSS SNR is 12 dB to 14 dB lower than the OFDM SNR. Therefore, DSSS is able to transmit symbols under extreme SNR conditions at a rate far below the channel capacity (i.e. 1000 bits/second with a bandwidth of 500 Hz at -4 dB SNR [*Shannon*(1948)]). Whereas OFDM is able to transmit symbols below the channel capacity with higher SNR (i.e 650 bits/second with a bandwidth of 200 Hz at +7 dB SNR [*Shannon*(1948)]) using channel coding and interleaving techniques.

These two approaches enable to access the medium (HF channel) from two different ways. The first (DSSS) would permit transmitting long periods of time below the noise floor and therefore minimizing the interference to other users; whereas, the second (OFDM) would permit transmitting short and sporadic bursts of data, also minimizing the interference, with good channel conditions. As a result of this comparison we

Symbol characteristics	BW [Hz]	Symbol time [ms]	BER ($P = 30\%$)	SNR ($P = 80\%$)[dB]	Bit rate [bps]	Spc. Eff. [bps/Hz]
31 chips	500	62	0	-4.9	16.3	0.032
31 chips	250	124	0	-3.7	8.06	0.032
63 chips	1000	63	0.04	-5.5	15.87	0.016
63 chips	500	126	0	-5.8	7.94	0.016
50×8 BPSK	160	53	0.11	8.8	125	0.786
70×16 BPSK	228	73	0.15	7	91	0.799
90×32 BPSK	355	93	0.21	6	71	0.806

Table 6.3: Summary of the best outcomes of DSSS and OFDM receptions. The sequence length and the number of samples per chip are shown for DSSS and for OFDM the symbol length, the number of subcarriers and the constellation.

propose the following strategy: for the unidirectional Antarctic channel, when the forecast channel [*Vilella et al.*(2008), *Ads et al.*(2012)] is poor use DSSS but when the channel is good use OFDM combined with channel coding and interleaving.

6.6 Acknowledgments

This work has been funded by the Spanish Government under the projects CGL2006-12437-C02-01, CTM2008-03536-E, CTM2009-13843-C02-02 and CTM2010-21312-C03-03.

Bibliography

[US Department of Defense (1991)] US Department of Defense (1991), MIL-STD-188-110A, Military Standard: Interoperabilty and Performance Standards for Data Mo dems.

[*NATO*(1999)] NATO (1999), STANAG 4415, Characteristics of a robust, non-hopping, serial-tone modulator/demodulator for severely degraded HF radio links, Edition 1, 21 June 1999.

[*Ads et al.*(2012)] Ads, A., P. Bergadà, C. Vilella, J. Regué, J. Pijoan, and R. Bardají (2012), A Comprehensive Sounding of the Ionospheric HF Radio Link from Antarctica to Spain, *Radio Science*, *doi:10.1029/2012RS005074*.

[*Andersson*(1994)] Andersson, P. (1994), Performance of Frequency-hopping Radio Systems on Interference-limited HF Channels, in *6th International Conference on HF Radio Systems and Techniques*, York, UK.

[*Baum et al.*(1997)] Baum, K., I. Schaumburg, and N. Nadgauda (1997), A Comparision of Differential and Coherent Reception for a Coded OFDM System in a Low C/I Environment, in *Global Telecommunications Conference*, vol. 1, pp. 300–304, Phoenix, USA.

[*Bergadà et al.*(2009)] Bergadà, P., M. Deumal, R. Alsina, and J. Pijoan (2009), Time Interleaving Study for an OFDM Long-Haul HF Radio Link, in *11th International Conference on Ionospheric Radio Systems and Techniques*, Edinburgh, UK.

[*Bergadà et al.*(2009)] Bergadà , P., M. Deumal, C. Vilella, J. R. Regué, D. Altadill, and S. Marsal (2009), Remote Sensing and Skywave Digital Communication from Antarctica, *Sensors*, *9*(12), 10,136–10,157, *doi:10.3390/s91210136*.

[*Deumal et al.*(2006)] Deumal, M., C. Vilella, J. Socoro, R. Alsina, and J. L. Pijoan (2006), A DS-SS Signaling based System Proposal for Low SNR HF Digital Communications, in *10th International Conference on Ionospheric Radio Systems and Techniques*, London, UK.

[*Dorazio et al.*(2007)] D'Orazio, L., C. Sacchi, and F. D. Natale (2007), Multicarrier CDMA for Data Transmission over HF Channels: Application to Digital Divide Reduction, in *IEEE Aerospace Conference*, Big Sky, USA.

[*Engels and Rohling*(1995)] Engels, V., and H. Rohling (1995), Multilevel Differential Modulation Techniques (64-dapsk) for Multicarrier Transmission System, *European Transactions on Telecommunications*, *6*, 633–640.

[*Forestier et al.*(2004)] Forestier, S., P. Bouysse, R. Quere, A. Mallet, J.-M. Nebus, and L. Lapierre (1995), Joint Optimization of the Power-added Efficiency and the Error-vector Measurement of 20-GHz pHEMT Amplifier through a New Dynamic Bias-control Method, *IEEE Trans. Microwave Theory and Tech.*, *52*, 1132–1140.

[*Furman et al.*(2012)] Furman, W.N., and J.W. Nieto (2012), Latest on-air testing of U.S. MIL-STD-188-110C appendix D wideband HF data waveforms, *12th IET International Conference on Ionospheric Radio Systems and Techniques*, pp. 1-5, 15-17 May 2012, York, UK.

[*Gherm et al.*(2005)] Gherm, V., N. Zernov, and H. Strangeways (2005), HF Propagation in a Wideband Ionospheric Fluctuating Reflection Channel: Physically based software simulator of the channel, *Radio Science*, *40*.

[*Gold*(1968)] Gold, R. (1968), Maximal Recursive Sequences with 3-valued Recursive Cross-Correlation Functions, *IEEE Transactions on Information Theory*, *IT-14*, 154–156.

[*M.C. Gill and Ball*(1995)] M.C. Gill, T. G., S.C. Cook, and J. Ball (1995),A 300 to 3600 bps Multi-rate HF Parallel Tone Modem, in *Military Communications Conference*, vol. 3, pp. 1066–1070, San Diego, USA.

[*S.W.Golomb*(1967)] S.W.Golomb (1967), *Shift Register Sequences*, Holden-Day, San Francisco.

[*Hoeher et al.*(1997)] Hoeher, P., S. Kaiser, and P. Roberston (1997), Two-dimensional Pilot-symbol Aided Channel Estimation by Wiener Filtering, in *International Conference on Acoustics, Speech and Signal Processing*, Munich, Germany.

[*Johnson*(2009)] Johnson, E.E. (2009), Performance Envelope of Broadband HF Data Waveforms, *IEEE Military Communications Conference*, pp.1-7, 18-21 Oct, Boston, USA.

[*Moose*(1994)] Moose, P. (1994), A Technique for Orthogonal Frequency Division Multiplexing Frequency Offset Correction, *IEEE Transactions on Communications*, *42*, 2908–2914.

[*Myung and Goodman*(2008)] Myung, H. G., and D. Goodman (2008), *Single Carrier FDMA: A New Air Interface for Long Term Evolution*, John Wiley & Sons, Hoboken.

[*Nieto*(2008)] Nieto, J. W. (2008), An Investigation of Coded OFDM and COFDM Waveforms utilizing different Modulation Schemes on HF Channels, in *6th International Symposium on Communication Systems, Networks and Digital Signal Processing*, Reykjavik, Iceland.

[*Peled and Ruiz*(1980)] Peled, A., and A. Ruiz (1980),Frequency Domain Data Transmission Using Reduced Computational Complexity Algorithms, in *IEEE International Conference on Acoustics, Speech and Signal Processing*, pp. 964–967, Denver, USA.

[*Voacap*(2013)] Perkiomaki, J. (2013), HF Propagation Prediction and Ionospheric Communications Analysis, *www.voacap.com*.

[*Peterson et al.*(1995)] Peterson, R. L., R. E. Ziemer, and D. E. Borth (1995), *Spread Spectrum Communications Handbook*, Prentice Hall, Upper Saddle River.

[*Proakis*(2000)] Proakis, J. (2000), *Digital Communications*, McGraw Hill, New York.

[*Sandell et al.*(1995)] Sandell, M., J. van de Beek, and P. Börjesson (1995), Timming and Frequency Synchronization in OFDM Systems Using the Cyclic Prefix, in *IEEE international Symposium on Synchronization*, Saalbau, Germany.

[*Schmidl and Cox*(1997)] Schmidl, T., and C. Cox (1997),Robust Frequency and Timming Synchronization for OFDM, *IEEE Transactions on Communications*, *45*, 1613–1621, Manchester, UK.

[*Shannon*(1948)] Shannon, C.E. (1948), A Mathematical Theory of Communication in *The Bell System Technical Journal*, vol.27, pp.379-423, 623-656, July, October, 1948.

[*Smith et al*(2001)] Smith, O.J., M.J. Angling, P.S. Cannon, V. Jodalen, B. Jacobsen, and O.K. Gronnerud (2001), Simultaneous measurements of propagation characteristics on noncontiguous HF channels, *11th International Conference on Antennas and Propagation*, vol.1, pp. 383-387.

[*Tourtier et al.*(1993)] Tourtier, P., R. Monnier, and P. Lopez (1993), Multicarrier Modem for Digital HDTV Terrestrial Broadcasting, *Signal Processing: Image Communication*, *5*, 379–403.

[*Vilella et al.*(2008)] Vilella, C., D. Miralles, and J. Pijoan (2008), An Antarctica-to-Spain HF Ionospheric Radio Link: Sounding Results, *Radio Science*, *43*.

[*Vilella et al.*(2009)] Vilella, C., D. Miralles, D. Altadill, F. Acosta, J. Sole, J. Torta, and J. Pijoan (2009), Vertical and Oblique Ionospheric Soundings over a Very Long Multihop HF Radio Link from Polar to Midlatitudes: Results and Relationships, *Radio Science*, *44*.

[*Wagner et al.*(1989)] Wagner, L.S., J.A. Goldstein, W.D. Meyers and P.A.Bello (1989), The HF Skywave Channel: measured Scattering Functions for Midlatitude and Auroral Channels and Estimates for Short-term Wideband HF Rake Modem Performance, *IEEE Military Communications Conference*, vol.3, pp.830-839, 15-18 Oct 1989, Boston, USA.

[*Zhang et al.*(2005)] Zhang, H., H. Yang, R. Luo, and S. Xu (2005), Design Considerations of a new HF Modem and Performance Analysis, in *IEEE International Symposium on Microwave, Antenna, Propagation and EMC Technologies for Wireless Communications*, Beijing, China.

Part III

Concluding remarks

Chapter 7

Conclusions

After eleven years of research on HF communications we can conclude that over-the-horizon communication between Antarctica and Spain is feasible. Such a long haul ionospheric link can be used to transmit data from sensors of unattended stations at low rate (i.e., < 200 bps). Other applications can also be approached but we must carefully consider the tough impairments that show this HF channel. That is, daily frequency availability variations, highly interfered and low SNR scenario at the receiver, and time-frequency dispersive impulse response.

In case of designing a simplex link, like ours, a previous frequency availability study is mandatory since there is no feedback channel to inform the transmitter about the best channel to hop and avoid long fadings, as many link protocols do. Therefore, it is important to configure the carrier frequency to the point with the highest availability and the lowest interference occurrence. Regarding this issue we have implemented an oblique narrowband sounder to study frequency availability and SNR at the receiver. We have improved this study by dividing the received period into smaller periods to detect and discard short burst of narrowband interference signals.

HF channel can also show short fading due to its multipath behavior which can lead to irrecoverable bursts of errors. Moreover, its impulse response varies in time due to the fact that the electron density of each ionospheric layer also varies, mostly because of the sun radiation activity. Since the channel impulsive response is required to implement the physical layer of the modem, we have studied the Antarctic channel by means of wideband signals (i.e., pseudonoise sequences) to measure its main characteristics: the composite multipath and Doppler spread.

In both cases, narrowband and wideband sounding, we have observed a clear difference between day and night. Regarding narrowband sounding, the best frequencies at night are those below 19 MHz decreasing towards 7 MHz at dawn when there is a sudden increase to frequencies from 11 MHz to 23 MHz. Regarding the wideband sounding the channel is more turbulent (i.e., higher composite multipath and Doppler spread) at night rather than at daytime. This phenomenon can be attributed to the

fact that during daytime the D layer shows its highest thickness, that is its highest ionization level (i.e., 10^2 and 10^4 e^-/cc, below 90 km) hence its high attenuation factor. Whereas, after sunset, this D layer gets thinner and consequently more paths, which are refracted at the upper layers (E, F_1 and F_2 during daytime and F at night), are able to arrive to the receiver with enough SNR. Therefore, the higher the number of paths that reach the receiver the higher the probability to measure higher delay between paths and higher Doppler spread. Moreover, layer E (10^4 and 10^5 e^-/cc, between 90 km and 160 km) tends to disappear at night since the primary source of ionization is no longer present. Critical frequency drops about an order of magnitude from its daytime value, which results in an increase in the height where ionization peak occurs because recombination is faster in lower levels. This phenomenon can explain the fact that in our channel the range of radio wave frequencies that can travel through this layer and finally arrive at the receiver extends from around 10 MHz, during daylight, up to more than 20 MHz at night.

When implementing the physical layer of the modem we have experimented with two techniques: DSSS and OFDM. Regarding DSSS, the main goal has been to study which symbol length and bandwidth are optimal for our channel. We have showed that the longest symbols do not perform better than the shortest ones because the length of long symbols are near the coherence time of the channel. However, the shortest symbols are not the best solution either, since these symbols have wide bandwidth and consequently very low SNR at the receiver. So, there is a trade-off between the PN sequence length and the bandwidth. To get the best symbol time length, which ranges from 62 ms to 126 ms, we can use short sequences (31 chips) and narrow bandwidth (i.e., 250 Hz and 500 Hz) or longer sequences (63 chips) and wider bandwidth (i.e., 500 Hz and 1 kHz). To get similar results with longer PN sequences (127 chips) wider bandwidth (i.e., 2 kHz) must be used. In all these tree cases the bit rate is approximately between 7 bps and 15 bps. In 30% of the received symbols these best configurations achieve BER=0. However, when considering the 50% of the symbols the BER worsens to 8.3×10^{-2}.

Regarding OFDM, we have experimented with the symbol length, the number of subcarriers, modulation and IBO of the symbol. Short symbol ($T_s < 50ms$) perform bad because they suffer from a lack of SNR and only poor channel estimation is achieved. Long symbols ($T_s > 70ms$) also perform bad because, despite achieving the highest SNR, their bandwidth is narrower than the coherence bandwidth of the channel. Then, intermediate symbol length ($T_s = 50ms$, $T_s = 70ms$) have shown the best performance. From the results, we can assure that BPSK always outperforms QPSK due to the 3 dB penalty in the energy per bit; and, also from the results, we can assure that as the number of subcarriers increases the performance decreases due to the lower energy per subcarrier. However, in longer symbols this rule is not so clear and even the 10% of the 32 subcarriers symbols of 90 ms length outperform 8 subcarrier and 16 subcarrier symbols. This phenomenon can be related to the higher frequency diversity that can experiment wider frequency symbols, which in average can have more subcar-

riers not effected by deep fadings of the channel or narrowband interference. Regarding the high fluctuations of OFDM symbol envelope we have limited the maximum IBO by means of a softlimiter at the expense of generating distortion. The results have shown that neither symbols with low IBOs (1 dB and 3 dB) nor symbols with high IBOs (9 dB and 11 dB) are the best solution for this link. Intermediate IBOs (5 dB and 7 dB) show a good trade-off between average transmitted power and distortion. The 10% of the received OFDM symbols show a BER lower than 4.0^{-2}, but when considering the 50% of the received OFDM symbols the error rate worsens to 1.2×10^{-1}. The best combinations (i.e., 50 ms-8 subcarriers-BPSK, 70 ms-16 subcarriers-BPSK and 90 ms-32 subcarriers-BPSK) achieve a bitrate that ranges from 71 bps to 125 bps.

When using both techniques, i.e., DSSS and OFDM, FEC code and interleaving should be used to improve the performance against fast fading of the channel and sporadic narrowband interference. The depth of the interleaving should be higher than the coherence time of the channel (approximately 5 seconds in the case of the slowest channel at 16 UTC and 15 MHz). The high delay introduced by the interleaving/deinterleaving is not a concern in our case since it is a broadcast application. In the OFDM case we expect better performance if an interleaving is applied in the time and frequency dimension to benefit from time and frequency diversity. DSSS shows better performance than OFDM at the expense of a throughput between 10 and 15 times lower within in the same bandwidth. However, for a given BER the required SNR of DSSS signal is 12 dB to 14 dB lower than the required SNR of OFDM wave. Therefore, according to the oblique channel soundings and to the data transmission experiments, we propose to use DSSS waveform in poor scenarios to transmit long streams of data minimizing interference on other HF users. Whereas, we could use OFDM waveform in the best scenarios (approximately, 10% of the cases) to increase the spectral efficiency by transmitting short bursts of data at high bit rate.

Chapter 8

Future work

In the HF channel the overlapping signals generated by multipath time-variant phenomenon create fluctuations in the received signals amplitude and phase. Moreover, scintillation, which is a name used to describe the multipath fading caused by the variation in the density of ions in the ionospheric layers, randomly degrades the received signal characteristics. Another disturbance that may affect transmitted signals through the ionosphere consists in the polarization fading between the ordinary and extraordinary waves [16]. The ionosphere is an anisotropic medium due to the earth magnetic field, and consequently, two solutions are possible for the propagation of the electromagnetic waves: ordinary and extraordinary mode. In each of them the electromagnetic wave is elliptically polarized and for a given propagation direction, these two modes are orthogonal; in particular, they present the same direction but opposite sense. Each of this two modes of propagation have a different speed of propagation in the plasma, which leads to different group delay and to different channel impulse response. Since channel impulse response of ordinary and extraordinary modes can be low correlated, this diversity can lead to higher channel capacity in a multiple input multiple output (MIMO) link or to higher reliability in a single input multiple output (SIMO) link.

We have already started to study the feasibility of applying polarization diversity in the HF channel between Antarctica and Spain. The goal is to implement a SIMO (single input multiple output) link to increase the low SNR available at the receiver. The first stage of this study is to characterize the polarization diversity that exists at the receiver between the data gathered from a vertical polarized antenna (i.e., a monopole) and from a horizontal polarized antenna (i.e., an inverted V antenna), both with similar gain. In order to characterize this polarization diversity we have started by correlating a non modulated carrier gathered simultaneously at both antennas, over a range of frequencies and hours. Preliminary results show that a low correlation (lower than 0.7) between both signals exists and that it varies depending on frequency and time. The second step will be to combine the data gathered from the two antennas to improve the SNR.

Since high envelope fluctuation of multicarrier waveforms is a major concern on HF waveforms, mainly if higher power efficiency is needed, a constant envelope solution could be explored for this HF link. A possible candidate could be the Single Carrier-Frequency Division Multiple Access (SC-FDMA) modulation adapted to a single user solution with a frequency or time equalization technique to overcome ISI. As a result, using a single user SC-FDMA solution the average transmitted power could be similar to the saturation power of the amplifier and hence increase the SNR available at the receiver. The downside of this technique is the higher computational complexity and signal processing at the receiver compared to the OFDM scheme. Interleaved and localized subcarrier mapping could be studied to find which solution best fits the HF channel. Interleaved mapping allocates the output of the DFT across the entire available bandwidth and applied a zero padding to the unused subcarriers. It provides better frequency diversity as well as lower PAPR; however, it is more sensitive against carrier frequency offsets [13]. Whereas, localized mapping allocates the frequency samples into contiguous subcarriers. Due to the blockwise structure, it provides good robustness against frequency carrier offset, at the expense of lower frequency diversity.

Although the bit rate achieved in DSSS tests was enough to transmit data from the sensors placed in Antarctica, a signaling technique could be approached to increase the spectral efficiency of the link for future use on higher demanding applications. The starting point could be using the best combinations of symbol period and bandwidth in terms of BER, already obtained in DSSS, and using the in-phase and quadrature component of a signaling technique to increase efficiency. A second experiment could consist in transmitting symbols with wider bandwidth, which enable higher throughput in signaling schemes and higher frequency diversity, while maintaining equal time length as DSSS solution by using longer PN sequences.

The radio modem should also include, apart from the modulation techniques discussed in this thesis, other parts such as source coding algorithms, channel coding and interleaving. As explained in appendix C, the INTERMAGNET frame should be modified to match a point to point HF transmission. Due to the low variability of the four components of the Earth magnetic field, a differential encoder plus a Huffman coding, based on a static dictionary determined before coding, could be a good option to reduce the redundancy of the data and come near the entropy of the source. Then, the compressed data could be divided into a number blocks and we could apply a channel coding based on concatenated codes. The outer code could be a Reed Solomon applied to each block and the inner coder could be a turbo coder applied to the whole amount of data. To reduce the probability of long burst of erroneous data, after each coder a random interleaving of the whole amount of data could be applied. In order to benefit from time diversity, we could merge the data of a whole day into the same file to have a sufficient long stream of data to be transmitted. Finally, we could transmit the file corresponding to each day several times and apply voting techniques to decide whether each transmitted bit is a zero or a one.

Part IV

Appendices. Other contributions

Appendix A

Channel estimation for long distance HF communications based on OFDM pilot symbols, in Proceedings of the IRST 2006

Channel Estimation for Long Distance HF Communications based on OFDM Pilot Symbols

R. Aquilué, P. Bergadà, I. Gutiérrez, J.L. Pijoan

{raquilue, pbergada, igutierrez, joanp}@salle.url.edu
Comunications and Signal Theory. La Salle Engineering. Ramon Llull University.

Keywords: Ionospheric communications, HF channel estimation, OFDM.

Abstract

Although HF communications have mostly been used for voice purposes, since the growing of digital systems, they are becoming a true alternative to satellite communications when talking about long distance and low bit rate demanding applications. The choice is very attractive since the equipment costs are dramatically reduced and it can overcome the targeting problem of GEO satellites from the poles. Ionospheric propagation suffers from serious impairments, i.e. long delay spreading, high attenuation, frequency dependent signal-to-noise ratio and high level of interference. In this paper, an OFDM (Orthogonal Frequency Division Multiplexing) based channel estimation is presented in order to cope with low SNR HF links. It has been tested out in a long distance (12700 Km) HF link that has been established between the Spanish Antarctic Base in Livingston Island and the Ebre Observatory (Spain).

1 Introduction

Long distance ionospheric communications are turning out to be a good alternative to satellite communications. The advantages are being taken of the hardware equipment costs, independence of satellite and good targeting on polar caps.

For all these reasons, the Electromagnetism and Communications Research Group of La Salle Engineering School of the Ramon Llull University, with previous experiences in the field of wideband modulations through HF channels [6], is developing a research project, called SANDICOM (Sounding System for Antarctic Digital Communications). The topic of the research is the study of the ionospheric channel characteristics, as SNR, delay and doppler spread, between the Spanish Antarctic Base Juan Carlos I (SAB), located in Livingston Island (62.6ºS,60.4ºW) and the Ebre Observatory (EO) in Spain (40.8ºN, 0.5ºE). Another important goal of the project is to develop a digital radiomodem specially adapted to HF long distance links, achieving the maximum bit rate at minimum power consumption.

This project has been divided in three Antarctic campaigns. During the first one (2003-2004), a ionospheric sounder was carried out with standard HF transceivers with 3 KHz bandwidth. Preliminary results on channel availability, narrowband multipath channel properties as time spread and doppler spread were found [10].

During de second campaign (2004-2005) a new digital transceiver was developed. It was based on a digital platform with FPGAs, ASICs and high speed A/D/A converters. It allowed to easily change the main characteristics of the transceiver, as the frequency carrier (3 to 30 MHz), the signal bandwidth (up to 100KHz) and modulation. More precise measurements of availability, time dispersion and doppler spread were carried out with pseudo-noise sequences with good autocorrelation properties [10].

During the third campaign (2005-2006) pseudo-noise sequences have been intensively used in order to improve the accuracy of the previous measurements. In addition, an alternative method for channel sounding has been introduced. It consists in a multi carrier modulation, such as OFDM (Orthogonal Frequency Division Multiplexing) containing pilot carriers. This is expected to be a first step in order to evaluate the success of a multi-carrier modulation scheme to transmit data through such a long link (12700 Km), with path losses up to 150 dB and very low SNR [9,10].

In this paper a deeply explanation about ionospheric channel estimation with multi-carrier modulation, between SAB and EO is fulfilled. Furthermore, OFDM modulation has been tested to transmit data and some preliminary outcomes are shown. Finally, some conclusions are drawn out from the achieved results and future work is proposed.

2 Measurement method description

The sounding system used to perform the ionospheric channel estimation consists on a digital transmitter and receiver, installed in the SAB and in the EO, respectively. The reader is referenced to [10] for more information about the architecture of the system employed in these channel measurements.

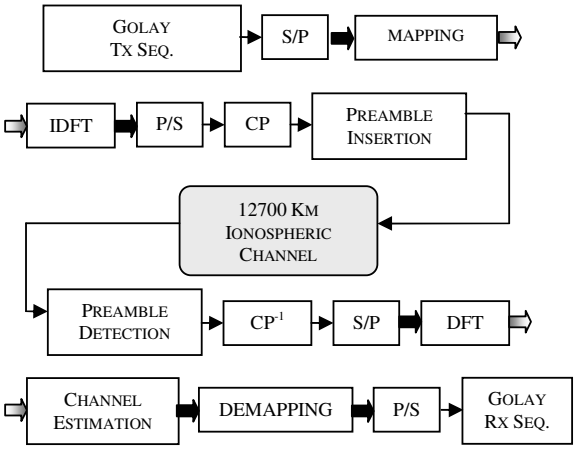

Figure 1: System block diagram.

The system permits the configuration of the initial and the final hour of the sounding sessions for each day. Sounding signals can be sent during the first 56 minutes of each hour. The remaining 4 minutes are used for system parameters reconfiguration and analog devices initialization. Each minute is divided in three time intervals:

- The first interval is used to tune both antennas at the desired transmission / reception frequency. This is done by transmitting a low power tone (<20W).

- A tone is transmitted at full amplifier's power in the second time interval. This is used to perform a channel link availability study in an easy way. Due to the transmission chain frequency response, the maximum transmission power fluctuates widely, between 250W and 120W in the worst case. The non flat transmitter frequency response is compensated at the receiver.

- Sounding and channel estimation waveforms are sent in the last time interval. Channel characteristics as time variability and delay spread are studied based on transmissions in this interval. Some of the subcarriers, among data ones, are considered as pilots in order to perform data aided channel estimation at the receiver. From figure 1, it can be seen that after OFDM modulation, a cyclic prefix is inserted to avoid inter-symbol interference. The signal crosses a 12700 Km ionospheric channel before arriving at the receiver, where a correlation based preamble detector feeds the synchronized data to the OFDM demodulation stage. Single tap channel estimation is performed and data is delivered for BER cumputing.

In order to explore the maximum usable bandwidth, channel estimation has been performed for different bandwidth up to 5 KHz.

2.1 Synchronization and frame design

Synchronization is one of the most critical points related to an OFDM system performance. Clock frequency mismatch between transmitter and receiver results in inter-carrier interference and FFT window misalignment. Time and frequency synchronization issues are discussed below.

Based on first and second campaign channel measurements [10], the symbol designed has the parameters listed in table 1, considering a doppler spread from 0.5 to 1.6 Hz and a delay spread ranging from 1 to 2 msec:

DFT window width	ts = 48 msec
Cyclic prefix length	Tg = 2.8 msec
Symbol length	T = 50.8 msec
Sub-carrier spacing	Δf = 20.833 Hz
Number of sub-carriers	N = 16

Table 1: OFDM symbol parameters.

According to [3], the maximum variability that can be expected is related to a coherence bandwidth of Δfc = 500 Hz and a coherence time of Δtc = 312 msec. The symbol waveforms are stored in a flash memory, able to store 245759 IQ pairs with 16 bits of resolution. In order to increase the alias rejection capabilities of the Digital Up Converter CIC interpolation filters, the signal has been stored and sampled at 37500 samples per second. If T = 50.8 msec, the memory can store up to 131 symbols or 21 frames of 6 symbols per frame, that can be cyclically read.

Oscillator deviation between transmitter and receiver causes a progressive and accumulative windowing position offset. Assuming perfect acquisition with an initial PN sequence, the accumulated timing offset caused by clock maximum tolerances of 1 ppm is shown in (1). This tolerance causes a maximum timing offset deviation 5 symbols after the synchronization sequence of:

$$5 OFDM symbol \times T \times 1 ppm = 254 n \sec. \qquad (1)$$

With a downsampling factor in the receiver of 1200 (RF sampling frequency / BB sampling frequency), these 254 nsec. cause, a timing offset of ±0.0127 samples before DFT demodulation.

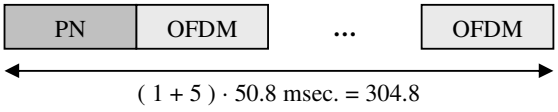

Figure 2: Frame format.

Figure 2 shows the frame structure based on one 127 chips PN sequence at 2.5 Kcps followed by 5 OFDM symbols. Timing synchronization is performed based on the well known autocorrelation properties of the Maximal Length

sequences. The frame duration is shorter than the channel coherence time, so it can be ensured that if the largest correlation peak is chosen as the acquisition point, the system will demodulate the pilot signals provided by the strongest path. Therefore timing tracking algorithm is not needed if, according to (1) an offset of one sample is applied, in the direction of the cyclic prefix, over the estimated window position.

As high stability clocks could not have been used yet, frequency offsets up to 60 Hz can be expected. The second interval signal mentioned before is used as frequency offset correction signal [2]. A non modulated sinusoid are sampled at 50 KHz and frequency deviation estimation is performed by doing a DFT. This method has an estimation uncertainly of 0.2 Hz, less than the 1% of the sub-carrier spacing (Δf = 20.833 Hz) [8]. As it will be shown, although this restriction can be relaxed in this application due to the fact that the effective inter-carrier spacing is larger than Δf = 20.833 Hz, the approach explained before is the one used to estimate the frequency offset deviation.

2.2 Pilot frame architecture

Due to the SAB strict power consumption restrictions, served only by wind and solar power in winter, transmitted power levels have been below 250 W. In frequencies where propagation has been favourable [10], transmission power has not been over 140 W. The antennas used in this third campaign have been the same antennas of the previous campaigns, when the main goal was channel sounding. Due to this fact, wideband monopole elements with no directivity have been employed. For these reasons, the SNR was extremely low for data transmission and the channel had to be estimated in sub-channels with few subcarriers, as will be explained later. In the next campaign, directive antennas will be used in order to increase the SNR available at the receiver.

From previous measurements [10], it can inferred that taking the subcarrrier spacing from table 1, the mean SNR avaliable at the receiver versus the number of subcarriers used is the one shown below.

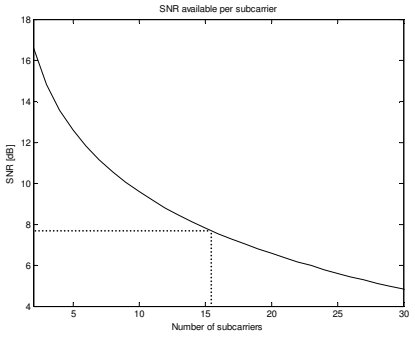

Figure 3: SNR available at the receiver versus number of SC.

The number of carriers was chosen N=16. If *ts* = 48 msec is taken as the useful symbol time, the intercarrier spacing is Δf = 20.833 Hz and the OFDM symbol bandwidth equals 333.3 Hz. As the coherence bandwidth allows a greater intercarrier spacing in order to correctly estimate the channel, 2 virtual subcarriers are inserted between the active ones. This lays in the ODFM symbol bandwith shown in (2).

$$\Delta f \times (N \times 3) = 1KHz \tag{2}$$

Since previous channel variability estimations showed a coherence time ranging from 0.312 to 1 seconds, 6 OFDM symbols of T = 50.8 msec of duration can be fit into the strictest constraint. This allows the transmission of one preamble and five 1 KHz OFDM symbols following the frame scheme of figure 2. OFDM subcarrier positions are frequency shifted from symbol to symbol in order to estimate a total bandwith of 5 KHz (Figure 4).

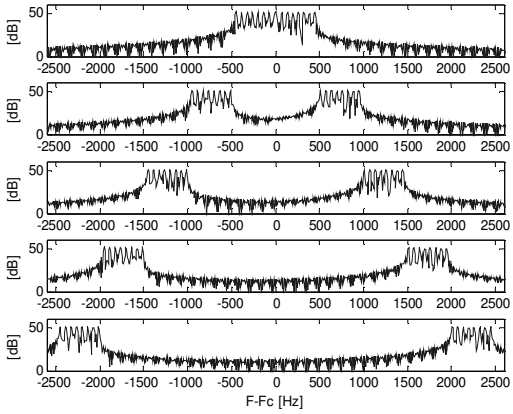

Figure 4: OFDM estimation symbols.

As input to the mapping stage, figure 1 shows that 16 chips long Golay sequences are BPSK modulated in each subcarrier. After IDFT modulation, Golay sequences generate a time domain waveform with peak to average power ratio (PAPR) equal or below 3 dB [1]. PAPR is particularly critical when talking about long distance HF communications, where SNR levels are very low and interference amplitudes are larger than the signal of interest. In this context, increase the mean power of the transmitted signal by reducing signal peaks and make the amplifier work on its transfer function lineal zone is essential.

Channel transfer function has been estimated by Least Squares (LS), considering some of the carriers as pilots. This estimator minimizes the expression (3):

$$(Y - XH)^H (Y - XH) \tag{3}$$

where $(\cdot)^H$ denotes the transposed conjugation and X is the signal matrix at the input of the IDFT block at the transmitter.

$$X = diag\left[X_1 X_2 X_3 ... X_K\right]^T \quad (4)$$

Y is the signal matrix at the otput of the DFT block at the receiver:

$$Y = \left[Y_k\right]^T = XH + N \quad (5)$$

$$H = DFT_N\{\left[g_k\right]^T\} \quad (6)$$

$$N = DFT_N\{\left[n_k\right]^T\} \quad (7)$$

Where g_k and n_k (6,7) are the impulse response and noise. It can be demonstrated that the LS estimator for *H* is given by [7]:

$$\hat{H}_{LS} = X^{-1}Y = \left[\frac{Y_k}{X_k}\right]^T \text{ (k=0,1…,N-1)} \quad (8)$$

Rectangular and Hexagonal [4] pilot patterns with various pilot densities have been proposed and tested. In figure 5, an hexagonal pilot patterns are depicted. Once channel has been estimated at pilot positions, the frequency – time channel matrix is interpolated using biarmonic splines [5].

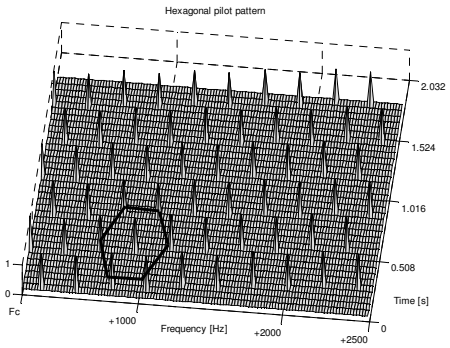

Figure 5: Hexagonal pilot pattern.

3 Results

In this section, results of the channel estimation with OFDM pilot symbols are presented.

Rectangular and hexagonal pilot patterns have been used to place pilots in a time-frequency lattice. Moreover, different pilot densities have been taken into consideration and 2, 4 and 8 carriers out of *N* are considered as pilots. In table 2, outcomes of BER without applying channel coding are shown, as well as the achieved bit rate with 16 subcarriers. The following statistics have been measured with SNR > 10 dB over 333.3 Hz occurrences, mainly at high frequencies [10]. All results from table 2 are measured at the same carrier frequency (Fc=16.130 MHz).

Pilot distribution	Pilot Density	BER without coding	Bit rate (bps)
Rectangular	2 / 16	2.9e-2	222.6
	4 / 16	1.5e-2	193.6
	8 / 16	1.2e-2	129.3
Hexagonal	2 / 16	1.6e-2	225.6
	4 / 16	1.1e-2	194.6
	8 / 16	1.0e-2	162.3

Table 2: Outcomes for different distributions and densities of pilots.

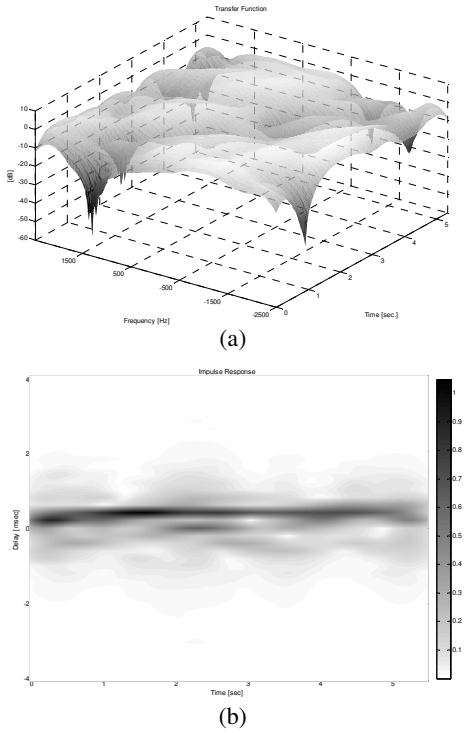

Figure 6: Channel transfer function (a) and evolution of the impulse response (b), with a carrier frequency of Fc = 16.130 MHz (20:55 UTC, February 21st, 2006).

From table 2 it can be derived that better bit error rates can be achieved applying hexagonal pilot pattern distribution rather than with rectangular distribution. So, assuming a 1:4 pilots to carrier ratio would be the best trade-off in order to minimize BER and maximize bit rate. In figure 6 (a, b) a picture of the transfer function and impulse response, respectively, with a carrier frequency of 16.130MHz are depicted. Channel estimation was done with rectangular pilot pattern distribution, with 4 pilot out of 16 carriers per symbol. The estimated channel bandwidth was 5 KHz during a period of 6 seconds. Using OFDM pilot symbols doppler spread values from 0.3 to 1.4 Hz and a delay spread ranging from 1 to 2 msec have been measured. Similar results, with a smaller

estimation bandwidth, were provided using PN sequences in [10]. The channel scattering function depicted at figure 7, which was measured at the same time and frequency as the previous figure, shows that the channel time spread at that moment was around 1 mseg and the channel doppler spread was approximately 1Hz.

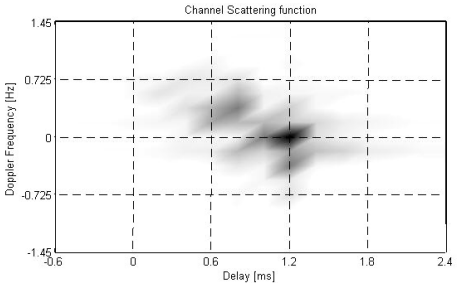

Figure 7: Channel Scattering function (21/02/06), with a carrier frequency of F_c = 16.130 MHz (20:55 UTC, February 21st, 2006).

4 Conclusions

In this paper OFDM modulation has been introduced as a possible technique to properly estimate ionospheric channel characteristics. It has been tested in a radio channel between the SAB and the EO in Spain. Some results about delay and doppler spread have been shown. In addition, OFDM has also been used to transmit data and some outcomes of BER and spectral efficiency have been measured.

For the following Antarctic campaigns, it is expected to keep on measuring ionospheric channel characteristics with OFDM pilot symbols as means to reinforce previous measurements. Increase of received power by improving antenna gains is also scheduled. Due to the low SNR observed with the experiments explained in this paper at a bandwidth of 333 Hz, one could conclude that in order to transmit data with OFDM symbols, with intercarrier separation explained above, with all carriers mapped with data and with a signal bandwidth of 5 KHz, a 12 dB improvement of the SNR should be provided.

Another goal is the evaluation of several combinations of multi-carrier modulation with spread spectrum techniques, what is called as MC-CDMA and MC-DS-CDMA. The point is to take advantage of the processing gain provided by the spreading sequence and to maximise the spectral efficiency, robustness and flexibility of the data link.

Acknowledgements

The aforementioned SANDICOM project has been developed in the framework of the research project REN2003-08376-C02-01 and the complementary action CGL2005-24213-E funded by the Spanish Government.

References

[1] J.A. Davis, J. Jedwad “Peak-to-Mean Power Control in OFDM, Golay Complementary Sequences and Reed-Muller Codes”, IEEE Transactions on Information Theory, vol 45,Nº 7, November 1999.

[2] G. Duprat “Demodulation and decoding studies of the 39-tone MIL-STD-188-110A HF signal” Defence R&D Canada.

[3] K. Fazel, S. Kaiser, Multi-Carrier and Spread Spectrum Systems, John Willey & Sons Ltd, 2003.

[4] M.J.F.-G. García, S. Zazo, J.M. Paez-Borrallo, “Pilot patterns for channel estimation in OFDM”, IEEE Electronic Letters, Vol 36, 8 June 2000 Pages 1049-1050.

[5] D.T. Sandwell, "Biharmonic Spline Interpolation of GEOS-3 and SEASAT Altimeter Data", Geophysical Research Letters, 2, 139-142,1987.

[6] J.C. Socoró, J.A. Moran, J.L. Pijoan, F. Tarres, A blind joint channel and data estimation algorithm for DS-SS ionospheric radiolink, International Conference on Achoustics, Speech and Signal Processing (ICASSP'2001), Salt Lake City, USA, 2001.

[7] J.J. van de Beek, M. Sandell, O.P. Börjesson, “On channel estimation in OFDM systems”, 45º IEEE Vehicular Technology Conference, Chicago,I1, vol.2,pp.815-819, July.

[8] R. van Nee and R. Prasad, “OFDM for Wireless Multimedia Communications”. Artech House, 2000.

[9] C. Vilella, D. Miralles, J.C. Socoró, J.L. Pijoan, R.Aquilué, "A new sounding system for HF digital communications from Antarctica", 2005 International Symposium on Antennas and Propagation (ISAP2005), 3-5 August 2005, Seoul, Korea.

[10] C. Vilella, J.C. Socoró, D. Miralles, J.L. Pijoan, P. Bergadà, “HF channel measurements for digital communications from Antartica”, 11th International ionospheric Effects Symposium IES 2005, Alexandria, Virginia, USA, May 2005.

Appendix B

Multicarrier symbol design for HF transmissions from the Antarctica based on real channel measurements, in Proceedings of the MILCOM 2006

MULTICARRIER SYMBOL DESIGN FOR HF TRANSMISSIONS FROM THE ANTARCTICA BASED ON REAL CHANNEL MEASUREMENTS

Ricard Aquilué
Pau Bergadà
Marc Deumal
and
J.L. Pijoan
Dept. of Communications and Signal Theory
La Salle Engineering, Ramon Llull University
Pg. Bonanova 8, Barcelona, Spain

ABSTRACT

Last fifteen years improvements in HF digital systems have made ionospheric communications a true alternative to low bit rate, long distance links, especially in the polar caps where alignment with geostationary satellites is not always possible. Our previous research efforts were focused on using pseudo-noise (PN) sequences and Orthogonal Frequency Division Multiplexing (OFDM) pilot symbols to evaluate the 7900 miles link from the Spanish Antarctic Base Juan Carlos I to Spain, crossing the equatorial belt. In this paper we face the problem of designing the OFDM physical layer. Two multicarrier transmission schemes are proposed and compared based on channel measured transfer functions and noise plus interference records. Special attention is paid to pilot pattern design in order to maximize the system performance while assuring high power and bandwidth efficiency. The quality and throughput in real transmissions from the Antarctica, as well as the evolution of BER in front of interferences, are studied.

INTRODUCTION

Data communications from the Antarctica is mainly achieved via satellite. However, since communication with geostationary satellites is not always possible from the poles, skywave ionospheric radiocommunications have become a good and inexpensive alternative. The Research Group in Electromagnetism and Communications from La Salle School of Engineering, Ramon Llull University, is working on the design of a robust unidirectional system for very long distance HF communications. The transmitter is located at the Spanish Antarctic Base (SAB) in Livingston Island (62.6ºS,60.4ºW) and the receiver is located at the Ebre Observatory (EO) in Spain (40.8ºN, 0.5ºE).

As a first step towards the implementation of the radiomodem the significant parameters of the ionospheric link between the Antarctica and Spain were measured. In that sense a sounding system, named SANDICOM (Sounding System for Antarctic Digital Communications), was designed. SANDICOM is based on a digital platform with high speed A/D/A converters and FPGA devices. The signal is fully processed digitally and, as a result, only amplification and some filtering are performed in the analog domain [1,2].

Although channel measurements are still being done to obtain sufficient statistics of the channel, current work is mainly focused on the preliminary design of the system for data transmissions. Two major advanced modulation techniques are being evaluated: Direct-Sequence Spread-Spectrum (DS-SS) Signaling [3] and Orthogonal Frequency Division Multiplexing (OFDM) [4]. In this paper we will focus on the design and evaluation of OFDM as a system candidate. In an OFDM system the data are transmitted over a number of parallel frequency channels, modulated by a baseband PSK symbol. The advantage of this technique is that it has an intrinsic robustness against multipath fading channels and narrowband interference.

In [4] we presented a preliminary OFDM system that was used to evaluate the success of multicarrier modulations in long distance data communications. The work was focused on evaluating the channel estimation capabilities in long-distance low-SNR HF link. In this paper, the channel measurements from the link between the Antarctica and Spain are used to find the optimum parameters of the OFDM physical layer, from theoretical analysis and exhaustive simulations. Subsequently, a physical layer technique that reduces the effect of interferences is evaluated. Simulation results with recorded interferences at the receiver site are used to evaluate the performance improvement capabilities of an OFDM system exploiting this technique compared to a conventional OFDM system.

SYSTEM ARCHITECTURE

The system that was designed for channel sounding (SANDICOM) is also used for preliminary data transmissions. One of the major considerations to be considered for the design of the physical layer is the strict power consumption restrictions at the transmitter site. Since the SAB is only served by wind and solar power during 8 months per year, a power amplifier capable of transmitting at a maximum power of 250 watts is used.

As multiple frequencies in the HF band are used, a broadband antenna is required. A monopole and an antenna tuner have been employed both in the emitter and in the receiver because of the ease of installation and the acceptable performance they show in the frequency range from 4 to 18MHz.

Both, transmitted power and antenna restrictions, imply that low SNR will be obtained at the receiver site. For instance, when a transmission bandwidth of 300 Hz is used an average SNR at the receiver of 8 dB has been measured when the channel is available [5]. In the next campaign, a directive antenna will be used at the receiver site in order to increase the available SNR up to 10 dB in a 1 KHz. This is the condition assumed it the following design.

SYMBOL DESIGN

Channel state information prior to the demodulation stage is needed at the receiver in order to compensate the different attenuation and phase rotations of the subcarriers introduced by the channel. First, the pilot pattern has to be designed. We define the efficiency of an OFDM system as a function of the pilot density, and it can be approximated as:

$$\rho_{PD} \approx \frac{N_T \cdot N_F - 1}{N_T \cdot N_F} \tag{1}$$

Where N_T and N_F are the pilot spacing in the time and frequency directions, respectively. If the pilots are too close to each other, an oversampling of the channel will occur causing an unnecessary penalty of the system efficiency. On the other hand, if pilot spacing is too large, channel variations will go unnoticed, dramatically reducing the system performance. In order to get a good estimation of the channel, the pilot grid has to fulfill the two-dimensional sampling theorem [6-8]. This theorem restricts the pilot spacing in the time domain to fulfill the following expression:

$$\frac{1}{2 \cdot N_T \cdot T_S} \geq f_D \tag{2}$$

Where f_D is the maximum Doppler frequency and T_S is the OFDM symbol time. The pilot spacing in the frequency domain has to fulfill:

$$\frac{1}{N_F \cdot \Delta f} \geq \tau \tag{3}$$

Where τ is the maximum delay spread of the channel and Δf is the subcarrier separation.

Next, a cyclic prefix is added at the beginning of each OFDM symbol in order to assure that no inter symbol interference (ISI) occurs. Let T_{CP} be the length of the cyclic prefix and T_U the length of the useful part of the symbol. The total symbol time becomes $T_S = T_{CP} + T_U$. The efficiency of an OFDM system due to the cyclic prefix can be expressed as

$$\rho_{CP} = \frac{T_U}{T_U + T_{CP}} \tag{4}$$

Note that in order to increase both the spectral and power efficiency, large values of ρ_{CP} should be used, i.e. the useful symbol time should be much larger than the length of the cyclic prefix. Let us define the efficiency of the OFDM system from (1) and (4) as:

$$\rho = \rho_{PD} \cdot \rho_{CP} = \frac{N_T \cdot N_F - 1}{N_T \cdot N_F} \cdot \frac{T_U / T_{CP}}{T_U / T_{CP} + 1} \tag{5}$$

Figure 1 represents the efficiency of the system as defined in (5). It can be appreciated that for T_U / T_{CP} values over 16, efficiency improves slowly.

We recall from [5] that typical 10dB-delay spread of 2.5 msec and maximum 10dB-doppler frequency of 1.6 Hz have been observed during the sounding survey. In order to avoid ISI, the cyclic prefix is set to be T_{CP} = 3 milliseconds. From the sampling theorem introduced in (2) and (3), the maximum spacing between time and frequency pilots can be obtained.

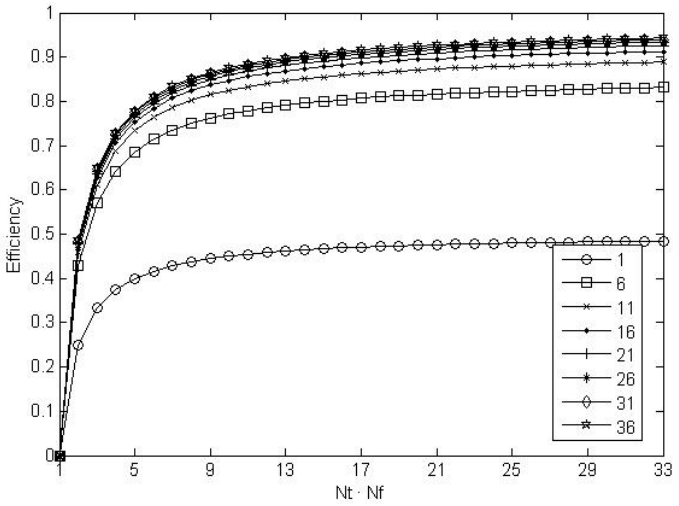

Figure 1. Efficiency of the system as a function of the pilot density and the ratio T_U / T_{CP}

Choosing a useful time in order to get a $\rho_{CP} > 0.95$, we have T_U = 60 milliseconds (T_U / T_{CP} = 20). If 60 milliseconds is used as the useful symbol time, we have:

$$N_F \le \frac{1}{\tau \cdot \Delta f} = \left\lfloor \frac{1}{0.0025 \cdot 1/0.06} \right\rfloor = 24 \qquad (6)$$

$$N_T \le \frac{1}{2 \cdot f_D \cdot T_S} = \left\lfloor \frac{1}{2 \cdot 1.5 \cdot 0.063} \right\rfloor = 5 \qquad (7)$$

The sampling theorem assumes a frequency doppler caused by different celerity vectors between transmitter and receiver and a uniform power density of the channel scattering function [9]. Moreover, some "rule of thumbs" can be found in the literature [8,10,11] that suggest a minimum oversampling of 2x or even more exhaustive channel sampling. If we focus on the ionospheric channel, spreading values varies widely from one path to another, so it is possible that the strongest signal path is not affected by the fastest variations. If dealing with low SNR levels, the effects of the weakest paths will go unnoticed, so if we synchronize to the strongest path, there is no need to track other paths variability if their relative level is low enough, yielding a more relaxed design. In addition, the fastest ionospheric layers variance occurs during the sunrise and sunset periods. If the channel propagation is not favourable for an OFDM transmission, the effects of these periods should not be taken into account [5]. There are several combinations of $N_T T_S$, $N_F \Delta f$ and T_U that meet the sampling requirements shown in (1) and (2) respectively. Using channel measurements when propagation has been favourable enough for an OFDM transmission, a global best solution will be fulfilled.

The maximum useful symbol time will be found using the simulation scheme of Figure 2. Random data is generated and after a serial to parallel conversion, data is mapped into a BPSK constellation space. Multipath ionospheric channel realizations taken from real measurements are applied in the frequency domain. The transfer function is directly extracted from the estimations of [4], so, no channel model is used. In order to find the maximum symbol time, white gaussian noise (AWGN) is added as the first approach. Beginning with an oversampled channel estimation, several pilot densities will be tested in order to search the optimum symbol time for this channel.

Table 1. Optimum symbol time – Initial search parameters

SNR	10 dB
T_{CP}	3 msec
T_U	5, 55, 105, 155, 205, 255, 305 and 355 msec
N_T	2, 3, 4, 5, 6, 7
N_F	2, 3, 4, 5, 6, 7
Channel estimation method	Least Squares
Interpolation method	Nearest pilot padding
Runs for each T_U, N_T and N_F combination	1.000
Total runs	288,000

Table 1 shows the simulation parameters: Six values of N_T and of N_F are evaluated based on hexagonal pattern locations [4,12] among several useful symbol times ranging from 5 to 355 msec. In order to compensate for the channel effects with reduced complexity methods (real time operation oriented), the channel is estimated with the Least Squares method [13] and interpolated with the novel Nearest Pilot Padding method [14]. This interpolation technique offers similar performance than other more complex methods in low SNR scenarios.

When the pilots are close enough to each other, many values of the symbol time result in a good channel estimation. This circumstance is exposed Figure 3 (N_T = 2 N_F = 2), where the channel is sampled over the minimum sampling frequency and the BER will not improve even though the pilot density is increased.

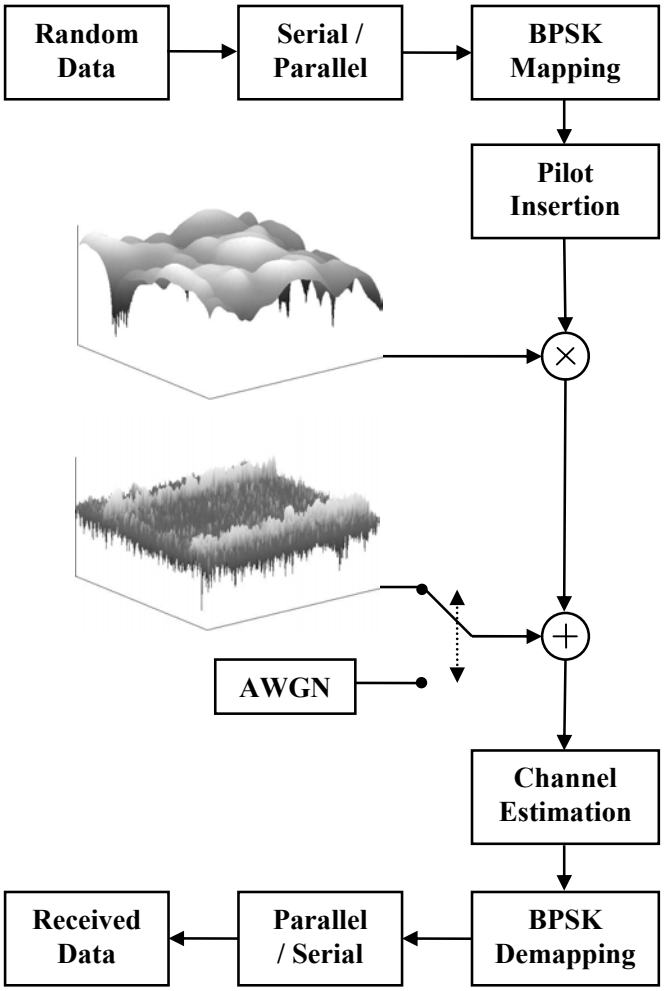

Figure 2. Simulation block diagram with real channel measurements

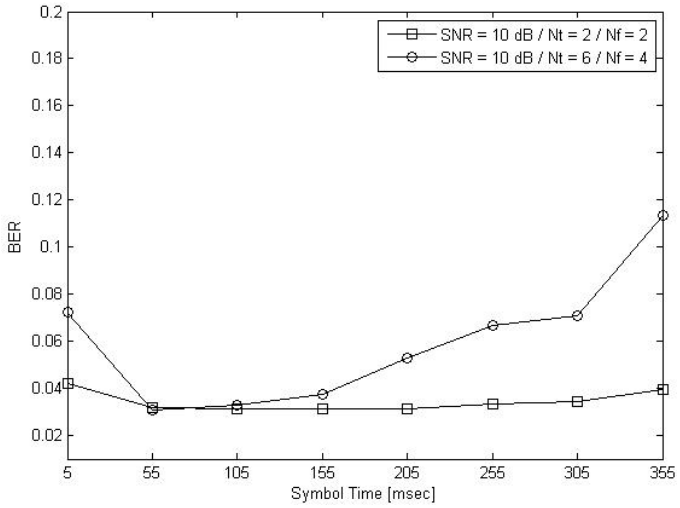

Figure 3. BER and useful symbol time (N_T = N_F = 2 and N_T = 6 N_F = 4)

As pilot spacing increase, BER levels begin to rise. However, there is an optimum symbol duration that exhibits the same BER than before. From Figure 3 (N_T = 6 N_F = 4), an optimal symbol time around 55 msec can be guessed.

A finest search is required, since a precision of 50 msec is not enough. The parameters used in order to find the exact value of the optimum symbol time are shown in Table 2.

Table 2. Optimum symbol time – Fine search parameters

T_{CP}	3 msec
T_U	25, 30, 35, 40, 45, 50, 55, 60, 65, 70, 75, 80, 85, 90, 95, 105 110 and 115 msec
N_T	5, 6, 7
N_F	5, 6, 7
Channel estimation method	Least Squares
Interpolation method	Nearest pilot padding
Runs for each T_U, N_T and N_F combination	1.000
Total runs	153,000

From Figure 4 we can state that the maximum useful symbol time for low BER values is 75 msec. Once the symbol time is fixed, simulations for finding the optimum value for N_T and N_F are performed.

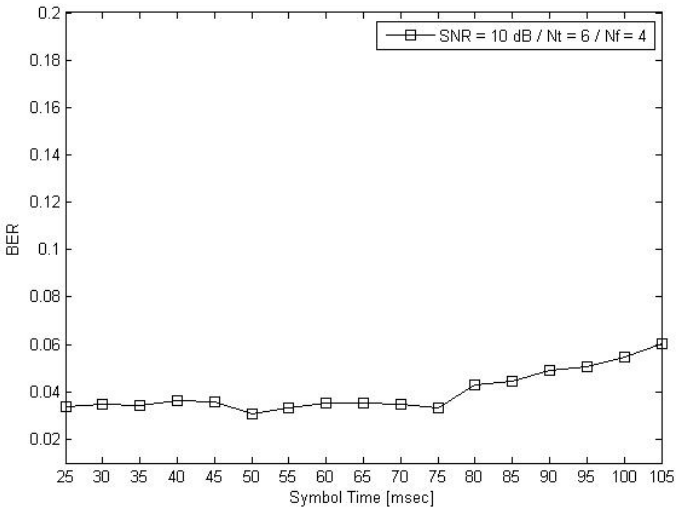

Figure 4. Detail of BER and symbol time (N_T = 6 N_F = 4)

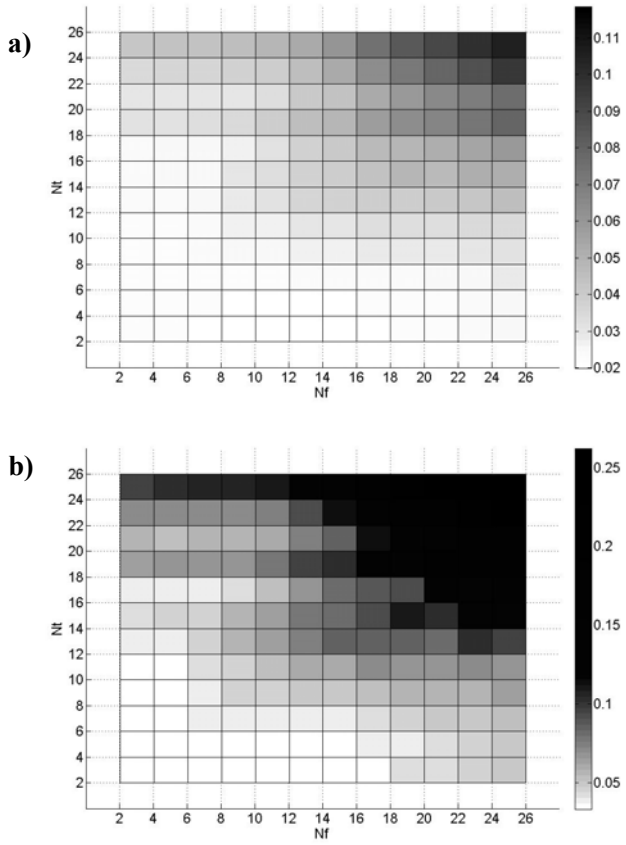

Figure 5. BER and pilot densities from $N_T = N_F = 2$ to $N_T = N_F = 26$ (a. average channel and b. worst channel)

In Figure 5, the study for the average and worst channel is shown. If focused on the worst case, the maximum pilot spacing in the time domain without BER degradation is $N_T = 12$ and $N_F = 18$ for the frequency domain. Taking into account the pilot number efficiency, the maximum expected SNR at the receiver and following the balanced design approach defined in [8], the selected values for the OFDM symbol are presented in Table 3:

Table 3. Frame and symbol parameters

T_{CP}	3 milliseconds
T_U	75 milliseconds
T_S	78 milliseconds
Δf	13.33 Hz
N_T	6
N_F	12
ρ_{CP}	0.9615
ρ_{PD}	0.9861
ρ	0.9481
N_{SC}	73
R_B	948 bps

Where N_{SC} is the number of subcarriers per OFDM symbol and R_B is the raw modulation bit rate.

INTERFERENCE EFFECTS

In HF channels, the level of interference is usually the limiting factor, more than SNR and multipath effects. In this section, measured interference records have been used to compute the robustness of two multicarrier modulations against interference.

First, a conventional OFDM modulation with the parameters shown in Table 3 will be tested under the measured multipath channel and AWGN (OFDM AWGN). Then, recorded noise plus interference (OFDM AvgNPI) samples will be used instead of AWGN and finally, OFDM performance will be evaluated under the worst interference conditions found during the sounding campaign (WstNPI). The OFDM AvgNPI simulation will show the average performance of the link. This is computed using the average interference found among all the situations during the sounding survey. Interferences in the HF band are usually slow variant, so they could be avoided if a feedback channel exists. In a simplex communication system, the interference location is unknown at the transmitter site, so the use of frequency diversity will guarantee the best average performance of the link.

Table 4. Interference effects – Simulation parameters

Num. subcarriers	73
T_{CP}	3 milliseconds
T_U	75 milliseconds
T_S	78 milliseconds
Δf	13.33 Hz
OFDM BW	1KHz
N_T	6
N_F	12
Hopping rate (h_R)	0 Hz (hop every 0 symbols) 12.82 Hz (hop every 1 symbol) 1.83 Hz (hop every 7 symbols) 0.41 Hz (hop every 31 symbols)
Hopping frequency	1KHz
SNR	0 to 14 dB (1 dB step)
Runs for each h_R and SNR combination	1.000
Total runs	60,000

OFDM has an intrinsic robustness against narrowband interference since the missing data of one subcarrier can be recovered if the information has been properly coded. This is only true when the interference bandwidth equals the subcarrier bandwidth and below. If interference

bandwidth is wide enough that equals the whole OFDM bandwidth, the multicarrier modulation sees the interference as a single carrier modulation would do, that is, as a global decrease of the SNR available at the receiver. In this situation, a frequency hopping approach with multicarrier modulation makes sense. Therefore, a frequency hopping OFDM modulation will be tested (Table 4) in order to approach the average performance of the conventional OFDM (OFDM AvgNPI).

In Figure 6, a conventional OFDM is compared with the results obtained by hopping the whole OFDM symbol by 1KHz frequency shift signal every 1,7 and 31 symbol times in order to evaluate the performance degradation due to the increase of the estimation error at the borders of the frequency / time matrix [9].

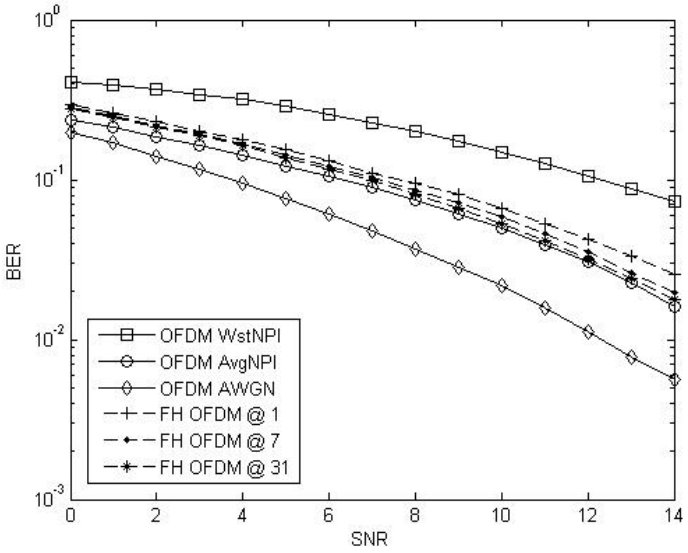

Figure 6. OFDM and FH-OFDM performances

There is a slightly decrease of the performance as the hopping rate increases. This is due to the fact that the area decreases faster than the perimeter of the frequency / time matrix and the ratio between the pilots located at the borders and the total number of pilots increases, yielding a decrease of the system performance. For hopping rates slower than 0.41 Hz, the performance almost equals the average performance of a standard OFDM.

Although slow hopping increases the estimation accuracy, fast hopping increases the diversity order, enhancing the correction capabilities of coding since errors are spread in time. However, this problem can be overcome by a deep interleaving, consequently the transmission delay will be penalised [15].

Interferences cause a serious impact on the system performance. From Figure 6, if we want to achieve the BER for the AWGN case, we are forced to reduce the number of active subcarriers in order to increase the SNR available at the receiver.

CONCLUSIONS

In this paper, the complete design of the most efficient useful symbol time and pilot density have been found for this trans-equatorial-belt 7900-miles-long ionospheric channel. On one hand, if the pilots are too close, the channel is oversampled and the efficiency is reduced without improving the estimation error. On the other hand, if the pilots are excessively spread along time and/or frequency dimension, the system performance will be dramatically reduced by channel aliasing. Although a generalized sampling theorem based on several mobile radio channel assumptions exists, a mismatch between the evaluation of that theorem and the exhaustive search for optimum symbol parameters has been exposed. In order to *a priori* properly estimate the pilot spacing requirements, several inputs are needed. First, an accurate path based channel sounding must be carried out in order to make the appropriate distinctions between path and multipath delay and doppler spread values. Second, without spreading gain, slightly high positive values of signal to noise ratio are needed in order to establish a reliable long distance link for low rate demanding applications. The OFDM has to be designed specifically for the time intervals where the propagation is good enough to transmit a non spread modulation.

Since a feedback channel is not available, frequency location information can not be known at the receiver. The risk of being jammed by a wideband interference can be overcome by hopping the OFDM signal among different carrier frequencies. Otherwise, if the carrier frequency is chosen based on link availability issues only, there is a risk of being jammed by wideband interference. The obtained results approach the average performance that we would get with a standard OFDM but without the risk of being continuously jammed.

In the next Antarctic campaign, an OFDM ionospheric link is expected to be established between SAB and OE based on the parameters found in this paper. The poor SNR available and the high interference level will constraint the maximum numbers of active subcarriers. A hexagonal pilot pattern with approximately 12 and 6 pilot spacing in frequency and time respectively will be used. Low complexity methods such Least Squares estimation and Nearest Pilot padding interpolation will be implemented

since a real-time FPGA based system is used for prototyping.

ACKNOWLEDGEMENTS

The aforementioned SANDICOM project has been developed in the framework of the research project REN2003-08376-C02-01 and the complementary action CGL2005-24213-E funded by the Spanish Government.

REFERENCES

[1] C. Vilella, J.C. Socoró, D. Miralles, J.L. Pijoan, P. Bergadà, "HF channel measurements for digital communications from Antartica", 11th International ionospheric Effects Symposium IES 2005, May 2005.

[2] C. Vilella, P. Bergadà, M. Deumal, J. L. Pijoan and R. Aquilué, "Transceiver Architecture and Digital Down Converter Design for Long Distance, Low Power HF Ionospheric Links", Proc. Ionospheric Radio Systems and Techniques, July 2006.

[3] M. Deumal, C. Vilella, R. M. Alsina, J. L. Pijoan, "A DS-SS Signaling Based System Proposal for Low SNR HF Digital Communications", Proc. Ionospheric Radio Systems and Techniques, July 2006.

[4] R. Aquilué, P. Bergadà, I. Gutiérrez, J.L. Pijoan, "Channel Estimation for Long Distance HF Communications based on OFDM Pilot Symbols", Proc. Ionospheric Radio Systems and Techniques, July 2006.

[5] C. Vilella, J. Socoró, J. L. Pijoan, I. Gutierrez and D. Altadill "An Antarctica to Spain HF Link. Oblique Sounding Results", Proc. Ionospheric Radio Systems and Techniques, July 2006.

[6] P. Hoeher, S. Kaiser, and P. Robertson, "Two-dimensional pilot-symbol aided channel estimation by Wiener filtering", in Proc. ICASSP, Apr. 1997, pp. 1845–1848.

[7] F. Sanzi and J. Speidel, "An adaptive two-dimensional channel estimator for wireless OFDM with application to mobile DVB-T", IEEE Trans. Broadcast., vol. 46, pp. 128–133, June 2000.

[8] P. Hoeher, S. Kaiser, and P. Robertson, "Pilot-symbol-aided channel estimation in time and frequency", Proc. Int. Workshop Multi-Carrier Spread-Spectrum, Apr. 1997, pp. 169–178.

[9] K. Fazel, S. Kaiser, Multi-Carrier and Spread Spectrum Systems, John Willey & Sons Ltd, 2003.

[10] Meng-Han Hsieh, Che-Ho Wei, "Channel estimation for OFDM systems based on comb-type pilot arrangement in frequency selective fading channels", IEEE Transactions on Consumer Electronics, Volume 44, Issue 1, Feb. 1998 Page(s):217 – 225.

[11] Morelli, Mengali, "A comparison of pilot-aided channel estimation methods for OFDM systems", IEEE Transactions on Signal Processing, Volume 49, Issue 12, Dec. 2001 Page(s):3065 – 3073.

[12] M.J.F.-G. García, S. Zazo, J.M. Paez-Borrallo, "Pilot patterns for channel estimation in OFDM", IEEE Electronic Letters, Vol 36, 8 June 2000 Pages 1049-1050.

[13] Van de Beek, Edfors, Sandell, Wilson, Borjesson, "On channel estimation in OFDM systems", Vehicular Technology Conference, 1995 IEEE 45th Volume 2, 25-28 July 1995 Page(s):815 - 819 vol.2.

[14] I. Gutierrez, J.L. Pijoan, F. Bader , R. Aquilué, "New Channel Interpolation Method for OFDM Systems by Nearest Pilot Padding", in Proc. European Wireless 2006, March 2006.

[15] L. Hanzo, S. X. Ng, T. Keller, W. Webb, "Quadrature Amplitude Modulation: From Basics to Adaptive Trellis-Coded, Turbo-Equalised and Space-Time Coded OFDM, CDMA and MC-CDMA Systems", John Wiley & Sons, Ltd. 2004.

Appendix C

Codificación de fuente y señalización OFDM ad-hoc para enlace HF de larga distancia, in Proceedings of the URSI 2008

Codificación de fuente y señalización OFDM ad-hoc para enlace HF de larga distancia.

J. Mauricio[(1)], P. Bergada[(1)], J.L. Pijoan[(1)], S. Marsal[(2)], J.M. Torta[(2)]
jmauricio@salle.url.edu, pbergada@salle.url.edu, joanp@salle.url.edu, smarsal@obsebre.es, jmtorta@obsebre.es
(1) Dpto. de Comunicaciones y Teoría del Señal. Ingeniería La Salle. Universidad Ramon Llull.
(2) Observatori de l'Ebre. CSIC. Universidad Ramon Llull.

***Abstract*- HF communication systems are a reliable alternative as a backup system for slow speed data communications. This can be achieved since the growing of the digital systems and the reduction of the equipment costs. The Research Group on Communications (GRECO) from Ramon Llull University, has been sounding the ionospheric channel between Livingston Island (Antarctica) and Ebro Observatory (Spain) for five years. In the present stage, a modem is being designed to transmit geomagnetic data on real time from Livingston Island, and cover the 12700 Km ionospherfic radio link. In this paper an ad-hoc source coder design and an OFDM based signalling system are approached.**

I. INTRODUCCIÓN

Este trabajo se enmarca dentro del proyecto "Monitorización de la variabilidad geomagnética e ionosférica en la Isla Livingston. Técnicas avanzadas para su caracterización y transmisión de los datos en HF".

Uno de los objetivos principales de dicho proyecto es la implantación de una estación geomagnética en la Base Antártica española Juan Carlos I (BAE), situada en la Isla Livingston (62.6ºS, 60.4ºW). Los datos que genera dicha estación geomagnética son capturados por un sistema de adquisición digital que posteriormente serán usados para el estudio de la variabilidad geomagnética en la Isla Livingston.

Por otro lado, se ha realizado un sondeo vertical y oblicuo entre la BAE y el Observatorio del Ebro (OE) en España (40.8ºN, 0.5ºE) durante las últimas cinco campañas antárticas. A partir del sondeo oblicuo se han deducido las características de la variabilidad de la ionosfera entre dichos puntos, tales como: disponibilidad, relación señal-ruido (SNR) y dispersión temporal y frecuencial. A partir de los resultados estudiados durante los últimos cinco años, se pretende implementar un módem capaz de transmitir los datos generados por el sensor geomagnético anteriormente citado.

El enlace ionosférico comprendido entre la BAE y el OE cubre una larga distancia (12700 Km), con más de 150 dB de pérdidas en algunos casos y con altos niveles de interferencia en el receptor [1]. Además, debido a restricciones energéticas en la BAE, la potencia de transmisión no supera los 250W, lo que supone bajas SNR en el receptor. Las antenas utilizadas son monopolos sintonizables, las mismas que en la fase de estudio del canal, ya que la disponibilidad de la ionosfera tiene dependencia en tiempo y frecuencia. En esta fase final del proyecto se prevé utilizar una antena directiva en recepción con el objetivo de mejorar la SNR y reducir el nivel de ruido. En el transmisor se conservará el monopolo debido a la no viabilidad de la instalación de una antena directiva en la BAE.

El estudio del canal ionosférico entre la BAE y el OE reveló que la ionosfera podía ser caracterizada como un canal dispersivo en tiempo y frecuencia. Tal como está extensamente explicado en la literatura [2], una modulación multiportadora, como es OFDM (*Orthogonal Frequency Division Multiplexing*), actúa eficientemente contra un canal multicamino, ya que puede sacar provecho de la diversidad frecuencial si se aplica codificación a los símbolos transmitidos; además de reducir la complejidad del sistema de detección y ecualización respecto a un sistema monoportadora.

En este trabajo se estudiará el uso de una codificación de fuente más óptima que la utilizada actualmente, *INTERMAGNET*, con el objetivo de reducir la cantidad de datos a transmitir y también se estudiará la viabilidad de un sistema de señalización mediante símbolos OFDM, para obtener una tasa de transferencia de bits suficiente como para transmitir los datos que genera el sensor teniendo en cuenta los bajos niveles de SNR en el receptor, la poca disponibilidad del canal y la no viabilidad de la implementación de un canal de retorno.

En el apartado II se explica la codificación de fuente aplicada a los datos generados por el sensor geomagnético. En el apartado III se detalla la implementación de la señalización mediante símbolos OFDM. En el apartado IV se mostraran los resultados obtenidos y finalmente en el apartado V, las conclusiones a las que se ha llegado a partir de los resultados obtenidos.

II. CODIFICACIÓN DE FUENTE

En todo sistema de transmisión digital, la codificación de fuente es una de las piezas clave del sistema. En los casos en que los datos siguen unos ciertos patrones, el estudio de la fuente que los genera es más que recomendable.

El primer paso será estudiar el sensor que proporciona los datos. En la Figura 1 se puede observar el diagrama de bloques del sensor geomagnético:

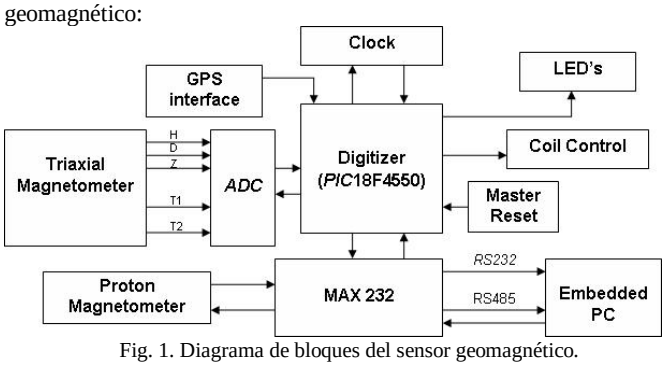

Fig. 1. Diagrama de bloques del sensor geomagnético.

El sensor está formado por un magnetómetro de protones digital y un magnetómetro triaxial analógico con dos sensores de temperatura cuyas señales son digitalizadas por un conversor analógico-digital (ADC). El dispositivo que controla los magnetómetros es un microcontrolador PIC18F4550, que tomará

decisiones en función de la trama horaria obtenida a través del módulo GPS, y transmitirá los datos a un *Embedded* PC a mediante dos puertos serie.

El *Embedded* PC se encarga de guardar los datos en una memoria Flash y de reducir el volumen de los datos para poder ser transmitidos vía satélite o a través del transmisor HF. Dicha reducción consiste en calcular el promedio de las muestras comprendidas entre cincuenta segundos antes y cincuenta segundos después del minuto a promediar con una función peso gausiana. En la siguiente expresión [3] se observa en que consiste el cálculo:

$$\langle x \rangle = \sum_{\substack{t_i=-50s \\ \Delta t_i=10s}}^{50s} c_{t_i} x_{t_i} = A \sum_{\substack{t_i=-50 \\ \Delta t_i=10s}}^{50} x_{t_i} \exp\left(-\frac{t_i^2}{2\sigma^2}\right) \quad (1)$$

Cada minuto se generaran un total de cuatro valores: H, D, Z y F correspondientes a las medidas de campo magnético. En el caso de H, Z y F las unidades son de nano-Teslas (nT) y la resolución deseada es de décimas de nano-Teslas (dnT). En el caso de D las unidades son minutos de arco (') y la resolución deseada es de centésimas de minuto de arco.

Una vez transcurridos doce minutos se genera una trama *INTERMAGNET* IMF v2.83 que contiene los cuatro valores de los últimos doce minutos. Dicha trama tiene una longitud de 126 bytes tal como se explicita en la Figura 2.

#Time (3B)	Offset (4B)	Flags (2B)	ω , φ (3B)	Padding (18B)
Data (96B)				

Fig. 2. Formato de la trama IMF v2.83.

$$Offset_i = floor\left(\frac{\min(DataIN_i)}{8192}\right) \quad (2)$$

$$Data_{i,j} = DataIN_{i,j} - Offset \cdot 8192 \quad (3)$$

Gracias a la codificación del *offset* por separado, se pueden codificar los valores con dieciséis bits.

Teniendo en cuenta que las variaciones del campo magnético durante doce minutos no superaran los 100 nT, se observa que esta codificación es poco óptima. Además, en esta trama hay muchos valores que sí tienen sentido para la comunicación vía satélite, pero no para la comunicación punto a punto HF, de manera que se propone una estructura de trama alternativa, la GCF v1.00:

#Frame (8b)	DataLen (16b)	Hmin (18b)	Dmin (17b)	Zmin (19b)	Fmin (19b)
Data (-TBD- b)					

Fig. 3. Formato de la trama GCF v1.00.

$$Data_{i,j} = DataIN_{i,j} - HDZT\min_i \quad (4)$$

$$DataLen_i = \log_2[\max(Data_{i,j})] \quad (5)$$

Se intenta reducir al máximo todos los campos que no aporten información magnética y se codifican los datos de forma variable. A partir del cálculo iterativo de la longitud de trama en función de la cantidad de minutos a transmitir en la misma trama, se ha determinado que el número de minutos por trama que minimiza la cantidad de datos a transmitir es de quince minutos.

Se envía íntegramente el valor de los cuatro mínimos, sobre *DataLen* se indica el número de bits que son necesarios para enviar los cuatro tipos de valores diferencia, y sobre *Data* habrá dichos valores diferencia respecto el mínimo. Las ventajas más destacables son su sencillez y su optimización respecto a la trama *INTERMAGNET*. Como desventaja está su longitud variable: un error en los campos de longitud de los datos no solamente comportará un error en la transmisión de la trama actual, sino que también puede afectar a tramas posteriores.

Otra estrategia posible es transmitir tan solo los valores diferencia en complemento a dos (CA2) respecto el minuto anterior y tampoco transmitir el primer valor, sino el valor diferencia respecto a un valor inicial conocido, ya que las variaciones de los valores a transmitir en un año están acotadas dentro de las desviaciones que se describen en la Tabla 1:

ΔH	ΔD	ΔZ	ΔF
± 30000 dnT	± 400.00'	± 30000 dnT	± 30000 dnT

Tabla 1. Máximas desviaciones de H, D, Z y F.

Por lo tanto, se propone la estructura de trama GCFv1.10:

#Frame (8b)	DataLen (12b)	ΔH1 (16b)	ΔD1 (17b)	ΔZ1 (16b)	ΔF1 (16b)
Data (-TBD- b)					

Fig. 4. Formato de la trama GCF v1.10.

$$Data_{i,j} = DataIN_{i,j} - DataIN_{i,j-1} \quad (6)$$

$$DataLen_i = \log_2[\max(|Data_{i,j}|)] + 1 \quad (7)$$

El formato de trama es muy similar a la GCF v1.00. Lo más destacable es que en este caso los datos ya no dependen del valor mínimo, sino que sólo dependen del minuto anterior, de manera que los valores diferencia serán menores. Este hecho no solamente hará que la longitud de la trama disminuya, sino que se requerirán menos bits para indicar la longitud de los datos. Además, ya no se envían los cuatro valores de referencia, sino que se envía el valor de desviación respecto unos valores preestablecidos, con lo que se consigue optimizar un poco más la trama.

La principal ventaja es que previsiblemente será capaz de comprimir más los datos que la propuesta de trama anterior. Las desventajas son las mismas que las de la trama GCF v1.00.

Por lo tanto, se han propuesto dos estructuras de trama que intentan minimizar la cantidad de bits a transmitir. Una vez obtenidos los resultados se decidirá cual de las dos propuestas es la más adecuada.

III. Señalización mediante símbolos OFDM

En estudios anteriores se estimaron las características del canal ionosférico entre la BAE y el OE mediante símbolos OFDM. Estas pruebas se realizaron símbolos pilotos en todas las subportadoras. De los resultados obtenidos con estas pruebas se pudo constatar el elevado nivel de ruido y la existencia de señales interferentes de gran potencia en el receptor.

Debido a estas evidencias se optó por trasmitir una secuencia pseudo aleatoria en las subportadoras de un símbolo OFDM (N subportadoras) y éste mapearlo en uno de los M *slots* frecuenciales dentro del ancho de bando utilizado (BW_u). El procedimiento consiste por un lado en utilizar uno de los M *slots* frecuenciales disponibles en función de la información a transmitir y por otro, mapear sobre dichos símbolos una secuencia pseudo aleatoria de longitud N.

Uno de los problemas más críticos de una modulación OFDM es la gran fluctuación de la envolvente de los símbolos. Cuando las N señales senosoidales que lo componen se suman coherentemente, la potencia de pico de la envolvente es $\sqrt{N}$ veces superior a la potencia media de la envolvente. Para caracterizar dicha variación se puede utilizar el parámetro PAPR (*Peak to Average Power Ratio*) que indica la relación entre la potencia de pico y la potencia media del símbolo OFDM.

Tal como se ha explicado en la introducción, la potencia de la señal que se espera recibir puede oscilar entre -80 dBm y -100 dBm.

Este hecho provoca que la potencia media en transmisión sea un factor muy crítico, no pudiéndose soportar elevados índices de PAPR que supondrían reducciones elevadas de la potencia media trasmitida. Por esta razón se decidió transmitir símbolos OFDM, mapeando secuencias *Golay* binarias en sus subportadoras, ya que dichas secuencias aseguran un PAPR inferior o igual a 3 dB [4].

En la Figura 5 se puede observar un esquema del procedimiento de mapeo de un símbolo OFDM con N subportadoras dentro de BW_u, compuesto por M *slots* frecuenciales, cada uno de longitud N.

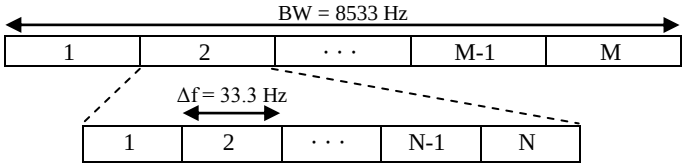

Fig. 5. M *slots* frecuenciales de N secuencias Golay.

A partir de los datos obtenidos en pruebas anteriores [5], el símbolo OFDM óptimo para el enlace ionosférico entre la BAE y el OE cumple con las características que se resumen en la Tabla 2.

Tiempo de símbolo útil	T_u = 30 mseg
Tiempo prefijo cíclico	T_g = 2.8 mseg
Tiempo símbolo	$T_s=T_u+T_g$ = 32.8 mseg
Separación entre subportadoras	Δf = 33.3 Hz
Ancho de banda símbolo OFDM	BW_1 = 266,44Hz, BW_2= 532,8 Hz
Ancho de banda utilizado	BW_u = 8533Hz
Longitud secuencia Golay = # subportadoras	N_1 = 8 , N_2= 16
Frecuencia de salto	FH = 30.48 Hz
Tasa de bits trasmitidos	243 bps

Tabla 2. Características del símbolo OFDM.

Para un símbolo OFDM se codifican $\log_2(M)$ bits para la selección del *slot* frecuencial y $\log_2(N)$ bits para la selección de la secuencia *Golay* a transmitir dentro de una familia de secuencias de longitud N. Por lo tanto, en cada símbolo se trasmitirán 8 bits, ya se use la configuración con 8 ó con 16 subportadoras.

En el receptor se aplica a la señal recibida la función *Maximum Likelihood* (ML) con todas las posibles N secuencias, con el objetivo de detectar en qué *slot*, de los M posibles, se ha transmitido el símbolo OFDM. En la ecuación (8) se describe el proceso que realiza el detector.

$$d[j]=\max_{k=1\ldots N}\left(\sum_{i=0}^{N-1} R[n+i+jN]\cdot seq_k[n+i]\right)\ldots j=1,\ldots,M \quad (8)$$

Donde max(d) indica el *slot* frecuencial donde se ha detectado con mayor probabilidad la secuencia seq_k trasmitida y R[n] es el símbolo recibido en el dominio de la frecuencia. En la Figura 6 se puede observar un diagrama de bloques del detector y del decodificador.

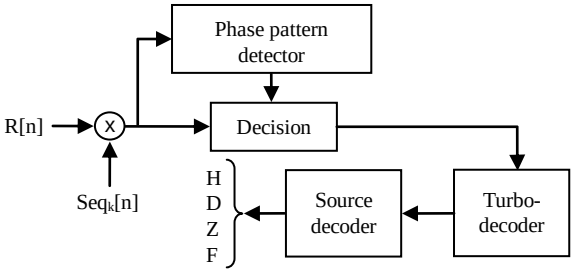

Fig. 6. Diagrama de bloques del receptor.

Los niveles de interferencia en el receptor son de elevada potencia; en el peor de los casos pueden superar la potencia de la señal esperada en 60-70 dB [6]. Este hecho provoca que la detección usando la función ML lleve a errores en casos con interferencias de elevada potencia.

Para poder detectar con éxito los símbolos OFDM y diferenciarlos de la señal interferente, se ha dividido el proceso de detección en dos fases: en la primera se obtiene una estimación del *slot* frecuencial usado, con la función ML; en la segunda se evalúa la relación de fase entre la secuencia recibida en el *slot* candidato y las N posibles secuencias trasmitidas. Se escoge como secuencia candidata aquella que presenta una variación de fase mínima entre muestras consecutivas, tal como se explica en la ecuación (9).

$$f[j]=\min_{k=1\ldots N}\left(\underset{i=1\ldots N}{angle}\left(\frac{R[n+i]}{seq_k[n+i]}\right)\right) \quad (9)$$

Si el sistema de detección de fase detecta que entre muestras consecutivas, en el *slot* candidato, la fase varía con brusquedad, se descarta el *slot* y se evalúa el siguiente candidato propuesto por el detector ML.

Pretendemos que este sistema de detección de fase junto al salto de frecuencia (FH) que experimenta el símbolo, combata con éxito las señales interferentes que aparecen en el receptor.

Para comprobar la fiabilidad de dicho sistema se han realizado dos experimentos (a) y (b), utilizando secuencias *Golay* de longitud 8 y 16 respectivamente, ocupando 32 y 16 *slots* respectivamente. En el caso (a) el ancho de banda ocupado por la secuencia es la mitad que en (b), lo que supone un incremento de 3 dB de SNR en el receptor. A su vez, el caso (a) contempla el doble de *slots* frecuenciales, lo que aumenta la incertidumbre de la detección del símbolo. En el caso (b), en cambio, la probabilidad que una señal interferente se solape con el símbolo trasmitido es mayor, pero a su vez la detección con la ecuación (8) contrarresta la pérdida de SNR al aumentar la ganancia de proceso ($10\log_{10}$ (N)) en 3 dB. Para evaluar cual de los dos casos optimiza el proceso de detección explicado anteriormente, se ha simulado dicho proceso para el caso de una longitud de secuencia *Golay* de 8 y 16 muestras. Las características del símbolo OFDM son las descritas en la tabla 2. En la tabla 3 se describen las características del canal utilizado en las simulaciones. Dichas características son las características que por término medio presenta este tipo de canal [1].

Número de taps	2
Delay Spread máximo (T_d)	2 mseg
Frecuencia *Doppler*	0.5 Hz

Tabla 3. Características canal simulado.

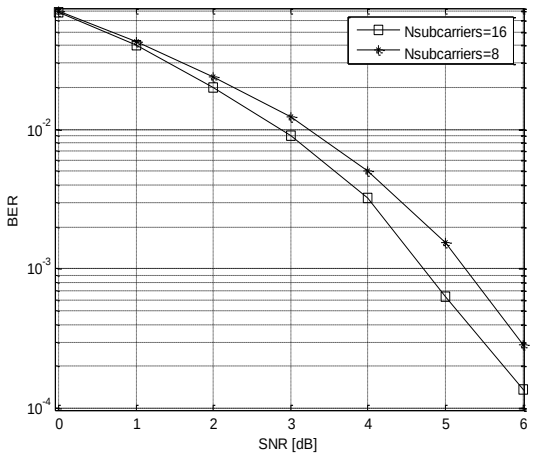

Fig. 7. Señalización con secuencias Golay de longitud N=8 y N=16.

Los resultados de la simulación, expuestos en la Figura 7, indican que el proceso de detección para una secuencia de longitud

16 es ligeramente mejor que para una secuencia de longitud 8. Se puede comprobar que la degradación de 3 dB de SNR en el caso de N=16 queda compensada por la diferencia entre las ganancias de proceso de dichas secuencias. La ligera mejora de 0.5 dB para SNR elevadas se puede achacar al hecho que la secuencia de mayor ancho de banda aprovecha mejor la diversidad frecuencial del canal. Para el caso de la simulación el ancho de banda de coherencia del canal $(0.61/T_d)$[5] se sitúa entre BW_1 y BW_2.

IV. Resultados

A. Codificación de fuente

A partir del histórico de datos magnéticos proporcionados por el OE [7], se ha analizado el rendimiento de las dos propuestas de codificador. Concretamente se han utilizado como referencia los datos magnéticos del año 2006 asumiendo que son suficientemente significativos como para que las conclusiones sean rigurosas.

Como se observa en la Figura 8 el segundo método de codificación de fuente (GCF v1.10) es más óptimo ya que consigue mejores tasas de compresión respecto a la codificación *INTERMAGNET*. Además, se han evaluado las prestaciones de los dos codificadores comparándolos con el algoritmo de compresión *RAR* en dos variantes: con bloques de quince minutos y con un solo bloque diario. Aunque *RAR* sea un algoritmo genérico de compresión que no tiene demasiadas similitudes con los codificadores propuestos, dará una visión cualitativa de los resultados y justificará el uso de un codificador *ad-hoc*.

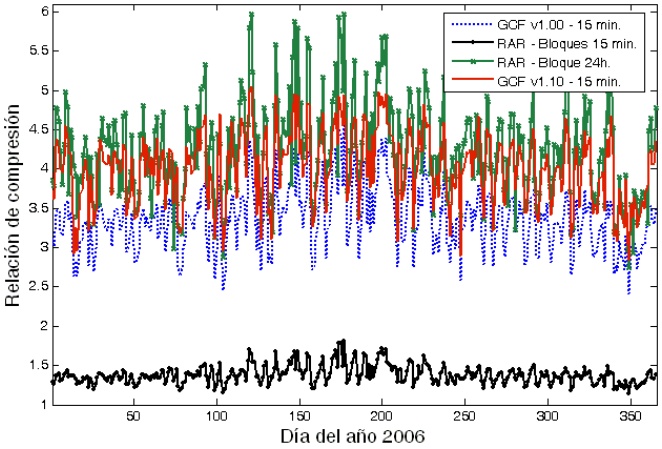

Fig. 8. Relación de compresión respecto codificación *INTERMAGNET*.

Se observa que en igualdad de condiciones (bloques de quince minutos), los dos codificadores propuestos superan al algoritmo *RAR*, ya que éste es un algoritmo genérico que comprime eficientemente cadenas binarias largas, como se observa en el caso de los bloques de 24 horas. El problema de generar un solo bloque diario es que un solo bit erróneo invalidará los datos de todo un día. En la Tabla 4 se observan los datos estadísticos de los diferentes métodos.

	RAR 15m	GCF v1.00	GCF v1.10	RAR 24h
Mín	1.1455	2.4116	2.8344	2.7969
Máx	1.8049	4.6033	5.0463	5.9692
μ	1.3820	3.3625	4.0122	4.2696

Tabla 4. Datos estadísticos de los diferentes métodos.

B. Señalización mediante símbolos OFDM

Durante la campaña 2007-2008 se transmitieron datos desde la BAE al OE aplicando la técnica de señalización explicada en el apartado III. En la Figura 9 se presenta la probabilidad de hallar una tasa de bits erróneos superior o igual a un cierto valor (BER_0), usando la función *Cumulative Distribution Function* (CDF). En dicha gráfica se puede observar que señalizar con longitudes de secuencia superiores mejora las prestaciones del sistema, tal como indicaba la simulación de la Figura 7. Estos resultados parecen indicar que obtienen mejores prestaciones aquellas secuencias que ocupan un ancho de banda que pueda introducir un mayor grado de diversidad frecuencial.

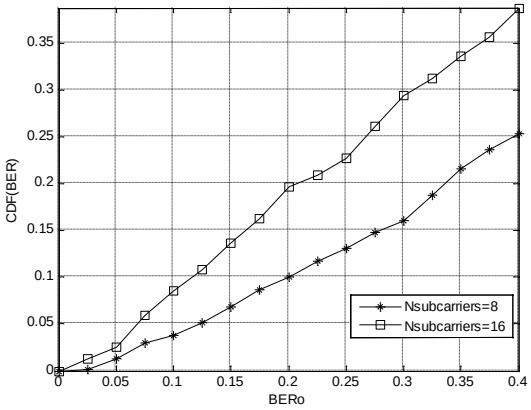

Fig. 9. Función de distribución acumulada del BER medido durante los días 15 y 16 febrero de 2008, con longitudes de secuencia N=8 y N=16.

V. Conclusiones

Se ha obtenido una tasa de compresión muy aceptable si se compara con los resultados de otros algoritmos. Una tasa de compresión estadística de 4.01 respecto a la codificación *INTERMAGNET*, permite el uso de un turbo código de velocidad 1/3 no solamente sin bajar la velocidad de bit efectiva, sino que aumentándola en comparación con un sistema con codificación *INTERMAGNET* y sin codificación de canal. Teniendo en cuenta la hostilidad del canal, BER obtenido después del turbo decodificador y la no viabilidad de implementar un canal de retorno, es necesario enviar los mismos datos más de una vez para poder aplicar técnicas *soft decision* que mejoren el BER.

Los datos estudiados hasta el momento indican que el sistema de señalización y detección descrito en este trabajo puede ser válido para transmitir datos en el enlace ionosférico entre la BAE y el OE. Se han realizado pruebas preliminares para evaluar el proceso de detección. Se ha llegado a la conclusión que utilizar secuencias cuyo ancho de banda supere el ancho de banda de coherencia del canal llevará a mejorar el funcionamiento del sistema. En futuros estudios se evaluará qué longitud de secuencia presenta las prestaciones óptimas, en cuanto a BER y tasa de bits trasmitidos.

Agradecimientos

Este trabajo de investigación se ha realizado en el marco del proyecto CGL2006-12437-C02-01 financiado por el Ministerio de Educación y Ciencia español.

References

[1] C. Vilella, D. Miralles, J.C. Socoró, J.L.Pijoan, R.Aquilué, "A new sounding system for HF digital communications from Antarctica.", 2005 International Symposium on Antennas and Propagation (ISAP2005), 3-5 August 2005, Seoul, Korea.

[2] J.J van de Beek, O. M. Sandell, O.P. Börjesson, "On channel estimation in OFDM systems.", 45th IEEE Vehicular Technology Conference, Chicago, IL, vol. 2, pp. 815-819, July 1995.

[3] D.F. Trigo, R. Coles, B. St-Louis, "INTERMAGNET technical referente manual version 4.2.", U.S. Geological Survey, 2004.

[4] J.A. Davis, J. Jedwad, "Peak-to-Mean Power Control in OFDM, Golay Complementary Sequences and Reed-Muller Codes.", IEEE Transactions on Information Theory, vol. 45, Nº 7, November 1999.

[5] P. Bergada, et al., "Multicarrier Modulation Proposal for Long Distance HF Data Links.", Ionospheric Effects Symposium, Alexandria 2008, USA.

[6] C. Vilella, et al. “On Site Receiver Testing. Application to Long Distance HF Links.”, Proceedings if International Symposium on Electromagnetic Compatibility EMC Europe, 2006.
[7] S. Marsal, et al., “Livingston Insland geomagnètic Observations, Antarctica, 2005 and 2005-2006 Survey.”, Observatori de l’Ebre. Roquetes, Tarragona.

Appendix D

Time interleaving study for an OFDM long-haul HF radio link, in Proceedings of the IRST 2009

Time Interleaving Study for an OFDM Long-Haul HF Radio Link.

P. Bergada*, M. Deumal*, R.M. Alsina*, J.L. Pijoan*

*GRECO, LA SALLE-Universitat Ramon Llull.
{pbergada, mdeumal, ralsina, joanp}@salle.url.edu

Keywords: HF communications, OFDM, Time Diversity.

Abstract

Communication with remote places is a challenge that in most cases is solved by means of satellites. However, for low-rate data transmission from remote sensors placed in Antarctic stations, this solution, a part from being too costly is of disadvantage since the geostationary satellite visibility is poor. In such scenarios, Skywave ionospheric communication systems represent a practical alternative to satellites.
HF communications suffer from impaired propagation, i.e. long delay spread, medium Doppler values, high level of attenuation and high level of interference. To cope with some of these impairments, in this paper, a study of the time interleaving effect applied to OFDM symbols transmitted through a multipath time-varying long-haul ionospheric channel is studied.

1 Introduction

The Research Group in Electromagnetism and Communications (GRECO) is studying the physical layer of a long-haul ionospheric digital data link between the Antarctic Spanish Base (ASB) in Livingston Island (62.6S,60.4W) and *Observatori de l'Ebre* (OE) in Spain (40.8N,0.5E). The major requirements of this data link include: i) Due to power restrictions in the Antarctic Base, the transmission power is strongly limited. ii) A very robust system capable of operating at very low SNR must be designed (135 dB of attenuation is expected at 10 MHz), especially if considering that since the transmission is simplex, (H)ARQ techniques can not be used. iii) Proper frequency scheduling is necessary to take full advantage of the reduced communication availability.
Previous studies of this link [1] have shown a strong correlation between the sunset and sunrise hours along the link and the frequency availability. Regarding multipath and Doppler spread, this channel exhibits typical values of 1.5 ms and 1 Hz, respectively, during calm hours whereas strongly variable values during sunset and sunrise hours.
A multicarrier modulation technique is being studied as a possible candidate to deal with time and frequency spread introduced by the ionospheric channel between the ASB and OE. Orthogonal Frequency Division Multiplexing (OFDM) has an intrinsic robustness against multipath delay spread because simultaneously transmit several symbols in parallel, so that OFDM symbol duration is greatly increased to eliminate the multipath delay spread effect. The greatly increased symbol duration makes it much vulnerable to the time-varying effect of the channel, which is inherent to a ionospheric link, due to the Doppler effect. On previous research studies OFDM symbols with different time duration were transmitted through this channel and conclusions about the optimum symbol length were reached [2]. Results showed that, in order to prevent from ISI and to guarantee a constant channel during the whole symbol, the OFDM optimum symbol length should be longer than 20 ms and shorter than 40 ms. Studies of the effects of time selective multipath fading on OFDM systems for mobile applications have shown that in order to achieve a 20 dB signal to noise and interference ratio, the OFDM symbol duration should be less than 8% of the channel coherence time [5].
In this paper the effect of time interleaving in a multipath time-varying long-haul ionospheric channel is studied. Time interleaver primary benefit is to provide time diversity, when combined with an error-correction coding. Transmitted symbols fully exploit time diversity when the time span over which the symbols are separated exceeds the channel coherence time and so, they are subjected to uncorrelated fading [3]. Therefore, what is expected is that performance improves when time interleaving depth gets nearer and beyond channel coherence time.
Moreover, for the real implementation a power amplifier (PA) operating close to saturation is used to increase power efficiency and at the same time maximize the transmission power, thus increasing SNR at the receiver. The PA input back-off is determined by properly clipping the OFDM symbol so that the full dynamic range of the D/A converter is exploited. BER performance degradation introduced by the clipping noise is negligible since small constellation sizes operating at low SNR are used [2].
This paper is organized as follows. First of all, on section two a brief description of the system used as HF transceiver as well as a fully explanation of the OFDM and time interleaver system is fulfilled. On section three results extracted from decoded OFDM symbols transmitted through the ASB-OE channel are exposed. Finally, some conclusions about which is the best time interleaving depth for a given channel, exploiting time diversity as fully as possible, are suggested.

2 System description

The system used to test the channel and to send data is a low power ionospheric radiomodem based on FPGA (Field Programable Gate Array) technology, AD and DA converters. A full explanation of its architecture can be found in [1]. The global positioning system provides the timing synchronization between emitter and receiver. Channel characteristics and data demodulation are obtained in non real time mode after using digital signal processing techniques.

OFDM symbols are used to test the performance of diferent time interleaving lengths. Figure 1 shows a block diagram of the OFDM transmitter. Firstly, data are encoded with a convolutional encoder. Its main main characteristics can be found on table 1. Afterwards, the encoded symbols are divided into N paths. On each of them a block interleaving is performed over a number of symbols. The size of the matrix (β_{IL}) of the block interleaver is only lower bounded by the expression (1).

$$\beta_{IL} \geq \frac{\Delta t_C}{T_S + T_{CP}} \quad (1)$$

Where Δt_C is the time coherence of the channel, T_S is the OFDM symbol length and T_{CP} is the cyclic prefix length. The size of the block interleaving matrix are specified this way since long burst of data symbols with low reliability corresponding to deep fadings of the channel transference function are avoided. In order to avoid the strong inter-daily channel variations to affect the conclusions of this study, four different data bursts are consecutively transmitted. Each burst is composed of a number of OFDM symbols and each burst performs different time interleaving depths. Table 1 summarizes the time interleaving length for each burst of symbols.

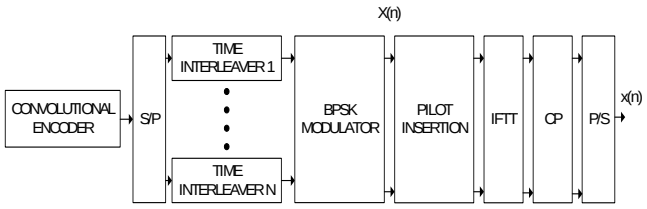

Figure 1. OFDM transmitter.

After the time interleaver data are modulated with a BPSK modulator. Before applying modulated symbols to the IFFT module, pilot symbols are inserted among data symbols. One pilot symbol is inserted every $4T_S$ in the time domain and every $3\Delta f$ in the frequency domain in consecutive symbols, hence Nyquist criteria is fulfilled in time and frequency domain since a Δt_C of 500 ms and a channel bandwidth coherence, BW_C, of 660 Hz are expected. In Figure 2 a picture of the time-frequency plan of the transmitted OFDM symbols is depicted.

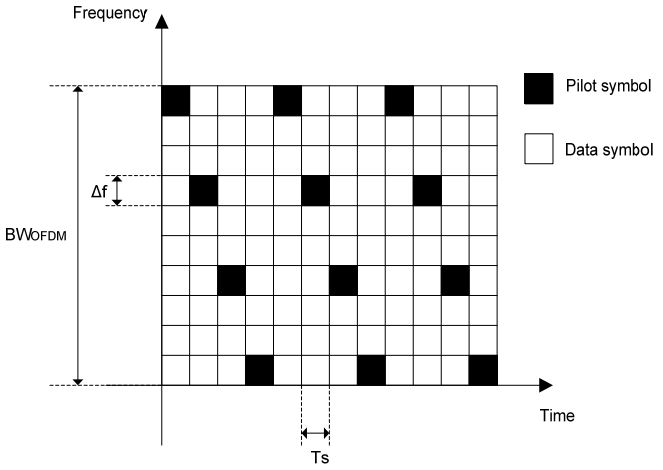

Figure 2. Pilot pattern used to estimate the channel.

OFDM symbol length	T_S: 30 ms
Cyclic Prefix length	T_{CP}:2.8 ms
Inter carrier frequency	Δf: 33.3 Hz
Number of carriers	N=10
OFDM symbol bandwidth	BW_{OFDM}=333.3 Hz
Modulation	BPSK
Interleaving time depth	T_{IL1}=131.2 ms, T_{IL2}=196.8 ms, T_{IL3}=262.4 ms, T_{IL4} =295.4 ms
Error correction code	Convolutional (code rate= ½, constraint length=7). Hard decisión Viterbi decoder.

Table 1. OFDM symbol characteristics.

Once pilot symbols are inserted among data symbols they are ready to be mapped to the IFFT module and create the time domain OFDM symbols. Equation 2 expresses the lowpass equivalent output of the OFDM modulator.

$$x(n) = \frac{1}{\sqrt{N}} \sum_{k=0}^{N-1} X(k) e^{j\frac{2\pi}{N}kn} \quad (2)$$

Where X(k) is the BPSK modulated pilot-data symbols in the frequency domain and N the number of subcarriers. The final module of this digital transmitter appends a cyclic prefix to each of the OFDM symbols to make it invulnerable to the multipath spread of the cannel. A cyclic prefix length longer than the maximum delay spread expected [1] is used.

At the receiver, inverse functions are applied in order to get the transmitted data (not shown for brevity). The cannel transfer function can be given by a Least Square estimator [6] from the received pilot symbols in the frequency domain as equation 3 expresses.

$$\hat{H}_{LS} = \frac{Y_K}{X_K} (K = 0,1,\cdots,N-1) \quad (3)$$

Where Y_K and X_K are, respectively, the received and transmitted pilot symbols in the frequency domain. Once the channel has been estimated at pilot positions, the time and frequency transfer function of the channel is interpolated using biarmonic splines [7].

3 Results

In order to test the performance of the proposed physical layer, from February the 11th to February the 13th of 2008, bursts of OFDM symbols were transmitted from the ASB to OE. Four burst of OFDM symbols with different time interleaving length were consecutively and constantly transmitted from 18h UTC to 09h UTC of the following day. Performance evaluation is shown as a function of the Cumulative Density Function (CDF) of the BER, i.e. the probability that the BER is less or equal to a given value that was obtained by doing bursts transmissions of 72 bits (144 coded bits), 162 bits (324 coded bits), 288 bits (576 coded bits) and 324 bits (648 coded bits) with time interleaving of $T_{IL1,}$ $T_{IL2,}$ $T_{IL3,}$ T_{IL4} respectively.

From the results we realized that there were basically two types of channels which appearance had a strong correlation with time. We realized that, approximately, from 18 UTC to 21 UTC, the channel showed high Doppler values and hence short coherence times and from 21 UTC to 04 UTC the channel showed lower Doppler values and hence longer coherence time values.

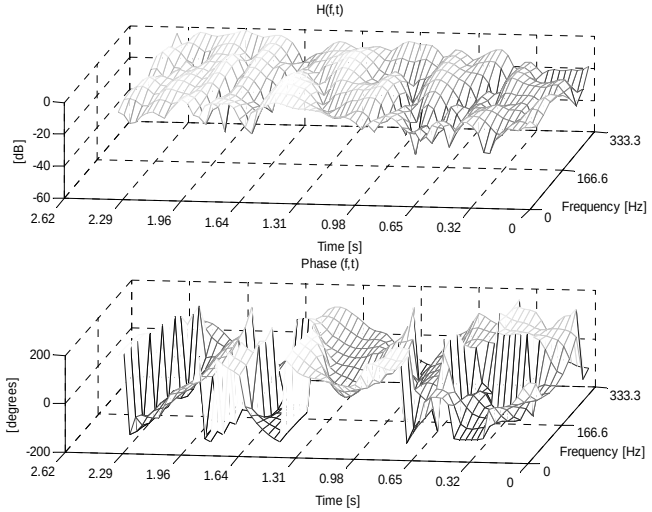

Figure 3. Amplitude Channel and Phase Channel Transfer Function sampled at 20:14 UTC the 11th of February 2008.

Figure 3 shows a 2.62 seconds sample of the time variant channel transfer function from which a value of channel coherence time of approximately 300 ms can be derived. This channel transfer function was sampled at 20:14h UTC when sunset was taking place near the receiver site. The same day between 18h UTC and 21h UTC the CDF of demodulated data was computed and shown in figure 4. As it is depicted in figure 4, bursts of symbols with long time interleaving perform slightly better than those with short interleaving. Very high differences of performance can not be observed between different bursts of symbols because time interleaving does not go far beyond the channel coherence time.

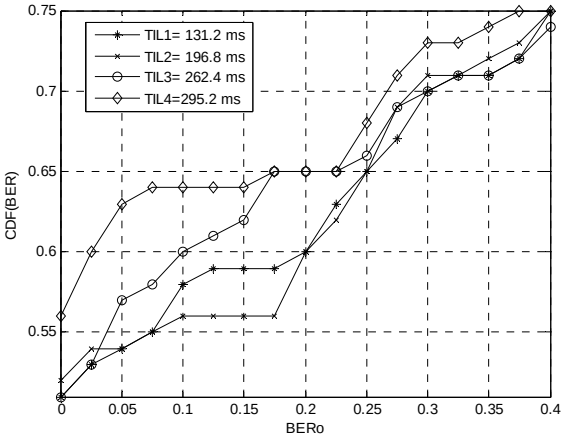

Figure 4. Cumulative Density Function of the BER of different burst of data with different time interleaving lengths (11th of February, approximately between 18h UTC and 21h UTC).

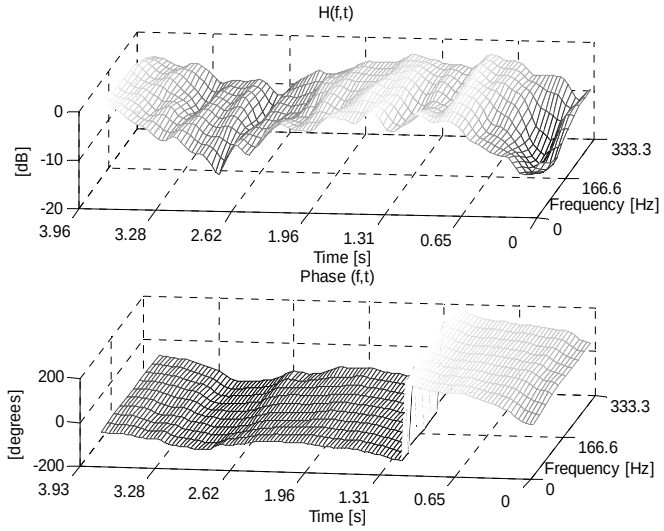

Figure 5. Amplitude Channel and Phase Channel Transfer Function sampled at 21:43 UTC the 12th of February 2008.

Figure 5 shows a 3.93 seconds sample of the time variant channel transfer function from which a value of channel coherence time of approximately 2 s can be derived. This channel transfer function was sampled at 21:43h UTC. The same day between 21h UTC and 04h UTC the CDF of demodulated data was computed and shown in figure 6. Two burst of symbols were transmitted. One with no time interleaving an another one with a time interleaving length of 295.2 ms. As it is depicted in figure 6, those symbols with interleaving time length much shorter than the channel coherence time do not assure a better performance than those symbols that do not apply time interleaving. Since there is no time diversity to exploit, data with time interleaved symbols does not perform better.

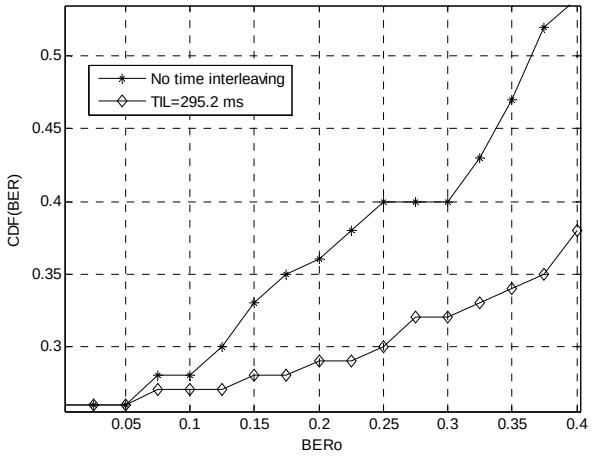

Figure 6. Cumulative Density Function of the BER of two bursts of data. One with no time interleaving and another one with 295.2 ms of interleaving length (Approximately, between 21h UTC of 11th and 04h UTC of 12th of February).

4 Conclusions and future work

OFDM symbols were transmitted between the Antarctic Spanish Base in Livingston Island and the *Observatori de l'Ebre* during 11th, 12th and 13th of Frebruary 2008. Data collected from these experiments showed that the Ionospheric Channel Transfer Function has a strong correlation with time, presenting different values of Doppler effects at different moments of day. Approximately, from 18 UTC to 21 UTC, the channel showed high Doppler values and hence short coherence time values and from 21 UTC to 04 UTC the channel showed lower Doppler values and hence long coherence time values. Through these two types of channel bursts of OFDM symbols with different interleaving lengths were transmitted and Cumulative Density Function of the BER was evaluated. Results showed that for fast fading channels (300ms of channel coherence time) long time interleaved symbols performed better than short time interleaved symbols. For slow fading channels (2 s of channel coherence time) data with interleaving length as long as 295.2 ms performed equal and even worse than data that not used time interleaving. So, time diversity can be only exploited in an ionospheric channel like the one under study when the time interleaving length applied to the transmitted symbols are equal or longer than the channel coherence time they are transmitted through.

Future studies will try to corroborate these first outcomes by transmitting symbols with time interleaving much more longer than the channel coherence time. Other works will try to combine frequency and time diversity of this multipath time-variant ionospheric channel in order to reduce high latency when transmitting through very static channels. Frequency hopping techniques will also be approximated to exploit the frequency diversity of the channel.

Acknowledgements

This work has been developed in the framework of the project CGL2006-12437-C02-01, funded by the Spanish Government.

References

[1]C. Vilella, D. Miralles, J.L. Pijoan. "An Antarctica-to-Spain HF Ionospheric Radio Link: Sounding Results". *Radio Science*, 2008.

[2]P. Bergada, M. Deumal, C. Vilella and J.L. Pijoan. "Multicarrier Modulation Proposal for Long Distance HF Data Link". 12th International Ionospheric Effects Symposium,IES 2008, Alexandria, Virginia, USA, May 2008.

[3]B. Sklar. *Digital Communications, Fundamentals and Applications.* Prentice Hall PTR, 2001.

[4]C. Vilella, J.C. Socoró, D. Miralles, J.L. Pijoan, P. Bergadà, "HF channel measurements for digital communications from Antarctica", 11th International Ionospheric Effects Symposium, IES 2005, Alexandria, Virginia, USA, May 2005.

[5]L. Junsong, "Effects of Time Selective Multipath Fading on OFDM Systems for Broadband Mobile Applications".IEEE Comunications Letters, Vol. 3, No. 12, December 1999.

[6] J.J. van de Beek, M. Sandell, O.P. Börjesson, "On channel estimation in OFDM systems", 45º IEEE Vehicular Technology Conference, Chicago,I1, vol.2,pp.815-819, July.

[7] D.T. Sandwell, "Biharmonic Spline Interpolation of GEOS-3 and SEASAT Altimeter Data", Geophysical Research Letters, 2, 139-142,1987.

Bibliography

[1] A. Ads, P. Bergadà, C. Vilela, J. R. Regué, J. L. Pijoan, R. Bardají, and J. Mauricio, "A comprehensive sounding of the ionospheric HF radio link from Antarctica to Spain," *Radio Science*, vol. 48, pp. 1–12, 2013.

[2] H. Aitken, *Syntony and Spark-The origins of Radio.* Wiley and Sons, 1976.

[3] C. Cahn, "Combined digital phase and amplitude modulation communication system," *IRE Transactions on Communications*, vol. CS-8, pp. 150–155, 1960.

[4] P. S. Cannon, M. J. Angling, N. C. Davies, T. Wilink, V. Joladen, B. Jacobson, B. Lunborg, and M. Broms, "Damson HF channel characterisation-a review," in *21st Century Military Communications Conference Proceedings*, vol. 1, Los Angeles, October 2000, pp. 59–64.

[5] R. S. Cheng and S. Verdú, "Guassian multiaccess channels with ISI: capacity region and multiuser water-filling," *IEEE Transactions Information Technology*, vol. 39, May 1993.

[6] S. C. Cook, "Advances in High Speed HF Radio Modem Design," in *Proceedings of the Nordic Shortwave Conference*, Faro, Sweden, 1995.

[7] J. A. Davis and J. Jedwad, "Peak-to-Mean Power Control in OFDM, Golay Complementary Sequences and Reed-Muller Codes," *IEEE Transactions Information Theory*, vol. 45, no. 7, November 1999.

[8] *MIL-STD-188-141A, Interoperability and Performance Standards for Medium and High Frequency Radio*, Department of Defense, USA Std., September 1991.

[9] M. Deumal, C. Vilella, J. C. Socoro, R. M. Alsina, and J. L. Pijoan, "A DS-SS Signaling based System Proposal for Low SNR HF Digital Communications," in *10th IET International Conference on Ionospheric Radio Systems and Techniques*, London, 2006.

[10] O. E. Dunlap, *Marconi, The Man on His Wireless.* Arno Press and New York Times, 1971.

[11] D. Elliott and K. Rao, *Fast Transforms Algorithms, Analyses, Applications.* Academic Press, 1982.

[12] K. Fazel and S. Kaiser, *Multi-Carrier and Spread-Spectrum Systems.* John Wiley and Sons, 2003.

[13] T. Frank, A. Klein, E. Costa, and E. Schulz, "Robustness of IFDMA as Air Interface Candidate for Future High Rate Mobile Radio Systems," *Advances in Radio Science*, vol. 3, pp. 265–270, 2004.

[14] R. S. Gallager, *Information Theory and Reliable Communications.* New York: Wiley, 1968.

[15] *Fedearal Standard 1045, Telecommunications: HF Radio Automatic Link Establishment*, General Services Administration Std., January 1990.

[16] B. Goldberg, "300 kHz-30 MHz MF/HF," *IEEE Transactions on Communication Technology*, vol. Com-14, no. 6, December 1966.

[17] S. W. Golomb, *Shift Register Sequences.* San Francisco: Holden-Day, 1967.

[18] M. Hervás, J. L. Pijoan, R. M. Alsina-Pagès, M. Salvador, and D. Badia, "Single-carrier frequency domain equalisation proposal for very long haul HF radio links," *IET Electronics Letters*, pp. 1–3, 2014.

[19] E. K. Hong, K. J. Kim, and K. C. Whang, "Performance evaluation of DS-CDMA system with M-ary orthogonal signaling," *IEEE Transactions on Vehicular Technology*, vol. 45, no. 3, pp. 57–63, February 1996.

[20] E. E. Johnson, E. Koski, W. N. Furman, M. Jorgenson, and J. Nieto, *Third-Generation and Wideband HF Radio Communications.* Boston: Artech House, 2013.

[21] R. W. Johnson, M. B. Jorgenson, and K. W. Moreland, "Error Correction Coding for Serial-Tone Transmission," in *7th International Conference on Radio Systems and Techniques*, Nottingham, UK, 1997.

[22] M. B. Jorgenson, R. W. Johnson, P. F. Jones, W. M. Bova, and K. W. Moreland, "Improving the LPI and self-interference characteristics of the STANAG 4415 very robust HF waveform," in *IEEE Milcom*, vol. 1, October 2002, pp. 115–119.

[23] B. S. Krongold and D. L. Jones, "PAR reduction in OFDM via active constellation extension," in *IEEE International Conference on Acoustics, Speech and Signal Processing*, vol. 4, April 2003, pp. 525–528.

[24] ——, "An Active-Set Approach for OFDM PAPR Reduction via Tone Reservation," *IEEE Transactions on Signal Processing*, vol. 52, no. 2, pp. 495–509, 2004.

[25] J. J. Lemmon, "Wideband model of man-made HF noise and interference," *Radio Science*, vol. 32, pp. 525–539, 1997.

[26] X. Li and L. J. J. Cimini., "Effects of clipping and filtering on the performance of OFDM," *IEEE Communications Letters*, vol. 2, pp. 131–133, May 1998.

[27] H. Ma and J. Wolf, "On Tail Biting Convolutional Codes," *IEEE Transactions on Communications*, vol. COM-34, pp. 104–111, 1986.

[28] H. G. Myung, J. Lim, and D. J. Goodman, "Single Carrier FDMA for Uplink Wireless Transmission," *IEEE Vehicular Technology Magazine*, vol. 1, pp. 30–38, 2006.

[29] *Standardization Agreement 4538, Technical Standards for an Automatic Radio Control System for HF Communication Links*, NATO Std., 2007.

[30] J. Nieto, "Does Modem Performance Really Matter on HF Channels? An Investigation of Serial-Tone and Parallel-Tone Waveforms," in *Nordic Shortwave Conference HF '01*, Farö, Sweden, 2001.

[31] ——, "Constant Envelope Waveforms for Use on HF Multipath Fading Channels," in *Proceedings of MILCOM2008*, San Diego, CA, 2008.

[32] ——, "An investigation of coded OFDM and CEOFDM waveforms utilizing different modulation schemes on HF channels," in *6th International Symposium on Communication Systems, Networks and Digital Signal Processing*, 2008.

[33] *Standardization Agreement 5066, Profile for High Frequency (HF) Radio Data Communications*, North Atlantic Treaty Organization Std.

[34] *Standardization Agreement 4285, Characteristics of 1200/2400/3600 Bits per Second Single Tone Modulators/Demodulators for HF Radio Links*, North Atlantic Treaty Organization Std., February 1989.

[35] *NATO STANAG 4415, Characteristics of a robust, non-hopping, serial-tone modulator/demodulator for severely degraded HF radio links*, North Atlantic Treaty Organization Std., 1999.

[36] I. Perez-Alvarez, I. Raos, S. Zazo, E. Mendieta-Otero, H. Santana-Sosa, and J. M. Páez-Borrallo, "Interactive Digital Voice over HF," in *IEE Ninth International Conference on HF Radio Systems and Techniques*, Bath, UK, June 2003.

[37] J. Perkiomaki, "HF Propagation Prediction and Ionospheric Communication Analysis," www.voacap.com, 2003-2013.

[38] R. L. Peterson, R. E. Ziemer, and D. E. Borth, *Spread Spectrum Communications Handbook*. Prentice Hall, 1995.

[39] J. G. Proakis, *Digital communications*, 4th ed. McGraw-Hill, 2000.

[40] S. Shepherd, P. van Eetvelt, C. Wyatt-Millington, and S. Barton, "Simple coding scheme to reduce peak factor in QPSK multicarrier modulation," *Electronics Letter*, vol. 31, pp. 1131–1132, July 1995.

[41] R. V. Sonalkar, "An efficient bit-loading algorithm for DMT applications," *IEEE Communications Letters*, vol. 4, pp. 80–82, March 2000.

[42] *MIL-STD-188-110B, Military Standard-Interoperability and Performance Standards for Data Modems*, U.S. Department of Defense Std., May 2000.

[43] R. van Nee and R. Prasad, *OFDM for Wireless Multimedia Communications*. Artech House Universal Personal Communications, 1999.

[44] C. Vilella, D. Miralles, and J. L. Pijoan, "An Antarctica-to-Spain HF Ionospheric Radio Link: Sounding Results," *Radio Science*, vol. 43, 2008.

[45] S. B. Weinstein and P. M. Ebert, "Data Transmission by Frequency-Division Multiplexing using the Discret Fourier Transform," *IEEE Transactions on Communication Technology*, vol. COM-19, pp. 628–634, 1971.

Notation

Acronyms

ALE	Automatic Link Establishment
ARQ	Automatic Repeat reQuest
ASIC	Application-Specific Integrated Circuit
AWGN	Additive White Gaussian Noise
BER	Bit Error Rate
BPSK	Binary Phase Shift Keying
CDF	Cumulative Density Function
CDMA	Code Division Multiple Access
CEOFDM	Constant Envelope OFDM
CPM	Continuous Phase Modulation
CW	Continuous Wave
D/A	Digital-to-Analog
DAB	Digital Audio Broadcasting
DAMSON	Doppler and Multipath SOunding Network
DEVM	Differential Error Vector Magnitude
DFT	Discrete Fourier Transform
DMT	Discret Multi Tone
DS	Direct Sequence
DSCDMA	Direct Sequence Code Division Multiple Access
DSP	Digital Signal Processing
DSSS	Direct Sequence Spread Spectrum
DVB-T	Digital Video Broadcasting-Terrestrial

EVM	Error Vector Magnitude
FEC	Forward Error Correction
FED-STD	Federal-Standard
FH	Frequency Hopping
FHSS	Frequency Hopping Spread Spectrum
FFT	Fast Fourier Transform
FPGA	Field Programmable Gate Array
FSK	Frequency Shift Keying
HF	High Frequency
HFC	Hybrid Fiber Coax
GMSK	Gaussian Minimum Shift Keying
GPS	Global Positioning System
GRECO	Research Group on Electromagnetism and Communications
IBO	Input Back Off
ICI	Inter-Carrier Interference
IFFT	Inverse Fast Fourier Transform
ISI	Inter-Symbol Interference
ITU	International Telecommunication Union
LMS-DFE	Least Mean Squares-Decision Feedback Equalizer
LTE	Long-Term Evolution
MC	Multicarrier
MC-CDMA	Multicarrier Code Division Multiple Access
MIMO	Multiple Input Multiple Output
MIL-STD	Military Standard
MLSE	Maximum Likelihood Sequence Estimation
OCXO	Oven Controlled Crystal Oscillator
OFDM	Orthogonal Frequency Division Multiplexing
OFDMA	Orthogonal Frequency Division Multiple Access
OSI	Open Systems Interconnection
PAM	Pulse-Amplitude Modulation

PAPR	Peak-to-Average Power Ratio
PAR	Power-to-Average Ratio
PN	Pseudo-Noise
PSK	Phase Shift Keying
QAM	Quadrature Amplitude Modulation
QPSK	Quadrature Phase Shift Keying
RRC	Root Raised Cosine
SAS	Spanish Antarctic Station
SDR	Software Defined Radio
SC-FDE	Single Carrier-Frequency Domain Equalization
SC-FDMA	Single Carrier Frequency Division Multiple Access
SF	Spreading Factor
SIMO	Single Input Multiple Output
SIR	Signal to Interference Ratio
SL	Soft Limiter
SLM	Selected Mapping
SNR	Signal-to-Noise Ratio
SS	Spread Spectrum
SSB	Signal Side Band
STANAG	Standardization Agreement
TDMA	Time Domain Multiple Access
WPLC	Wide Power Line Communication

Errata

List of corrigenda

- On page 73, last paragraph, instead of *In order to improve the robustness of the τ_c calculation, the power delay profile modified by subtracting...*, it should say *In order to improve the robustness of the composite multipath spread calculation, defined in equation 5.11, the power delay profile is modified by subtracting....*
- On page 74, in equation 5.7 the upper limit should be τ instead of τ_2.
- On page 80, in table 5.3, F_c stands for carrier frequency. Instead of τ_{eff} it should say τ_c.
- On page 82 and 84, there should be a cite to [Voacap(2013)] Perkiomaki, J. (2013), HF Propagation Prediction and Ionospheric Communications Analysis, www.voacap.com.
- On page 99, the caption of table 6.1 should say: *The values of BER at several points of accumulated probability are given for all designed combinations*, instead of *The values of Cumulative Distribution Function of the BER are given for all the designed combinations.*
- On page 104, the cite [9] should be [Deumal et al.(2006)].